Tooth Roots and the Periodontal Ligament: Morphology, Modeling and Behavior

Casey J Self

A dissertation

submitted in partial fulfillment of the

requirements for the degree of

Doctor of Philosophy

University of Washington

2015

Reading Committee:

Susan Herring, Chair

Christian Sidor

Sharlene Santana

Program Authorized to Offer Degree:

Biology

University of Washington

Abstract

Tooth Roots and the Periodontal Ligament: Morphology, Modeling and Behavior

Casey J Self

Chairperson of the Supervisory Committee:

Professor Susan Herring

Department of Biology

The relationship between tooth roots and diet is relatively unexplored, although a logical relationship between harder diets and increased root surface area is suggested. Two studies were done to address the interaction between tooth root morphology, diet and bite force in small mammals. In bats there was a clear relationship between food hardness and root surface area. In contrast, no strong relationship was found between estimated bite force and tooth root surface area in rodents. In general though, these studies combined show that microCT successfully allows the non-destructive quantification of previously difficult-to-access tooth morphology and shows the potential for tooth roots to provide valuable dietary, behavioral and ecological information in small mammals. The study of root morphology by microCT inevitably ignores the PDL fibrous component, yet this is also critical for mechanical behavior. Therefore, simplified single-rooted tooth geometry was used to make predictions about PDL fiber bundle organization under two types of habitual loading. The architectural hypotheses generated by FEA were generally supported by histological findings. An unanswered question is whether PDL architecture can be modified in response to altered diet. A rabbit model was used to investigate the effects of reduced loading on the morphology and composition of the PDL. This is not a change in diet hardness per se, but it was assumed that the animals could not bite with normal force. The expected changes in PDL shape and size, as a result of reduced loading, were not seen. There was no reduction in PDL area or collagen content, nor was the complexity of either the PDL or bone affected. This could indicate that PDL morphology cannot adapt to changed circumstances or that the change in loading was not sufficient to trigger adaptation.

Acknowledgements

I would like to thank my committee, Sue Herring, Christian Sidor, Sharlene Santana, Greg Wilson, Dwayne Arola, and Peter Mackenzie for being wonderful mentors. This work could not be done without museum collections and staff; specimens were kindly loaned from The University of Washington Burke Museum (UWBM) and The Museum of Vertebrate Zoology (MVZ) at the University of California, Berkeley. Jeff Bradley (UWBM) and Chris Conroy (MVZ) were especially helpful to this project. Tim Cox and Murat Maga at the Small ANimal Tomographic Analysis facility (SANTA) at Seattle Children's Hospital provided training and assistance with CT scanning, for which I am grateful. Thank you also to Xian-Qin Bai and Kathy Rafferty for helping me unravel the mysteries of a good histological section. Thanks to Tracy Popowics for sharing her wisdom regarding mice and always being willing to read a draft of something. Several undergraduate research assistants were integral to this project: Abby Payne, Rebecca Andersen, Anna Kovac and Sofie Bluvstein. The FEA model work could not have been completed without the help of Terry Polen, I am extremely grateful for his assistance and support. Mary Pat Wenderoth, Karen Petersen, Judy Farrow, Marissa Heringer, Mary Beth Cunningham, Carol Wiesenbach, and Leslie Zeman all helped me in different ways at different times. Thank you. Many thanks to my first academic mentor, David Daegling, for setting me on this path. Finally (again) many thanks to my advisor, Sue Herring, for her guidance and patience.

This project was supported by T32 DE07132 from NIDCR.

Contents

Chapter 1: Introduction 1

Production of Bite Force 2

Periodontal Ligament 3

Tooth Roots 17

Overview 18

Chapter 2: Dental root size in bats with diets of different hardness 21

Introduction 22

Material and Methods 25

Results 30

Discussion 34

Chapter 3: Cricetid rodents: Is molar root morphology an indicator of diet? 47

Introduction 48

Material and Methods 50

Results 54

Discussion 57

Chapter 4: Finite Element Analysis of Periodontal Ligament Fiber Bundle Orientation . 64

Introduction 64

Methods 72

Results 76

Discussion 77

Chapter 5: The Comparative Periodontium 87

Introduction 87

Methods 92

Results 94

Discussion 96

Chapter 6: The Effect of Reduced Loading on PDL Morphology 122

Introduction 122

Methods 124

Results 126

Discussion 128

Chapter 7: Conclusions and Future Work 136

Summary of Results 136

Future work 138

List of References 140

List of Tables

Table 2-1. Species studied according to diet and hardness classifications 40

Table 2-2. Size estimates for skull and body areas and surface areas root and the occlusal face of the crown 41

Table 2-3.Species means ± standard deviation and results of non-parametric species comparisons 42

Table 2-4. Product-moment correlation coefficients (r) of skull size and body size against bite force estimates 43

Table 2-5. Correlations among tooth variables in each species..... 44

Table 3-1. Rodent specimen information.....61

Table 3-2. Individual rodent tooth values. 62

Table 4-1. Experimentally determined properties of the tooth-bone interface 81

Table 4-2. Root apex displacement under two loading regimes for each fiber angle 83

Table 4-3. Normalized strain distribution around a horizontal section of the tooth socket. 81

Table 5-1 . Average values and standard deviation for bundle width and angle in the coronal plane 102

Table 5-2. Average values and standard deviation for PDL width in the four anatomical quadrants 103

Table 5-3. Response table for overall species difference in PDL bundle organization category 104

Table 5-4. Response table for PDL bundle organization category in the four anatomical quadrants for each species 105

Table 6-1. Comparison of PDL characteristics in normal and reduced loading cases 131

Table 6-2. PDL perimeter measurements and PDL area measurements for all studied species .132

List of Figures

Figure 1-1. Diagram showing dental structures and arrangement of collagen fiber bundles within the PDL 20

Figure 2-1. Isolated bat tooth rows, all to scale 45

Figure 2-2. Bivariate plot of mandibular largest tooth root surface area and estimated bite force using the beam method 46

Figure 3-1. Combined phylogeny, diet, and morphology of the rodents studied. 63

Figure 4-1. Diagram of the FEA model in the coronal plane 84

Figure 4-2. Diagram of the FEA model in the horizontal plane 85

Figure 4-3. Rotational movement of the tooth under horizontal loading 86

Figure 5-1. Comparison of skull morphology and primary chewing direction in the three study taxa 106

Figure 5-2. Predictions for PDL fiber orientation in the coronal plane 107

Figure 5-3. Predictions for PDL fiber orientation in the horizontal plane.....108

Figure 5-4. An overview of tooth root and PDL morphology in the coronal plane in the mid-first molar region of *N. vison*.....109

Figure 5-5. Detailed image of PDL fiber arrangement in the coronal plane for *N. vison* 110

Figure 5-6. An overview of tooth root and PDL morphology in the coronal plane in the mid-first molar region of *M. musculus*. 111

Figure 5-7. Detailed image of PDL fiber arrangement in the coronal plane for *M. musculus* ...112

Figure 5-8. An overview of tooth root and PDL morphology in the coronal plane in the mid-first molar region of *O. cuniculus*. 113

Figure 5-9. Detailed image of PDL fiber arrangement in the coronal plane for *O. cuniculus.* ...114

Figure 5-10. An overview of PDL morphology in the horizontal plane in the mid-first molar region of *N. vison* 115

Figure 5-11. Detailed image of PDL fiber arrangement in the horizontal plane of *N. vison* 116

Figure 5-12. An overview of PDL morphology in the horizontal plane in the mid-first molar region of *M. musculus.*.....117

Figure 5-13. Details of *M. musculus* PDL morphology in the horizontal plane.....118

Figure 5-14. An overview of PDL morphology in the horizontal plane in the mid-first molar regions of *O. cuniculus*. 119

Figure 5-15. Details of PDL morphology in the horizontal plane of *O. cuniculus* 120
Figure 5-16. Distribution and variation of bundle width measurements for each species.....121
Figure 6-1. Diagram of work-flow for parsing of digital images for the four PDL analyses 133
Figure 6-2. Detailed image of *O. cuniculus* PDL organization in the coronal plane 134
Figure 6-3. Detailed Image (Specimen 5218), horizontal section rabbit PDL 133

Chapter 1: Introduction

Morphology of jaws and teeth vary among mammals. Dental and other masticatory characters of extant animals strongly correlate with dietary adaptations, and their morphology can be used to interpret the fossil record. To infer the selective force acting on these features, a structural and functional awareness of the components of the masticatory system is required. Part of this process involves a clear understanding of the load pattern resulting from jaw activity (Hiiemae, 1984).

Dental morphology is a vital source of information for determining dietary behavior and phyletic relationships of animals. To do so, it is necessary to identify morphological correlates of behavior. Paleontology benefits from a deeper understanding of functional and evolutionary morphology. Questions pertaining to food choice in resource abundant areas or between sympatric species, resource partitioning, are often related to questions of anatomy. Studies of gut morphology have identified dietary constraints that restrict feeding behavior in sympatric primate species (Milton, 1981). Likewise, details of periodontal ligament (PDL) and tooth root morphology may shed light on behavioral constraints. Teeth are tools and the type of activity an animal is capable of, for example, grooming, nest building, or prey capture, will depend on the available tools. Additionally, association of structure and behavior can help identify constraints on dietary change. Many species take advantage of seasonally available food, changing their diets through the year. The ability of an organism to alter its diet is mediated by many biological constraints, not the least of which is food processing ability.

Production of Bite Force

Faced with physical barriers to obtaining nourishment, such as shells, chitin covering or seed coats, most mammals must process their food to some degree. The primary breakdown of food is caused by occlusal contact between the teeth. Occlusal force is generated when the muscles of mastication contract, and the temporomandibular joint allows complex jaw movements to occur. The rotational versus translational components of jaw movement vary among mammals, along with the morphology of the joint and the arrangement of the mastication muscles. In mammals the masseter, temporalis and pterygoideus groups are all involved in jaw closing but these muscles are complex, often subdivided and interconnected (Herring, 2007; Hiiemae, 2000). Carnivores generally exhibit larger temporalis muscles, which contribute to the simple hinge movement in their feeding behavior (Smith and Savage, 1959). Herbivores that produce a grinding action have masticatory muscles dominated by the masseter. Transverse grinding is associated with a strongly-developed pterygoideus in addition to the dominant masseter (Turnbull, 1970). In some animals such as rodents and elephants, there is a strong anteroposterior component during the chewing cycle (Hiiemae, 1978; Maglio, 1973).

Diet is linked to cranial structure through bite force (Meyers and Irschick, 2015). It is thought that bite force varies according to food material properties after controlling for body size; however, there are few studies that directly compare bite force measurements and diet. Aguirre et al. (2002) compared bite force measurements taken in the field with food choice in several species of insectivorous bats. Specializations such as nectivory and sanguivory were associated with reduced bite forces, and the authors suggested that food hardness is likely a limiting factor in food choice, especially for small bats (Aguirre et al., 2003). Similarly in a rodent study by Freeman and Lemen (2008b), two outliers from a bite force– body size

relationship were a nut-eating species and a fossorial species; both behaviors require a relatively higher bite force. These findings may support a correlation between hard foods and a high bite force.

Since obtaining bite force measurements from live animals is not often feasible, it is common practice to estimate bite forces from muscle attachment area measurements (Davis et al., 2010; Freeman and Lemen, 2010; Thomason, 1991b). In one such study of carnivores, Wroe et al.(2005) found a positive relationship between the bite force of the predator and the size of its prey, although prey size was not directly measured. Although the result supports the notion that structure can predict behavior, muscle attachment areas are very indirect indicators of bite force. In the case of museum specimens or extinct animals indirect measurement is all that is available. In this respect, PDL attachments are more clearly related to bite force mechanically, and should be less ambiguous to measure.

Periodontal Ligament

The periodontal ligament (PDL) functionally links the teeth to the alveolar bone. It provides support, protection and sensory input to the masticatory system. The PDL allows the teeth to change position under loading and maintains continuity between the two hard tissue components of the periodontal region: the alveolus and tooth cementum (Bondevik, 1984). In addition to its role as a support structure, the PDL also transmits blood vessels, supplies nourishment to the cementum and, through signaling from the mechanical loads, maintains and remodels the soft and hard tissue of the periodontal region. The PDL is a unique tissue. Its removal can cause loss of function of teeth and resorption of surrounding alveolar bone (Mitchell and West, 1975; Roberts, 1999). In mastication, its role is to provide sensory feedback during the

chewing cycle and to serve as a medium of force transfer between the teeth and alveolus (Roberts et al., 1981; Ten Cate, 1994).

Composition. A healthy, functioning PDL contains multiple cell types: fibroblasts, endothelial cells, sensory system cells, bone associated cells and cementoblasts. Collectively, these cells act to sense applied physical forces and respond to them by maintaining periodontal width and preserving cell viability (McCulloch et al., 2000). The main component of the PDL is fibroblasts; the amount of fibroblasts present is species dependent. In rodents, fibroblasts make up 35% of the volume of PDL space, in sheep closer to 20% and in humans approximately 25-30% (Beertsen, 1975; Berkovitz et al., 1981; McCulloch et al., 2000). Fibroblast number also appears to be affected by age. In humans, the number of fibroblasts is halved by age 50 (Krieger et al., 2013).

Morphology. The PDL is mostly composed of oriented bundles of collagen fibers, called principal fibers. In humans, the individual collagen fibers within the bundles are approximately 55 nm in diameter. These fibers are small compared to the 100-250 nm collagen fiber diameters observed in tendons. A large diameter is generally attributed to older fibers; the small diameter in PDL fibers is likely due to a high rate of collagen turnover (Sloan and Carter, 1995). Periodontal collagen turnover rate is very high, twice that of the gingiva, four times that of the skin, and six times that of alveolar bone (Sodek, 1977). Adult human fibrils are slightly thicker than those in rodents and several other mammalian species, indicating a variable rate in PDL turnover (Sloan and Carter, 1995). However, age can be a confounding factor in total collagen amount because there is a decrease in collagen-producing activity in the PDL with age (Moxham

and Evans, 1995). In all mammals, the fibers of the PDL tend to be wavy on their course from cementum to bone, which allows for movement of the tooth (Melcher and Eastoe, 1969). There does not appear to be a functional link between individual fiber thickness and mechanical response, at least in bovine PDL (Pini et al., 2002).

The PDL's collagen fiber bundles are primarily composed of interstitial collagens I and II. These collagens form banded fibrils (Bartold and Narayanan, 1998). Collagen V is also associated with the fibrils, however it is found either in the spaces between fibril bundles or within the core of the fibrils (Huang et al., 1991). Several other minor collagens are also found in the PDL, such as collagens VI and XII as well as other extracellular matrix proteins including some proteoglycans, fibronectin and plycoprotiens (Beertsen et al., 2000; Karring et al., 1993; McCulloch et al., 2000).

Of principal importance to the function of the PDL are the attachment sites to tooth and bone. Sharpey's fibers are the extensions of the principal fibers of the PDL into the hard tissues: cementum and bone. Once embedded into the wall of the alveolus or the cementum, Sharpey's fibers calcify and are associated with non-collagenous proteins commonly found in bone and tooth cementum (McCulloch et al., 2000). Sharpey's fibers tend to be longer on the tension side of the PDL (appositional side), suggesting interstitial fiber growth where the bundles are integrated into the surrounding bone (Beertsen et al., 2000). Sharpey's fibers are also associated with high levels of osteopontin and bone sialoprotien; this close association could possibly provide advantageous physical properties to the hard tissue – soft tissue interface. Bone remodeling severs Sharpey's fibers as old alveolar bone is replaced by new bone. The association with non-collagenous proteins would allow for continuous embedding of PDL fibers into the alveolar wall (McCulloch et al., 2000).

Fiber bundles appear to have constant orientation relative to their location (Fig. 1-1). Accordingly, PDL fibers have generally been classified into categories based on orientation: gingival, crestal, horizontal, oblique and periapical fibers (Bartold and Narayanan, 1998; Melcher and Eastoe, 1969; Sloan, 1978). Alveolar crest fibers run from the cementum of the tooth in an apically-slanted direction and towards the alveolar crest. Horizontal fibers run horizontally from the cementum covering the region of the tooth just inferior to the cementoenamel junction to the alveolar bone directly opposite. Oblique fibers run in an occlusally-slanted direction from the cementum covering the apical two-thirds of the root to the alveolar bone. Periapical fibers radiate from the cementum of the apex to the alveolar bone. Not all fiber bundles present in the PDL insert into alveolar bone. Gingival fibers run from the most cervical cementum into the lamina propria of the gingiva. Circumferential fibers originate in the most cervical cementum and run horizontally around the root and insert into the lamina propria of the gingiva. Transseptal fibers run from the cementum of one tooth, cross the interdental septum and insert into the cementum of the adjacent tooth. In multi-rooted teeth, interradicular fibers run from the interradicular septum into the cementum (Moss-Salentjin and Hendricks-Klyvert, 1990).

These classification schemes have been challenged, especially for animals with continually growing (hypselodont) teeth (Sloan and Carter, 1995). Indeed, histological work as a part of this project has identified issues classifying PDL regions by fiber arrangement in hypselodont species (Chapter 4). In continuously erupting (hypsodont) teeth, the alveolar region of the tooth is shortened throughout life, resulting in a reduced overall PDL attachment area with age. The reduction of PDL attachment results in increased masticatory forces on the remaining PDL attachment area with increasing age (Staszyk et al., 2006; Warhonowicz et al., 2006).

However, histological examination of hypsodont types of teeth have found three zones of PDL fiber arrangement, generally following that found in humans (Staszyk et al., 2006). In general, the organization of PDL collagen fibers is closely aligned with *in vitro* load characteristics (Viidik, 1980), indicating that PDL morphology is modified by applied loads in all species (Komatsu et al., 1998). This suggests a close link between PDL morphology and ability to withstand applied forces.

Development of the PDL. The PDL is produced before dental eruption mainly from fibroblasts that originate in the dental follicle and begin to differentiate during root development (Ten Cate et al., 1971). During apical development, the cells of the dental follicle differentiate into cementoblasts and form the cementum lining of the root surface (Grant and Bernik, 1972). Initially, collagen fibers become embedded in the cementum, and Sharpey's fibers are laid down in a coronal direction within the PDL region. The initial orientation is nearly parallel to the root surface. Fiber formation and deposition occur from the developing cementoenamel junction (CEJ) to the apex of the tooth. Those fibers deposited apical to the CEJ form the PDL. After one-third of root formation, fibers insert within the cementum matrix from the CEJ and continue coronally. This process closely follows the outline of the newly formed crown. No insertion of collagen fibers into the alveolar bone can be seen at this stage.

Loosely arranged fiber deposition and insertion continues along the developing root surface. Opposite this surface, fiber insertion also occurs along the lining of the bony socket wall. These fibers cross the ligament space in a similar fashion as the root side fibers. Both root and bone-side fibers ultimately come together in the middle of the ligament space to form the intermediate plexus. The orientation of these fibers is initially parallel to the root surface, but as

the teeth erupt, their orientation dramatically changes (Grant and Bernik, 1972), possibly as a result of the positional relationship of the erupting tooth to the adjacent teeth (Bartold and Narayanan, 1998).

PDL During Tooth Eruption. During eruption of teeth that will have closed roots, the dentogingival fibers align from the CEJ in the occlusal direction, terminating in the connective tissue of the gingiva. The transseptal fibers extend over the alveolar crest in an oblique direction toward the surface of the adjacent developing tooth root. The fibers of the cervical-most one-third of the root surface run obliquely in the apico-occlusal direction from cementum to bone. Although there is still no direct connection from the root and bone, fibers in the middle third of the root become more defined. Root formation is still occurring in the apical portion, and accordingly, fiber arrangement is poorly developed.

Upon full eruption and occlusal contact, the ligament fibers assume their final configuration. The dentogingival, transseptal and alveolar crest fibers originate at the CEJ. Within the coronal one-third of the root surface, the fibers are arranged horizontally. In the middle third of the root, the fibers run obliquely from the margin of the cementum border on the tooth to the alveolar bone. The apical third maintain an oblique arrangement, but the fibers run apically from the cementum surface to the alveolar bone (Bartold and Narayanan, 1998; Grant and Bernik, 1972).

Ligament formation in teeth with and without primary predecessors differs in structure to some degree. Grant et al. (1972) found that ligament formation in deciduous teeth differs from succedaneous teeth. However, the processes are not unique, as both classes of teeth follow the same stages; only the timing of development is delayed for secondary teeth. During the

preeruptive stage, the succedaneous premolar shows only a few fiber extrusions from the cementum, and no fibers are apparent from bone. Most of the PDL space is filled with loose collagenous elements, unlike a permanent molar which has well defined predentogingival and alvelodental fibers that extend between bone and cementum. Upon eruption, the succedaneous tooth only shows organized dentogingival, alveolar crest and horizontal fibers, leaving the rest of the ligament in developing stages. During initial occlusal contact, the succedaneous premolar demonstrates organized and continuous alveolodental fibers for the coronal two-thirds of the root and the principal fiber formation is still progressing in the apical one-third. The permanent tooth exhibits continuous periodontal ligament fibers. During full occlusal function, both the succedaneous and permanent tooth exhibit classically aligned and thickened PDL fibers. Although the developmental timing differs after eruption and a period of occlusion, the fibers in secondary and primary teeth thicken and become indistinguishable from each other (Grant and Bernik, 1972).

In mammals with hypsodont and hypselodont teeth, the initial development of the PDL is very similar to that of closed rooted teeth. In hypselodont mammals, a proliferative area for dentin and enamel is retained at the base of the tooth and is present throughout life (Oxberry, 1975; Phillips and Oxberry, 1972). In the area between the proliferative zone and the alveolar bone, a reduced tripartite dental follicle remains in that the apical fiber arrangement is different in ever-growing teeth. Additionally, there is a difference in the zone of transseptal fibers; ever growing teeth lack both alveolar crest and interraddicular fibers. (Oxberry, 1975). Along the rest of the tooth, the periodontium follows the development and classification scheme of closed-rooted mammals (Phillips and Oxberry, 1972).

Remodeling. The maintenance and remodeling of the PDL collagen fibers and Sharpey's fibers require a coordinated synchronized action of multiple cell types and signaling pathways. Non-human animal studies have indicated that there is an extremely high turnover rate for PDL matrix proteins (Sodek, 1989). Turnover differs from remodeling in that it constitutes no change in the structural organization of the tissue, while remodeling implies positional or functional changes in the tissue. Both processes occur simultaneously, and the speed of remodeling seen for the PDL contributes to the unique character suite that is part of its adaptability (Sodek, 1989).

The vascular elements and extracellular matrix proteins of the PDL function to allow teeth to adjust their position within the tooth socket, while remaining firmly attached. During remodeling, the collagenous mesh that stretches from bone to cementum must be rapidly broken-down and synthesized. Early studies of continuously growing molars had indicated that remodeling of the ligament is restricted to the mid-region, where fibers from the bone and teeth intermingle, the "intermediate plexus" (Sicher, 1942). More recent work in teeth with limited eruption found remodeling activity throughout the PDL from cementum to bone (Rippin, 1976). Fiber systems are broken down to adapt to changes in the position of teeth. The morphology of the PDL, as a stretched out net, allows for regional breakdown of the meshwork without compromising the integrity of the tissue (Beertsen et al., 2000; McCulloch et al., 2000).

Central to the remodeling activities are the PDL fibroblasts. The fibroblasts are responsible for the formation and remodeling of periodontal fibers. The process of collagen breakdown is controlled intracellularly through phagocytosis; an intracellular mechanism allows for the precise removal of collagen fibers (Beertsen et al., 2000). Extracellular breakdown of collagen is also seen, most often mediated by matrix metalloproteinases (MMPS) (Apajalahti et al., 2003; Ingman et al., 2005; Nahm et al., 2004; Redlich et al., 2001; Shibata et al., 2014).

Levels of MMP are thought to be the primary mode of remodeling in those mammals with ever-erupting teeth (Warhonowicz et al., 2007).

Sensory mechanisms and receptors in the PDL are still under investigation. In addition to neural pathways, PDL cells have mechanisms to respond directly to mechanical forces by activation of myriad mechanosensory signaling systems. These systems include stretch-activated adenylate cyclase ion channels and changes in cytoskeletal organization (McCulloch et al., 2000). There is a loss of actin fibers under stress (de Araujo et al., 2014). These changes in cytoskeleton organization and cell motility result in activation of signaling molecules in response to mechanical stimuli. These immediate responses to mechanical force result in the production of intracellular messengers. After physical osteoblast stretching, increased inositol phosphate concentrations have been observed (Saito et al., 1991a). Also, intracellular calcium ion concentration oscillations have been observed in PDL cells in response to substrate tension (Carvalho et al., 1994; Jones et al., 1991). *In vitro*, an increase in prostaglandin release in tension areas of the PDL has been demonstrated (Yeh and Rodan, 1984). In addition, the PDL maintains gap junctions, which play a role in hypoxia-induced regulation of remodeling through cell-to-cell communication (Kato et al., 2013).

Longer term responses to PDL loading include: altered collagen synthesis, promotion of collagenase activity, stimulation of cell division and release of transforming growth factor-ß (Carvalho et al., 1994; Curtis and Seehar, 1978; Jones et al., 1991; Klein-Nulend et al., 1995; Leung et al., 1976). These studies indicate that there are many potential routes that may lead to direct or indirect influence of the PDL on bone remodeling, however the exact pathway is still unclear. There is a reciprocal, dynamic relationship between activation of membrane-localized cation-permeable channels and cytoskeleton structure. Also, the fibroblasts and osteoblasts that

populate the PDL have the required signaling and effector mechanisms to sense and respond via remodeling to physical force (Beertsen et al., 2000). For example, intermittent pressure application to PDL cells increases bone resorption (Saito et al., 1991b). Although the exact signaling and cellular mechanisms responsible for PDL behavior are still under study, it is evident that the PDL is a requirement for rapid remodeling of bone via application of physical forces to the teeth through its role as a transducer of mechanical stress into biological signaling.

Functions of the PDL. One of the main functions of the PDL in the masticatory cycle is to provide sensory feedback during chewing. Humans are capable of detecting the presence of very small particles between the occlusal surfaces of teeth. The teeth also can serve as an excellent judge of material properties. There are proprioceptive sensors in the PDL that provide sensory information about how fast and how hard to bite (Hannam, 1982). While there are other concentrations of sensory fibers in the oral cavity, the PDL plays a substantial role in providing unconscious feedback for the masticatory system.

Lund and Lamarre (1973) anesthetized patients' teeth and found a 40% reduction in bite force applied, indicating that PDL proprioceptors are important in the control of bite force. Cathelineau and Yardin (1982) found that patients with advanced periodontal disease had an increased threshold in detection of vibrations sent through the teeth, most likely the result of inflammation of the ligament. Edentulous individuals still display proprioceptive abilities, but dentate individuals have the ability to produce much higher interocclusal forces and differentiate between fine particles with higher accuracy (Hannam, 1982). Edel and Wills (1975) and Williams et al. (1987) found that individuals with loss of periodontal bone but no tissue inflammation had no significant differences from a control population in perception of axially

applied forces. Williams et al. (1985) anesthetized teeth and TMJs to measure differences in inter-incisor bite force. They found discrimination of bite force was significantly impaired only when the teeth were anesthetized, again implicating the PDL in a sensory feedback role. These studies indicate feedback mechanisms of the PDL play a significant role in the proper mechanical function of the masticatory system by assisting in particle identification and maintaining appropriate force application.

The PDL is subjected to forces during mastication, speech and orthodontic tooth movement. The PDL acts as a medium of force transfer during these behaviors and it displays some unique mechanical properties that may be ascribed to loading regimes commonly observed in mastication. The PDL is confined in the alveolus and loads resulting from tooth-tooth contact during mastication are not purely axial. A such, the PDL experiences both compression and tension during a regular loading scheme (Pini et al., 2002). The mechanical strength of the PDL is derived from the molecular structure of the type I collagen and its arrangement into fibers (McCulloch et al., 2000). There appears to be regional variation in the biomechanical properties of the PDL, which may depend on the developmental stage of the collagen fibers as well as arrangement, diameter and density of the collagen fiber bundles (Komatsu et al., 1998). The PDL is also highly vascularized, a trait that contributes to its viscoelastic behavior. Matsuo and Takahashi (2002) found that the blood vessels in the PDL may contribute to "shock absorber" behavior of the PDL, cushioning the alveolus from the occlusal load. Exact behavior of the PDL during mastication is still somewhat unclear, and *in vivo* research on human subjects is difficult to come by. Most experimental studies of PDL response to load *in vivo* have been done on rodents. Interspecific variation in the mechanical properties of the PDL has been attributed to

differences in the width and crimping of the PDL, as well as the species-specific strength and stiffness of the periodontal collagen fibers (Komatsu et al., 1998).

Despite some uncertainties about detailed behavior and remodeling effects of the PDL, research has demonstrated broad cross-species trends in PDL behavior. For example, the PDL exhibits viscoelastic behavior, where the stiffness of that material changes with the rate of load application. As increasing rates of force are applied to the tooth the force-displacement curve is non-linear. The initial stiffness is low, but as the force is increased the resistance increases until at high forces, the additional displacement is very small (Wills and Picton, 1978). Ralph (1982) found that, in tension, human PDL exhibited viscoelastic behavior in both extrusion and intrusion and suggested that the close interaction of PDL fibers and capillaries may produce a closed fluid system in the PDL space which would allow for distribution of large masticatory loads to the alveolar wall. Results of experimental extrusion and intrusion of human teeth produced stress-strain curves that had distinct toe and linear regions indicating a nonlinear response to load (Toms et al., 2002a; Toms et al., 2002b). The response varied according to the age of the PDL donors, region of the PDL measured and direction of load application. Toms et al. recommend the inclusion of these unique viscoelastic properties into computer simulations of orthodontic tooth movement.

Pini et al. (2004) found that bovine PDL exhibited non-linear mechanical behavior. They also found that the maximum tangent modulus, strength, strain and strain energy density all increased with depth of location for the incisor and for the molar (except for the apical region of molars), supporting earlier work that the properties of the PDL vary along the length of the root. Their results indicate that the PDL should be viewed as a biphasic material, similar to articular

cartilage in future experimental work and that the compressive behavior of the PDL is highly influenced by interstitial fluid flow.

In conjunction with viscoelastic behavior, the PDL also exhibits an initial loading range where relatively large increments of strain occur with low changes in stress, a toe region. This is counter to early work assuming a linear response to load. Komatsu et al. (1998) found that the maximum functional shear stress exerted on the PDL is approximately 0.335 MPa, a value that corresponds generally to the upper limits of the toe region. If this is true, the PDL naturally operates within the toe region, and the linear stress-strain curve would not be readily observable in normal loading scenarios. The toe region is generally attributed to fiber reorganization with no significant change in stress. With further displacement, the load continues to increase non-linearly, probably the result of principal fibers aligning with the direction of force application. Once the fibers are uncoiled, a linear stress-strain curve is usually observed and attributed to the mechanical stretching of the collagen fibers (Pini et al., 2002).

Experimental intrusion of teeth is affected by the rate of load application and the interval between loads (in macaques (Parfitt, 1960)). Wills and Picton (1978), using two rates of load application, 4 $Nsec^{-1}$ and 12 $Nsec^{-1}$ and human PDL samples, found that slow application of force results in more tooth movement than rapid force application. The slower movement allows the extracellular fluids within the PDL to move, whereas a rapid application would trap them causing restriction of tooth intrusion. Under high loading rates, all of the components of the PDL, both fibers and extracellular fluid, remain in place and act as a single unit to transmit loads (Wills et al., 1976).

The values for rate dependency of ligament load responses under monotonic loading vary widely. Some rabbit knee ligament data indicate minimal rate dependency (Woo et al., 1990),

while rat PDL appears to have a higher level of rate dependency. Komatsu and Chiba (1993) examined the mechanical responses of rat PDL at molar and incisor locations at various load rates. Mechanical strength, stiffness and toughness were greater for the molar than the incisor ligament, indicating that the molar ligament probably has a different fiber arrangement than the incisal ligament. However; both the incisor and molar ligament demonstrated mechanical differences based on loading velocity. Their primary finding was that stress levels were reduced at lower loading velocities. Pini et al. (2002) found no rate dependency of stress as a function of strain in bovine PDL push-pull tests. However in similar experiments with torsion using human PDL, there appeared to be a rate dependency for hysteric effects (Daly et al., 1974).

Hysteresis is the lag in the response of a material to the application or removal of a load. It is a key characteristic of viscoelastic materials and a measure of the ability of a material to store and dissipate energy. Purely elastic materials produce identical load-deformation curves for the loading and unloading phases. In viscoelastic materials, the area under the loading curve is greater than the area under the unloading curve. The difference between the two is a measure of hysteresis, the energy lost during the load cycle (Martin et al., 1998). Mechanical push-pull tests on bovine PDL suggest the PDL response in the range of physiological compression exhibits high levels of hysteresis (Pini et al., 2002). Hysteresis resulting from tension is due to the uncoiling and friction between principal fibers (Pini et al., 2004). Some of the stiffness in PDL response to small loads has been attributed to its high level of vascularization, which also may account for some level of the hysteric behavior seen in the PDL. Additionally, the level of vascularization may affect the accuracy of small loads (0.5N-3.5N) used in *in vitro* studies due to lack of a maintained circulatory system (Pini et al., 2002; Wills et al., 1976).

The PDL is an integral part of the masticatory system, and its organization and functional role should not be overlooked. Investigations of the PDL can potentially inform a myriad of masticatory inquiries, from processes of bone metabolism to biomechanics and masticatory physiology. Furthering our knowledge of the PDL on the physiological and biomechanical fronts are imperative to a clearer understanding of masticatory system as a whole.

Tooth Roots

In the absence of observation and field study, morphological data can be used as a proxy for behavior. Accurate bite force measurements can be difficult to obtain (Dumont, 2007; Thomason, 1991a) and root surface area is a potential surrogate for bite force (Spencer, 2003), but despite early interest in the topic there is still very little work on the subject (Kloehn, 1938). A typical mammalian tooth consists of three layers of mineralized tissue; enamel, dentin and cementum. Enamel is the outermost tissue of the tooth crown and is a highly mineralized tissue derived from mouth epithelium. Dentin is the foundation of the whole tooth, a mineralized tissue derived from mouth mesenchyme. Tooth roots are composed of a central dentin core pierced by a longitudinal canal for passage of nerves and vasculature to the pulp. The root dentin is covered by a thin coat of cementum, which provides anchorage for the PDL. Teeth can be single or multi-rooted. In mammals, the large teeth at the back of the mouth are usually multi-rooted for increased stability under load (Lucas, 2004). The forms of tooth roots are likely related to their mechanical role, but little has been done in the way of direct observation, despite Kloen's (1938) assertion that "the tooth is a tool, and the root is the handle by which it is held and through which it receives its support." The surface area of the root determines the area available for attachment

of the PDL and directly affects the resistance of a tooth to translational forces (Hillam, 1973; Kovacs, 1979; Nikolai and Schweiker, 1972).

Roots with greater surface areas are likely able to withstand higher forces than those with smaller areas. Increase in tooth root surface area can be achieved by lengthening and widening the roots or by increasing the root number. Although gross root morphology has been used to establish evolutionary relationships in primates and fossil hominids, root surface area appears to correlate more closely between unrelated animals with a similar diet (Kupczik and Dean, 2008). Hard diets, whether herbivorous, carnivorous or omnivorous, require larger forces to break down food (Lucas, 2004). Larger root surface areas could theoretically function to reduce stress concentrations in the tooth and alveolar bone that result from large masticatory forces. In summary, the dietary choices of mammals are tied to their ability to produce bite force and to their habitual chewing directions. Both bite force and chewing movements are mediated by the PDL, which connects the tooth to bone. A study of the PDL will advance our understanding of feeding behavior and may provide surrogate measures where field observations are not feasible.

Overview

What follows is a discussion of periodontal ligament and tooth root morphology as they relate to diet, bite force and mastication. Chapter 2 is analysis of tooth root form in phyllostomid bats and the relationship to known dietary habits in these species. Chapter 3 addresses root surface area in sigmodontine rodents along similar lines. Chapter 4 is a review of finite element modeling practices and includes an evaluation of studies relevant to the role of the PDL from the clinical and comparative perspectives. Additionally, a simplified geometric model is created to predict periodontal ligament fiber orientation in various chewing modes. Chapter 5 tests these

model assumptions in a histological investigation of periodontal ligament architecture of three species with distinct chewing modalities. To evaluate the role of changes in loading on PDL morphology, Chapter 6 is a brief analysis of periodontal ligament morphology under a reduced occlusal loading regime.

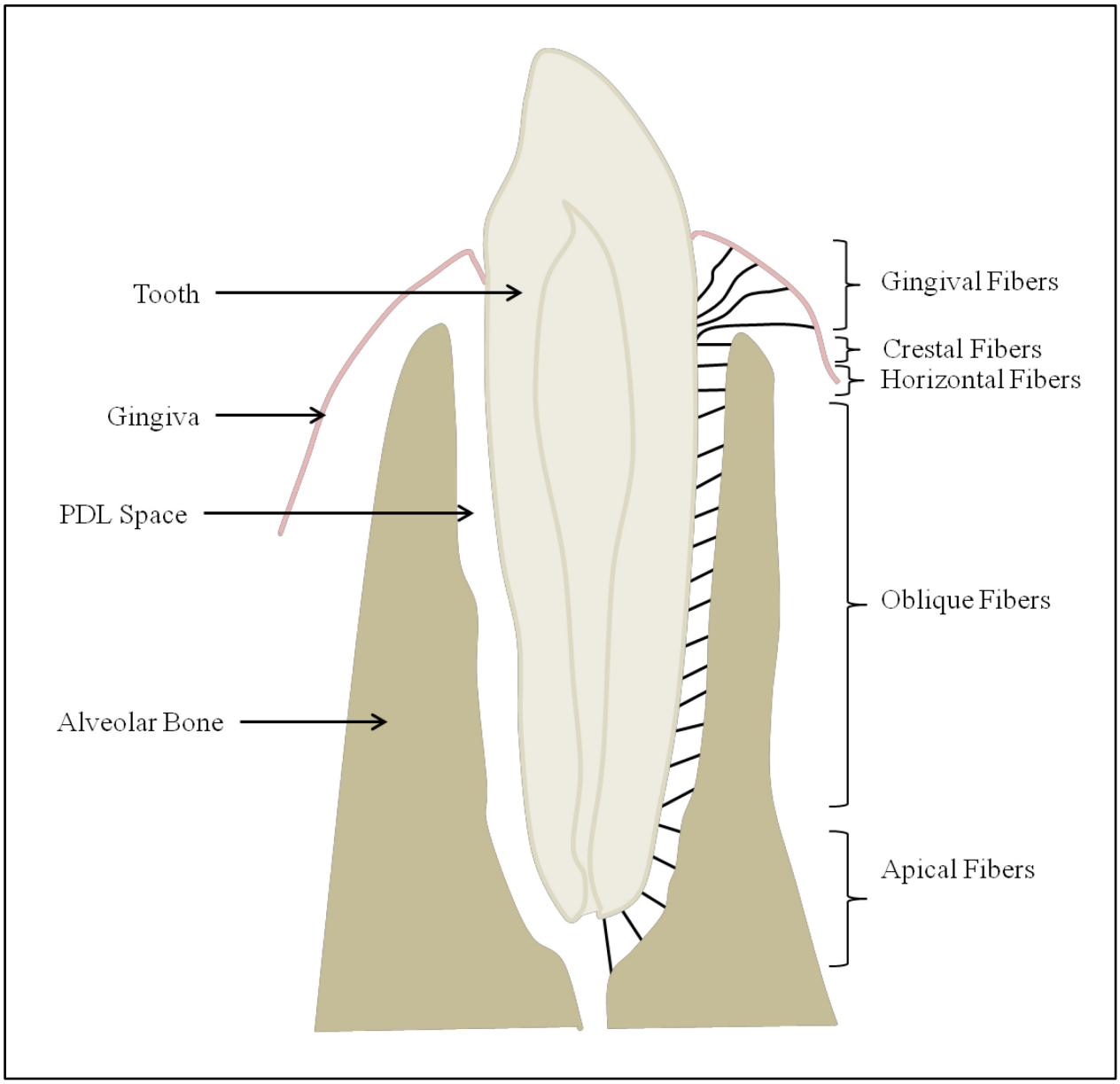

Figure 1-1. Diagram showing dental structures and arrangement of collagen fiber bundles within the PDL.

Chapter 2: Dental root size in bats with diets of different hardness

Self, C.J., 2015 Journal of Morphology

Abstract

The relationship between tooth roots and diet is relatively unexplored, although a logical relationship between harder diets and increased root surface area is suggested. This study addresses the interaction between tooth morphology, diet and bite force in small mammals, phyllostomid bats. Using micro computed tomography (microCT), tooth root morphology of two fruit-eating species (*Carollia perspicillata* and *Chiroderma villosum*) and two insect-eating species (*Mimon bennettii* and *Macrotus californicus*) was compared. These species did not differ in skull or estimated body size. Food hardness, rather than dietary classification, proved to be the strongest grouping factor, with the two insectivores and the seed-processing frugivore (*C. villosum*) having a larger root surface areas ($p < 0.001$). Bite force was estimated using skull measurements; bite force significantly correlated with tooth root surface area ($r = 0.76$, $p = 0.001$) but not with body size. Although the three durophagous species did exhibit larger crowns, the area of the occlusal surface did not vary among the four species. There was a linear relationship between root size and crown size, indicating that the roots were not expanded disproportionately; instead the entire tooth was larger in the hard diet species. MicroCT allows the non-destructive quantification of previously difficult-to-access tooth morphology; this method shows the potential for tooth roots to provide valuable dietary, behavioral and ecological information in small mammals.

Introduction

The teeth and jaws of an organism provide critical information regarding the potential dietary niches it may occupy. Many species take advantage of seasonal availability of food, changing their diets throughout the year (Teaford and Robinson, 1989). On a larger time scale, permanent dietary shifts can be observed in the fossil record (Pilbeam et al., 2008). The ability of an organism to alter its diet is mediated by many biological constraints, not the least of which is food processing ability. Teeth are valuable indicators of diet and past behavior, be it the recent past or millions of years ago.

Like tooth crowns, the forms of tooth roots are likely related to their mechanical role. Tooth crowns have been studied in detail, but tooth root morphology is understudied and may be able to provide additional information regarding habitually encountered diets. Little is known in a comparative context about root size variation outside of humans and carnivores (Kupczik and Stynder, 2012; Stynder and Kupczik, 2012). Even less is known about the mechanical consequences of those root variations on stress resistance in the jaws (Spencer, 2003). In primates tooth root surface area varies along the tooth row (Jespen, 1963; Kupczik and Dean, 2008; Kupczik et al., 2003; Watt et al., 1958) and is correlated with maximum bite force production, indicating that root surface area may be an effective indicator of typical occlusal loads (Kupczik and Hublin, 2010; Spencer, 1998a). A relationship between root surface area and bite force is logical; an increase in surface area would enlarge the space available for attachment of the periodontal ligament (PDL) fibers.

The periodontium is a multifunctional connective tissue. It serves proprioception, signaling, and healing, but its major role is probably mechanical and depends on collagen fibers of the PDL, along with their proteoglycan matrix (Beertsen et al., 2000). The PDL transmits

occlusal forces from the tooth into the surrounding alveolar bone (Hillam, 1973; Kovacs, 1979; Naveh et al., 2013; Nikolai, 1996) via this network, and a proteoglycan matrix. Principal fiber bundles of the PDL run from the cementum layer of the tooth into the alveolar bone (Melcher and Eastoe, 1969). In addition to providing support for the tooth in its socket, the bundles allow precise occlusion via small adjustments in tooth position, but also prohibit large tooth movements, thereby preventing damage to surrounding tissue. For both support and adjustment functions, increasing the number of fiber bundles would be a major way to adapt to higher loads. An increased number of bundles would require a root with larger surface area for their attachment. Hence, root surface area would be expected to enlarge for diets requiring elevated bite force.

Difficult diets may involve foods with varying material properties, including hardness (ability to withstand deformation), yield strength (amount of stress required to produce plastic deformation), and fracture toughness (amount of energy required to propagate a flaw). In this paper the terms “hard diet” and “durophagous” are used broadly to reflect foods with high hardness, high yield strength or increased toughness. The bite force required to process hard foods is likely a determining factor in dietary choices (Aguirre et al., 2003). Non-feeding related behaviors, such as nest building, may also drive an increased bite force (Dechmann et al., 2009; Santana and Dumont, 2011). If harder items require larger forces for breakdown, then species consuming them should have larger root surface areas, which could theoretically function to reduce stress concentrations in the tooth and alveolar bone. If such an association exists, then tooth root surface area should allow for inferences of masticatory function. If a harder diet results in a larger root surface area, there may also be differences in the relative proportions of crown and root surface area for a given diet. It is unclear how the ratio of crown and root area varies

among species (Kupczik et al., 2009). Large crown areas, like large root areas, dissipate stress, but this may not be an advantage for fracturing a hard food item when a smaller tip of the tooth load would increase local stress and reach the yield stress at a lower load. A larger root surface area can be achieved by growing an overall larger tooth, or by preferentially increasing the size of the root. The latter method may be more favorable for harder diets, when an increase in crown size may not add to efficiency in food processing.

Traditional dietary classifications such as herbivore or carnivore overlook the material properties of foodstuffs, which may vary greatly within classifications. Ripe fruit is usually considered soft food while insects or seeds are usually referred to as hard food (August, 1981; Lucas et al., 2008). Nevertheless, there is a range of values even within these categories. Aguirre et al. (2003) used a small force transducer to measure the force required for different foods to fracture. The insects tested failed at between 3 – 34 N (coleopterans were generally on the higher end, Lepidoptera were lower) and fruits such as figs, solanum and piper failed at approximately 1 – 4 N.

Phyllostomid bats offer an excellent study group for comparison of root surface area with diet, as the family presents a large variety of dietary specialties. This study compares the post-canine tooth root morphology of durophagous species (*Chiroderma villosum, Mimon bennettii* and *Macrotus californicus*) to a soft food species (*Carollia perspicillata*). These species were primarily chosen for their similarity in body size and well documented dietary habits; additionally, there are existing bite force data for two of the studied species (*C. perspicillata* and *C. villosum*) (Freeman and Lemen, 2010). Bite force should be greater in *C. villosum* and the two insectivores (*M. bennettii* and *M. californicus*) than in *C. perspicillata*. Studies in primates

further show that tooth root surface area is greater in groups that process resistant seeds than in those that do not (Spencer, 2003).

Therefore, it was expected that among four bat species of similar body size, insectivores (*Mimon bennettii* and *Macrotus californicus*) and the seed processing species (*Chiroderma villosum*) would have a larger root surface than the frugivore (*Carollia perspicillata*). Furthermore, hard-food processors should show disproportionate increases in root surface area relative to crown area when compared with the soft diet frugivore. The relationship between diet, bite force and tooth morphology may be able to provide insight into the evolutionary past of an animal, as well as the potential for future behavioral change.

Material and Methods

Study group and diet classification. Phyllostomid bats are a large and diverse group in which species have become specialized for a wide variety of diets. This study compares the post-canine (i.e. premolar and molar) tooth root morphology of two fruit-eating species (*Carollia perspicillata* and *Chiroderma villosum*) and two insect-eating species (*Mimon bennettii* and *Macrotus californicus*). These species were chosen for their similarity in body size and well documented dietary habits. Current phylogenies place each of these species in a separate subfamily, with the two fruit eaters (*C. perspicillata* and *C. villosum*) most closely related and *M. bennettii* and *M. californicus* as progressively more distant (Agnarsson et al., 2011; Dávalos et al., 2012). The diets were obtained from the existing literature. The food hardness category was based primarily on the presumed relative hardness of the main food item. In the field, *C. perspicillata* feeds primarily on fruits from the family Piperaceae (Fleming, 1991). Changes in seasonal availability of *Piper* fruit can result in consumption of other soft fruits, including

Cecropia (which has fruit similar in style to *Piper*), and *Solanum* (which produces a tomato-like fruit), as well as some insects (Mello et al., 2004). In captivity *C. perspicillata* has also been observed eating insects (Ayala and D'Alessandro, 1973), however, only the soft parts were consumed, the remainder of the insect being thrown away. As such for this study, it was classified as having a diet category of "fruit" and a hardness category of "soft". The natural diet of *C. villosum* also largely consists of fruit, primarily figs (Gardner, 1977). However, *C. villosum* habitually processes seeds found in its preferred fruit; they were found to consume the nutrient rich center of the seed while discarding the coat as compact oral pellets (Nogueira and Perracchi, 2003). This seed crushing behavior would likely subject their teeth to more stress than soft fruit mastication. In order to account for the seed eating habits of *C. villosum* its diet was classified as "fruit" and its hardness category as "hard". *M. bennettii* eats a diet of arthropods (Carvalho et al., 2008) which it gleans from branches. *M. bennettii* fecal analyses have shown a high proportion of Coleoptera in the diet (Fenton et al., 1999). *M. californicus* feeds mainly on arthropods, specifically butterflies, cockroaches and moths (Bell et al., 1986) and in captivity is known to eat grasshoppers (Bradshaw, 1961). Arthropods are covered in chitin and there is variation in how difficult an insect can be to process based on chitin thickness and tooth crown morphology (Evans and Sanson, 2005a; Evans and Sanson, 2006; Freeman, 1979). Although there are not hardness values for the specific insects consumed by these bats, I am assuming here that the coleopterans consumed by *C. villosum* are similar in hardness to the cockroaches consumed by *M. californicus*. Since neither of these species has been observed discarding the hard parts of their prey, their diet was classified as insects, hard (Table 2-1).

Dried skulls (6-8 individuals per species, Table 2-1) were obtained from the mammal collections at the Burke Museum of Natural History and Culture (Seattle, WA) and the Berkeley

Museum of Vertebrate Zoology (Berkeley, CA). Only individuals with complete dentition, intact teeth, and minimal wear were chosen. Additionally all cranial bones were required to be present and intact. All specimens were fully adult. The post canine tooth row was chosen for study in order to evaluate the effect of occlusal forces during the process of chewing food. While post-canine teeth may sometimes be used in food acquisition (Dumont et al., 2003), they are always used in intra-oral processing of the bolus (Santana et al., 2011a).

Because the museum tags lacked body mass measurements for some individuals, the skulls were used to estimate body size (Radinsky, 1967), skull size, and bite force. Dental parameters were measured on the left side of each mandible. Although it was intended to include equal numbers of males and females, only one male specimen of *C. villosum* fit the selection criteria of complete dentition, intact teeth and minimal wear. Calculations were initially performed separately for males and females (Table 2-2). No consistent differences were seen in any parameter, so sexes were combined for further consideration (Table 2-3).

CT and 3D image processing. Mandibles were scanned using a Skyscan1076 microcomputed tomography scanner (Skyscan Inc., Belgium). An optimization study with two of the 26 individuals identified the most effective contrast settings: 9µm resolution scanned with a tube voltage of 50kv, an exposure of 180mAs and a 200ms exposure time. The post-canine tooth roots were manually isolated from their surrounding alveolar bone using CTAn 2.1 (Skyscan Inc., Belgium) and the resulting isolated tooth slices were rendered using a smooth-surface model with a double-time cubes algorithm. The resulting stereolithography (STL) models were used to measure tooth and crown surface area in RapidForm XOR (Rapidform Inc. Sunnyvale, CA). The root surface area for each post-canine tooth was quantified by manually selecting the

root surface area located below the cementoenamel junction, which was readily identifiable in the STL models. Occlusal surface (OSA) was quantified similarly by selecting the entire enamel covered surface visible when viewing teeth in the occlusal direction. Crown surface area (CSA) was quantified as the entire enamel covered surface.

Root surface area variables computed include RSA_{total}, the combined surface area of all post-canine roots; RSA_{M1}, the root surface area of M_1; and RSA_{max}, the surface area of the largest post-canine root. These three measures provide three perspectives on root surface area: area of the entire post-canine tooth row, a common tooth, and finally the largest tooth. Also, not all bat species had the same number of teeth (Table 2-2). RSA_{avg} is the total root surface area divided by the number of post-canine teeth present in each species. Occlusal surface area variables were computed analogously. OSA variables were divided by comparable RSA variables to produce a ratio of occlusal area to root area (OCR). Total crown surface area was divided by RSA_{total} to produce the ratio of crown to root surface area (CRR).

Estimated bite force, skull size, and body size. Phyllostomid bats are frequently studied in the field, and published bite force data do exist for two of the species studied here, *C. villosum* and *C. perspicillata* (Freeman and Lemen, 2010), but could not be found for *M. bennettii* and *M. californicus*. Using a transducer- measured bite force for two species and an estimated bite force for the other two would have produced a biased result. Therefore, to allow comparisons among all four species, bite force was estimated using skull measurements. Because such estimates always rely on many assumptions, two quite different published methods were used, each using different measures. The first method, based on muscle attachment areas, produced a theoretical bite force at the M_1 using a modified equation from Thomason (1991b), following Christiansen

and Wroe (2007). Muscle areas and moment arms were measured from digital photographs of each skull and incorporated into an equation for bite force area M_1 using 370 kPa as value for muscle contractile force (Christiansen and Wroe, 2007). The second method was that developed by Freeman and Lemen (2010) for estimating bite force based on expected strength of the jaw bone, but using the M_1 rather than the canine. Since this model was designed for bats, it was considered an appropriate alternative approach to the more general Thomason method. By calculating the section modulus of the mandible as a simplified beam and incorporating the load arm, a relative index of strength is produced where $beamCalc = (htDent^2 * widDent/6)/loadArm$. The variables *htDent* and *widDent* are the height and the width of the beam, respectively (mm) and the *loadArm* is the length from just posterior to the last molar to the end of the load, in this case the M_1. Bite force from this beam model can then be estimated from *beamCalc* using the provided regression equations. Although the two methods produced different absolute bite force, the rank order of species was the same for both, as was the statistical significance of the findings. Therefore, only the beam model results (BF_{beam}) are reported here.

To adjust for individual size differences, estimates of skull size and body size were calculated. Skull size was approximated by calculating the geometric mean of five skull size variables: foramen magnum height and width, bizygomatic breadth, basicranial length and skull length. Foramen magnum area (FMA) was used as a proxy for body size (Radinsky, 1967); area was estimated by multiplying the height and width of the opening. These variables were all measured on the skulls with digital calipers.

Statistical analysis. The primary hypotheses are that bite force, root surface area and occlusal surface area will all be relatively larger in hard-diet species. Non-parametric tests were

used to determine significance. Mann-Whitney tests were used compare bite force, RSA_{total}, RSA_{M1} and RSA_{max}; occlusal surface area (OSA_{M1}); and occlusal to root area ratio (OCR); between food hardness groups.

To identify species specific relationships, species root and occlusal values were compared using a Kruskal-Wallis test with post-hoc Bonferroni correction for multiple testing. Post-hoc Mann-Whitney tests were also used in investigating differences in tooth root area between any two species. Additional tests were carried out to assay whether generalized diet categories (frugivore and insectivore), or phylogenetic relationships (sister group relationship between *C. perspicillata* and *C. villosum*) were associated with root surface areas. Testing for statistical significance in these groupings allows a cursory investigation of these issues, but a sample size of four species, necessitated by the labor-intensive methods, prohibits definitive ecological or phylogenetic interpretations.

To understand the relationship of dental variables to each other and to body size, bivariate associations were evaluated with a product-moment correlation. Because both the independent and dependent variables are subject to error, bivariate trends were modeled using a reduced major axis (RMA) regression. All values were $\log_{10}$ transformed for analyses. Analyses were carried out using PASW 18 (Polar Engineering and Consulting).

Results

Root Morphology. The species did not differ in either skull size (GM) or body size (FMA)(Table 2-3). Figure 2-1 is a surface rendering of the exposed tooth row for the phyllostomid species used in this study. Details for each tooth and crown are presented in Table 2-2. Species averages for root and crown areas, plus size variables and bite force estimates can

be found in Table 2-3. The largest values for RSA_{max} and $RSA_{average}$ were found in *C. villosum*; however RSA_{M1} and RSA_{total} were both larger in *M. bennettii*. The smallest root areas were in *C. perspicillata*. The largest root in the tooth row (RSA_{max}) was found at P_3 in *C. perspicillata* but was the M_2 for all other species (Fig. 2-1). The largest occlusal surface area did not correspond with the largest root area. While peak occlusal surface area was found for the M_2 in *M. bennettii* and *C. villosum*, it was actually the M_1 in *C. perspicillata* and *M. californicus*.

The smallest root area was variable among species and in some cases variable within a species. The smallest root was consistently at the M_3 for *C. perspicillata* although most of its roots were very similar in size (Fig. 2-1, Table 2-2). *C. villosum* has a drastically reduced P_3, but the next smallest roots, those of the P_4 and M_1,were very similar in size. *M. californicus* individuals varied between the P_2 and the P_4 as the smallest tooth root; on inspection the P_3 is a smaller tooth, but it is double rooted, accounting for its larger root surface area. *M. bennettii*'s smallest root was at P_3. *M. bennettii* was the only species that demonstrated sexual dimorphism in tooth size, skull size, and body size, with females being larger (Table 2-2). However estimated bite force, root surface area, and occlusal surface area were not significantly different between the sexes.

The summary values in Table 2-3 reveal interesting contrasts among the species despite their similarity in skull size proxy (Average GM 6.1-6.8 mm) and body size proxy (FMA, 16.4-18.4mm^2). Average root surface area (RSA_{avg}) per tooth was small in *C. perspicillata* and *M. californicus* (4.6-5.3 mm^2) and much larger in *M. bennettii* and *C. villosum* (17.2 – 18.4mm^2). When all roots were summed, *C. perspicillata* remained very low (23.0 mm^2) whereas *M. californicus* (31.8mm^2) was closer to *C. villosum* (37.0mm^2) and *M. bennettii* was clearly the

largest (42.3 mm^2). Average and total occlusal area showed essentially the same patterns as did root area.

Bite Force Estimates. Bite force estimates can be found in Table 2-1. *C. villosum* had the largest bite force followed by *M. bennettii* then *C. perspicillata*; *M. californicus* consistently ranked lowest in bite force (Table 2-3). The method of estimating bite force is likely to be very sensitive to size variation (Herrel et al., 2008; Santana et al., 2010). Table 2-4 reports the product-moment correlation values for the major variables. Bite force estimates were positively correlated with skull size, which is not surprising since both methods rely solely on skull measurements. There was not a significant correlation between BF_{beam} and the body size proxy despite the strong relation between skull size and body size. Occlusal surface area was, however, significantly correlated with the bite force estimate, as were most root surface variables. The highest correlation coefficient for bite force and root surface area (0.54) was between RSA_{max} and bite force (Table 2-4).

Root and occlusal surfaces. Root or occlusal surface area values were at best marginally correlated with skull size ($p = 0.04 – 0.10$; Table 2-4). Significance was slightly stronger for correlations with body size ($p = 0.015 – 0.10$), but still does not satisfy the more stringent Bonferroni correction for multiple comparisons ($p < 0.01$). The highest correlation coefficient was only 0.44 (RSA_{total} and FMA, Table 2-4). There were, however, a few significant correlations between RSAmax and some of the individual skull measurements that were used to generate the body size estimate. Specifically, skull length, bizygomatic breadth and mandible length were all correlated with tooth root surface area (r = 0.72, 0.49 and 0.75 respectively).

In two species (*C. perspicillata* and *M. bennettii*), there was a clear relationship between root surface area and occlusal surface area at each tooth; increased root size was correlated with a larger occlusal surface (Table 2-5). In the other two species, there was no correlation between root surface area and occlusal surface area (*C. villosum* and *M. californicus*). But when all species were pooled, the relationship between root surface and occlusal surface was very strong ($r = 0.93$, $p < 0.01$).

Overall, the occlusal surface was smaller than the root surface. The species average of OCR_{M1} was between 0.6 and 0.7 with no significant difference among species ($p = 0.210$). When the OCR was calculated for the other post-canine teeth and compared among species a significant difference was only found at the P_3 ($p < 0.01$); this was solely due to the extremely reduced crown of P_3 in *C. villosum*. All species except *M. bennettii* showed significant differences in OCR along the tooth row. The largest OCR occurred at M_1 except in *M. californicus* (P_3); the smallest at M_3 in *C. perspicillata* and *M. bennettii*, P_4 in *C. villosum* and *M. californicus* (Fig. 2-1).

Relationships among species and food types. Root surface area values were compared between each of closely related species pairs. The related frugivores *C. perspicillata* and *C. villosum* were significantly different from each other ($p < 0.001$). The two insectivores *M. bennettii* and *M. californicus* were similar to each other in root surface area ($p = 0.12$). A comparison of frugivores to insectivores showed no difference ($p = 0.312$). The same result was found for the other root surface area variables, occlusal surface area variables, and OCR.

Hypothesis testing: diet hardness, bite force, and root surfaces. If diet hardness dictates bite force and bite force dictates relative root size in these species, then *C. villosum*, *M. bennettii* and *M. californicus* should all show larger values with respect to *C. perspicillata*. Skull size between hardness categories was not significant ($p = 0.824$), nor was body size ($p = 0.657$). There was also not a significant difference in bite force ($p = 0.354$) due to the very small estimated value for *M. californicus*. The other two durophagous species (*C. villosum*, *M. bennettii*) did have larger estimated bite forces than the soft diet frugivore (*C. perspicillata*) ($p = <0.01$). There was a significant difference in root surface area between soft and hard diets, with the three harder diet species having a larger root surface area than *C. perspicillata* (For all RSA values: $p < 0.002$). Occlusal surface area was also larger in the hard diet group (for OSA_{M1}, $p < 0.001$). The occlusal and root surface of hard food eaters appear to increase at the same rate since OCR was not different between the two groups ($p = 0.66$). However, the entire crown was larger in hard food eaters than in the soft food frugivore because CRR was elevated ($p = 0.02$), indicating that the overall size of the crown increased more than the root in the durophagous species.

Discussion

Bite force estimates and hardness categories. If tooth root surface area was dominated by phylogeny, the RSA values for *C. perspicillata* and *C. villosum* would resemble each other most closely, which was not the case. The results of this study indicate that postcanine root size follows the expectations of diet hardness with higher estimated bite forces in two of the three hard-diet species and relatively larger roots in all of the hard-diet species than in the single soft-

diet species. In contrast, both phylogeny and the frugivory/insectivory comparison would predict *C. villosum* to be more like *C. perspicillata* than like *M. bennettii* and *M. californicus*.

It is generally thought that bite force increases with food hardness, and that root surface area increases with bite force (Spencer, 2003). There are few studies that directly compare bite force measurements and diet. Bite force is highly correlated with body size in phyllostomid bats, but after accounting for body size, specializations such as nectivory and sanguivory are still associated with reduced bite forces (Aguirre et al., 2002), and dietary specializations are also apparent in rodents after accounting for body size (Freeman and Lemen, 2008a). In this study bite force estimates did not correlate with food hardness categories because of the very small estimated bite force of *M. californicus* (Table 2-1). Freeman (1995) found *M. californicus* had a narrower palate than expected when compared to other insectivorous and animalivorous bats and a thinner than expected dentary width. The latter measurement was the primary driver of the small bite force estimate here. Unfortunately, actual bite force has not been measured in *M. californicus*. It is conceivable that this species, which captures and eats prey on the wing, has sacrificed bite force for other gains (i.e. speed of jaw closure). It is also conceivable that lepidopterans, rather than harder-bodied insects, dominate the diet of this species, and that despite its grouping with the other hard diet species in dental measurements, its diet is soft. More likely though, bite force was underestimated in *M. californicus*, because both occlusal and root values suggest that occlusal forces are high. The slender jaws would then suggest that safety factor, rather than bite force, had been sacrificed. Of the species studied here, bite force has been measured for only the two frugivores (Freeman and Lemen, 2010), showing that *C. villosum* (hard diet) does indeed have a significantly higher bite force (10.1 N) relative to the soft frugivore used in this study, *C. perspicillata* (5.6N). This extreme disparity in bite force,

probably related to *C. villosum*'s seed processing, corresponds very well to the high root surface area values observed.

Is root surface area a predictor of estimated bite force? A relationship between bite force and root surface area has been shown in some carnivores (Kupczik and Stynder, 2012; Stynder and Kupczik, 2012) and in some primates (Spencer, 1998a). In the present case, the relationship between estimated bite force and root area is significant, but not strong. The highest correlation (BF_{beam} and RSA_{max}) was 0.54 ($p = 0.004$; Table 2-4, Fig. 2-2), but this only accounts for approximately 30% of the variation in bite force, indicating a minimal predictive value. Nevertheless, considering that a relationship has now been found in three quite different groups of mammals, and the crude estimated bite force used in this study, I expect further studies in this vein will support the usefulness of tooth roots as an additional way to estimate bite force for fossil species with little discovered material, even single isolated teeth.

Root and occlusal surface ratio: larger teeth, not just larger roots. In contrast to the hypothesis that durophagous species would have relatively small occlusal surfaces, the major way these bats have enlarged root area is to enlarge the whole tooth. OCR ratios did not vary significantly among species even though the hard food consumers did have larger roots, indicating that generally as the root increases, so does the occlusal surface. The crown as a whole actually increased disproportionately. The larger CRR in hard-food bats is evident when looking at the tooth morphology (Fig. 2-1). All three hard-diet species exhibit sharper, more wedge-like crowns than the soft-fruit eater, *C. perspicillata*. However, even though crown height increased, the area exposed to occlusion did not vary among species. An increase in crown size would

certainly require a larger root to maintain stability within the jaw. The exact nature of the relationship between crown and root size has not been studied in a systematic manner outside of primates and ursids (Keene, 1991; Kupczik et al., 2009; Le Cabec et al., 2013). Although some work looking at complexity in bat occlusal surfaces has been done (Dumont and O'neal, 2004; Freeman, 1979; Santana et al., 2011b), it is clear that further work is required to separate out the complex relationship between optimal crown shape for food processing (Evans and Sanson, 2005b) and the reciprocal root shape best suited to handle the resulting occlusal load.

Root surface area correlates with diet hardness. There is a clear relationship between food hardness and root surface area, and while this study is not large enough to tease apart the relationship between crown and root morphology, it does lead to further interesting questions. Much plasticity in bat feeding behavior has been noted in regards to both niche partitioning and seasonal variation. Limitations to this kind of behavior could be identified with a detailed understanding of the mechanical potential of the food processing tools. There are few observational diet studies to provide insight into how these animals are processing their food (Santana et al., 2010; Santana et al., 2012), and bite force data remain lacking for most species. Also, while seed processing may be responsible for the large root surface area in *C. villosum*, some animals may exhibit non-feeding oral behavior that would result in a similar increase in root surface area. For example in bats, roost excavating may result in a robust feeding apparatus that is not actually the result of feeding behavior (Santana and Dumont, 2011).

Limitations. It is clear that microCT techniques offer accurate measurement of complex surface areas, even though the procedures are still time-consuming and labor-intensive. For this

reason, the technique has not often been applied to adequate sample sizes. The sample size of 6-8 per species employed here was adequate to characterize individual variation as well as to show statistical differences among species. The small size of bats was both an asset, in allowing the entire cheek tooth row to be measured, and a detriment, in that the periodontal space was too narrow for automatic recognition and had to be defined manually in each slice.

Because my focus in this contribution was on food processing rather than acquisition, the incisors and canine, highly variable in size among bats, were omitted. Aside from the role that anterior teeth play in feeding, their mere presence may affect the morphology of post-canine teeth. In New World monkeys, selection pressures on large incisors and canines may reduce selection pressure on post-canine roots resulting in reducing of variation (Spencer, 2003). Of the species studied here *C. villosum* has the most outsized canines, however the exact role canine size plays in post-canine root size is not well defined. Thus, I have assumed that the bats studied here habitually rely on post-canine food processing, and the signal from that behavior would be strongly present in premolars and molars.

Conclusions. Root surface area is a potential representative for bite force, but despite early interest in the topic (Kloehn, 1938), there is still very little work on the subject. Undoubtedly, this neglect stems from the difficulty of exposing the roots without damaging specimens, as well as from the difficulty of measuring surface area. Both of these difficulties have been removed by technology; micro CT scanning and computational power now make these measurements possible, and the present study shows their potential for comparative studies of dental function. This study indicates that tooth roots have the ability to provide data about the mechanical properties of the food exploited by these species, and that there is potential to

identify behaviors, such as seed processing, that can discriminate among species that would normally be placed in the same broader diet category. Furthermore, roots are typically present in fossil teeth and may be useful in interpreting dietary history from paleotaxa. Because tooth roots are part of the link between occlusal force and craniofacial bone, their potential for registering historical loading conditions is likely significant and deserves further study.

The final publication is available at Wiley via
http://onlinelibrary.wiley.com/doi/10.1002/jmor.20400/full

Table 2-1. Species studied according to diet and hardness classifications (S = Soft, H=Hard) and number of males and females studied. Estimated bite forces at the first molar using the beam properties of the bat mandible (BF_{beam}) (Freeman and Lemen, 2010).

	Diet	Material	Males	Females	Bf_{beam} (N)
Carollia perspicillata[1]	Fruit	S	4	4	21.24 ±6.70
Chiroderma villosum[2]	Fruit	H	1	5	53.26 ±16.51
Macrotus californicus[3]	Insects	H	3	3	10.18 ±1.79
Mimon bennettii[4]	Insects	H	3	3	29.82 ±6.90

[1]UWBM62083, UWBM62084, UWBM62086, UWBM62087, UWBM62089, UWBM62094, UWBM62096, UWBM62099; [2]UWBM62120, UWBM62121, UWBM63059, MVZ136523, MVZ136524, MVZ168873; [3]UWBM 51409, UWBM51410, UWBM51478, UWBM51479, UWBM51713, UWBM51720; [4]UWBM 62376, UWBM62377, UWBM62378, MVZ136405, MVZ154778, MVZ157659

Table 2-2. Size estimates for skull and body areas and surface areas root and the occlusal face of the crown (mm^2), mean and standard deviations (SD)

	Carollia perspicillata		*Chiroderma villosum*		*Macrotus californicus*		*Mimon bennettii*	
	Male (4)	Female (4)	Male (1)	Female (5)	Male (3)	Female (3)	Male (3)	Female (3)
Size	Mean ± SD	Mean ± SD	Mean ± SD	Mean ± SD	Mean ± SD	Mean ± SD	Mean ± SD	Mean ± SD
GM[1]	6.57 ± 0.27	6.30 ± 0.23	6.17 ± ---	6.92 ± 0.27	6.13 ± 0.40	6.10 ± 0.46	5.83 ± 0.09	7.25 ± 0.08
FMA[2]	16.81 ± 3.12	16.04 ± 1.93	16.88 ± ---	17.28 ± 1.12	19.19 ± 0.96	15.95 ± 1.03	14.51 ± 1.31	22.38 ± 0.87
Root Area								
RSA_{avg}[3]	5.18 ± 0.85	4.02 ± 0.68	9.6 ± ---	9.18 ± 0.88	5.26 ± 0.75	5.34 ± 0.13	7.38 ± 0.72	9.53 ± 1.20
RSA_{total}[4]	25.91 ± 4.26	20.11 ± 3.39	38.39 ± ---	36.72 ± 3.51	31.59 ± 4.48	32.05 ± 0.78	36.88 ± 3.61	47.64 ± 6.00
P_2					3.23 ± 0.64	3.19 ± 0.41		
P_3	6.03 ± 1.14	5.23 ± 1.13	1.63 ± ---	1.98 ± 0.33	3.68 ± 0.48	4.06 ± 0.06	3.95 ± 0.25	6.37 ± 0.74
P_4	5.29 ± 0.75	4.09 ± 0.87	9.70 ± ---	9.13 ± 0.54	3.51 ± 0.31	3.83 ± 0.08	6.39 ± 0.65	8.36 ± 0.81
M_1	5.26 ± 0.75	3.97 ± 0.75	9.64 ± ---	9.42 ± 0.96	6.26 ± 0.80	6.68 ± 0.15	8.91 ± 1.07	11.00 ± 1.53
M_2	5.21 ± 0.75	3.79 ± 0.47	17.42 ± ---	16.19 ± 2.97	7.91 ± 0.86	7.85 ± 0.49	10.37 ± 0.94	13.15 ± 2.46
M_3	4.13 ± 0.91	3.04 ± 0.42			6.99 ± 1.85	6.43 ± 0.70	7.27 ± 1.31	8.76 ± 1.43
Occlusal Area								
OSA_{avg}[5]	2.54 ± 0.41	2.34 ± 0.52	4.65 ± ---	5.45 ± 0.49	3.08 ± 0.29	2.98 ± 0.42	4.35 ± 0.43	6.35 ± 0.26
OSA_{total}[6]	12.68 ± 2.03	11.60 ± 2.62	18.60 ± ---	21.78 ± 1.98	18.50 ± 1.73	17.87 ± 2.54	21.74 ± 2.16	31.75 ± 1.30
P_2					2.21 ± 0.14	1.99 ± 0.17		
P_3	2.83 ± 0.38	2.65 ± 0.55	0.76 ± ---	0.86 ± 0.28	1.88 ± 0.08	2.04 ± 0.20	2.55 ± 0.28	4.17 ± 0.14
P_4	2.61 ± 0.36	2.57 ± 0.51	4.85 ± ---	5.53 ± 0.77	1.66 ± 0.16	1.75 ± 0.26	3.26 ± 0.32	5.29 ± 0.43
M_1	2.98 ± 0.50	2.60 ± 0.70	5.01 ± ---	6.29 ± 0.28	3.81 ± 0.49	3.82 ± 0.88	5.89 ± 0.51	8.05 ± 0.11
M_2	2.61 ± 0.46	2.30 ± 0.57	7.99 ± ---	9.10 ± 0.82	5.37 ± 1.03	4.98 ± 0.86	6.55 ± 0.64	8.85 ± 0.39
M_3	1.65 ± 0.43	1.58 ± 0.33			3.58 ± 0.15	3.28 ± 0.62	3.49 ± 0.68	5.39 ± 0.36

[1] Geometric mean of five facial dimensions (mm), [2] Foramen magnum area (mm^2), [3] Average root surface area of all teeth, [4] Total combined surface root area of all teeth, [5] Average occlusal surface area of all teeth, [6] Total combined occlusal surface area of all teeth

Table 2-3. Species means ± standard deviation (sexes combined) and results of non-parametric species comparisons.

	Carollia perspicillata	*Chiroderma villosum*	*Macrotus californicus*	*Mimon bennettii*	Kruskal-Wallis Significance
GM[1]	6.44 ±0.27	6.80 ±0.39	6.12 ±0.39	6.54 ±0.78	n.s
FMA[2]	16.43 ±2.44	17.21 ±1.02	16.57 ±1.12	18.44 ±4.43	n.s
RSA_{avg}[3]	4.60 ±0.94	9.25 ±0.80	5.30 ±0.48	8.45 ±1.47	P < 0.01
RSA_{total}[4]	23.01 ±4.72	37.00 ±3.21	31.82 ±2.89	42.26 ±7.37	P < 0.01
OSA_{avg}[5]	2.44 ±0.45	5.31 ±0.55	3.03 ±0.33	5.35 ±1.14	P < 0.01
OSA_{total}[6]	12.18 ±2.23	21.25 ±2.20	18.18 ±1.97	26.74 ±5.71	P < 0.01
OCR[7]	0.54 ±0.10	0.58 ±0.09	0.57 ±0.08	0.63 ±0.7	n.s.
CRR[8]	1.42 ±0.42	1.92 ±0.50	2.14 ±0.26	1.95 ±0.51	P < 0.01

1 Geometric mean of five skull dimensions (mm), 2 Foramen magnum area (mm^2), 3 Average root surface area of all teeth (mm^2), 4 Total combined surface root area of all teeth (mm^2), 5 Average occlusal surface area of all teeth (mm^2), 6 Total combined occlusal surface area of all teeth (mm^2), 7 Ratio of occlusal surface area to root surface area, 8 Ratio of crown surface area to root surface area

Table 2-4. Product-moment correlation coefficients (r) of skull size and body size against bite force estimates (BF_{beam}) root areas (RSA) and occlusal area (OSA_{M1}), and occlusal to root surface ratio (OCR). Correlations are for all individuals.

Skull Size (GeoSq)			Body Size (FMA)			BF_{beam}		
Variable	*r*	*P*	Variable	*r*	*P*	Variable	*r*	*P*
RSA_{M1}	0.35	0.085	RSA_{M1}	0.42	0.035	RSA_{M1}	0.44	0.025
RSA_{max}	0.39	0.050	RSA_{max}	0.33	0.099	RSA_{max}	0.54	0.004
RSA_{total}	0.33	0.097	RSA_{total}	0.44	0.015	RSA_{total}	0.29	0.152
RSA_{avg}	0.40	0.041	RSA_{avg}	0.39	0.049	RSA_{avg}	0.46	0.018
OSA_{M1}	0.35	0.085	OSA_{M1}	0.39	0.052	OSA_{M1}	0.54	0.005
OCR	0.18	0.382	OCR	0.12	0.565	OCR	0.42	0.033
BF_{M1}	0.51	0.008	BF_{M1}	0.36	0.073			
BF_{beam}	0.46	0.018	BF_{beam}	0.15	0.481			
FMA	0.64	<0.001						

Table 2-5. Correlations among tooth variables in each species, correlations are for all individuals.

	RSA_{M1} - OSA_{M1}		RSA_{avg} - OSA_{avg}	
	r	*P*	*r*	*P*
Carollia perspicillata	0.750	0.031	0.693	0.057
Chiroderma villosum	0.099	0.858	0.223	0.671
Macrotus californicus	0.166	0.750	0.139	0.793
Mimon bennettii	0.763	0.078	0.870	0.024
All Species	0.93	<0.01	0.92	<0.01

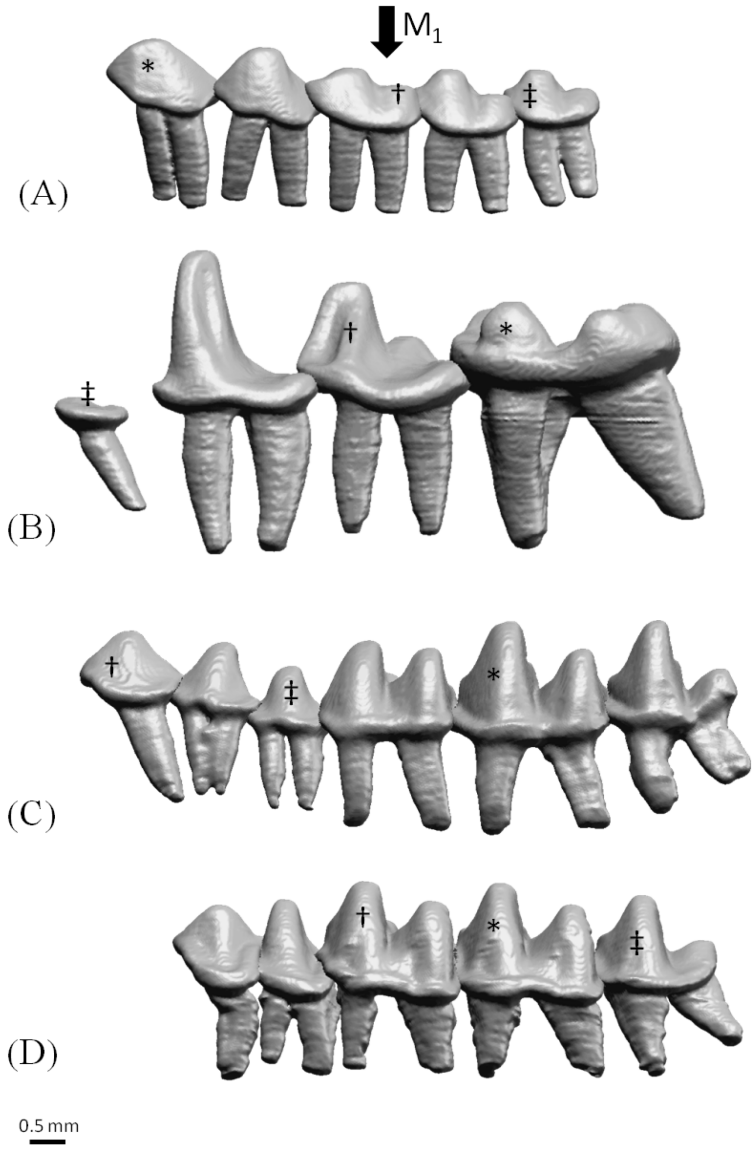

Figure 2-1. Isolated bats tooth rows, all to scale. (A) *Carollia perspicillata*, (B) *Chiroderma villosum*, (C) *Macrotus californicus*, (D) *Mimon bennettii*. * Tooth with the largest root surface, † tooth with the largest occlusal surface to root ratio, ‡ tooth with the smallest occlusal surface to root ratio.

Figure 2-2. Bivariate plot of mandibular largest tooth root surface area and estimated bite force using the beam method (Freeman and Lemen, 2010).

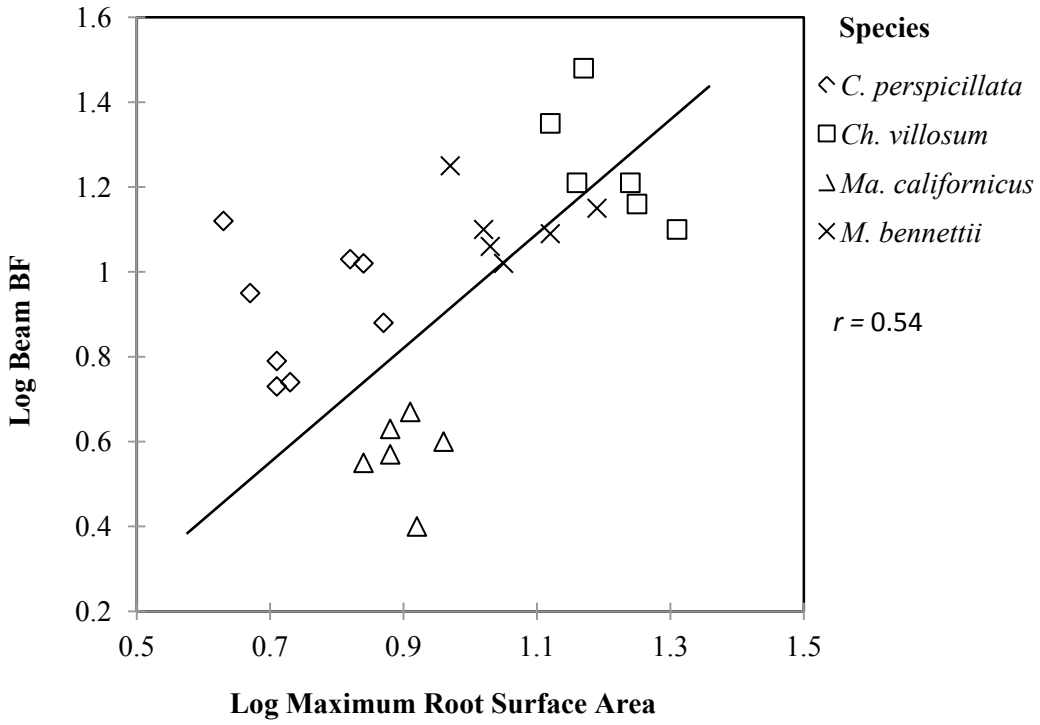

Chapter 3: Cricetid rodents: Is molar root morphology an indicator of diet?

Self, C.J., 2015 Zoomorphology: 134(2) 309-316

Abstract

The relationship between tooth roots and diet is largely unexplored, although a logical relationship between harder diets and increased root surface area is suggested. Existing studies of primates, carnivores and phyllostomid bats have indicated a relationship between diet hardness, bite force and tooth root surface area. The goal of this study was to determine if root surface area can act as a potential surrogate for bite force and diet in cricetid rodents. Using micro computed tomography (microCT) tooth root morphology from six species of rodents, two grass-eaters (*Calomys callosus* and *Reithrodon auritus*), two seed eaters (*Phyllotis darwini,* and *Ochrotomys nuttalli*) and two insect eaters (*Akodon azarae*, *Oxymycterus hispidus*), were compared. Similar to other studies, these rodents did exhibit differences in tooth root surface area based on diet classification, but food hardness did not seem to be a factor. Grass-eating species showed significantly larger roots relative to the other diet groups ($p = 0.001$). Bite force was estimated using skull measurements. Seed eaters were found to have a larger bite force, followed by grass and insect eaters, though the trend did not reach statistical significance ($p = 0.058$). No strong relationship was found between estimated bite force and tooth root surface area. In this study, the mechanics of grass-eating seem to have a stronger effect on tooth root surface area than bite force. MicroCT allows the non-destructive quantification of previously difficult-to-access tooth morphology; this method shows the potential for tooth roots to provide valuable dietary, behavioral and ecological information in rodents.

Introduction

Forces produced as a result of chewing are transmitted to cranial bone via a gomphosis, the periodontal ligament (PDL). This ligament runs the space between the tooth and the alveolar bone and inserts into the bone via Sharpey's Fibers. The attachment area of the PDL is likely a reliable indicator of habitually encountered chewing behavior (Spencer, 1998b). Previous positive relationships have been identified in carnivores (Stynder and Kupczik, 2012; Wroe et al., 2005) and primates (Spencer, 2003). To test whether this relationship also holds for rodents, I looked at root surface area in sigmodontine (Cricetidae) rodents with diverse feeding behavior. A clear relationship between tooth root area and diet would lead to increased reliability of behavioral predictions from the fossil record and shed insight on species whose feeding behavior has not been observed in the field.

Rodents are typically gnawers, a task that is achieved with ever-growing incisors. The incisors are kept short by sharpening (Druzinsky, 1995), but their role in food acquisition varies with species. Perhaps because of developmental constraints, the overall morphology of ever-growing incisors does not clearly reflect dietary differences even though their enamel microstructure is the most complex among mammals (Martin, 1993). To evaluate the relationship between diet hardness and tooth morphology, I turned to the molars.

Post-gnawing, food must still be masticated. It is ground between the rigid molars using a primarily posterior-anterior chewing motion (Kesner, 1980; Samuels, 2009). Rodent molars are often unrooted (ever-growing), but for this study species with closed roots were chosen to avoid confounding signals of continuous growth. Based on previous studies (Kupczik and Dean, 2008; Kupczik and Stynder, 2012), there seem to be two major correlates of tooth root surface area;

overall bite force and material properties of the food. These two correlates are obviously related to each other but are not identical. In particular, bite force and material properties of food may part company in grass eaters.

Although grass eaters are known to undergo high tooth wear (Rensberger, 1975; Williams and Kay, 2001), grass does not require the cracking of hard seed coats of chitin. Because of the lack of hard food cracking behavior, the estimated bite force is expected to be relatively low in grass eating species. Crown height of the molars is generally enlarged to compensate for wear in grass eating species (Williams and Kay, 2001), however whether the actual occlusal surface is relatively larger is not well studied. Grass is a high-fiber, low-nutrient availability food that requires significant mechanical digestion before chemical digestion can begin. To aid in that plant breakdown, grass eaters should show a larger occlusal surface, relative to root surface area, than insect and seed processors. If the occlusal surface of grass eating species is also enlarged, it should be reflected in the ratio of root area to crown area.

To evaluate the role of tooth root surface area as a predictor of diet, cricetid rodent species from three diet categories were chosen for measurement of tooth root surface area and estimation of bite force. Sigmodontines were chosen because they have a diverse set of feeding behaviors, and their phylogenetic relationships are fairly well understood. I hypothesize that there will be root surface area difference between the three modes of feeding, specifically that those species subsisting on a harder diet, the seed and insect eaters (*Akodon azarae*, *Oxymycterus hispidus*, *Phyllotis darwini,* and *Ochrotomys nuttalli*) would have the larger root surface area and the largest estimated bite force than grass eaters (*Calomys callosus* and *Reithrodon auritus*).

Material and Methods

Species selection and diet classification. The rodents selected all belong to the cricetid subfamily Sigmodontinae. One, *Ochrotomys nuttalli*, is sometimes placed in a separate subfamily (Neotominae). However, there is not a strong consensus for this placement (Reeder et al., 2006; Steppan, 1980). Species were chosen to represent three diet categories: Grass, Seeds and Insects. An overview of this classification can be found in Table 3-1 and Figure 3-1. To avoid technical issues with calculating surface area of a hypselodont tooth, one of the requirements for species selection was the presence of closed molar roots. Additionally to investigate the role of body size, diet groups were made up of one large species (average adult body size greater than 50g) and one smaller species. All specimens were adult individuals with minimal crown wear, although unavoidably the grass eaters had the highest level of wear. Six individuals per species were examined via microCT. Males and females were used in equal numbers when possible (Table 3-1).

Diet classification for this study was made based on a survey of existing literature for the habits of the six species. *Phyllotis darwini* is found along the central coast of Chile and weighs between 20 and 100g (Nowak, 1999). They eat primarily small seeds of grass and shrubbery, with some additional plant material and lichens (Meserve, 1981a). The percentage of seeds has been found to vary seasonally, with as low as six percent of the diet in the spring to up to 75 percent in the fall months (Meserve, 1981b). At low elevations, *P. darwini* does consume some insects (Pizzimenti and Salle, 1981) and is sometimes classified as omnivorous (Sabat and Bozinovic, 2000), however the most prominent food category is consistently seeds. For the purposes of this study, it was classified as Seeds. *Ochrotomys nuttalli* is found in the

southeastern United States and commonly weighs between 15 and 30g. Its diet consists mainly of seeds from grasses and small shrubs (Hall, 1981; Springer et al., 1981), also classified as Seeds.

Akodon azarae is found in southern Bolivia, Paraguay and southern Brazil. They commonly weigh between 10 and 45g (Nowak, 1999). The diet of *A. azarae* has been classified as partly herbivorous and partly insectivorous (Dalby, 1975), but stomach contents revealed 20 percent plant material and 70 percent invertebrates (Barlow, 1969). Thus for this study, its diet was classified as Insects. *Oxymycterus hispidus* is found in eastern and southern Brazil and in northeastern Argentina. Adults commonly weigh between 46 and 125g and use the snout to root for invertebrates in soil. The diet of *Ox. hispidus* is primarily composed of insects, however it is also known to consume other (presumably softer) small invertebrates and some plant matter (Barlow, 1969; Dalby, 1975). Although it does consume soft-bodied invertebrates, the harder shelled insects are considered the more challenging object and for the purposes of this study the diet is classified as Insects.

Calomys callosus is found in Bolivia and southern Brazil. Its diet is not well studied but seems to be primarily composed of grassy vegetation (Barlow, 1969). Adults commonly weigh between 30 and 38g. *Reithrodon auritus* is found in southern Chile. Adults, which weigh between 77 and 95g (Dalby and Mares, 1974) are primarily pastoral, feeding on grasses including the roots and tubers of some species (Pearson, 1988; Scaglia et al., 1982). For this study, both species are classified as Grass.

The general diet categories of Seeds, Insects and Grass were used to compare root surface area and bite force among the species. Getting at the material properties of these diets is more complicated, and speculative. It is generally thought that harder foods require more force to process, depending on crown characteristics. Hardness is most commonly measured via

indentation studies; however, the properties more relevant to mastication are likely stiffness, the resistance of a material to permanent deformation, and toughness, the energy needed to propagate a crack through a material. In light of these properties insect cuticle might be considered stiff, but could be cracked easily with pointed cusps whereas many seeds are both stiff and strong, in other words more tough. Although mechanical properties data for these dietary classifications are lacking, it was assumed that insects and seeds were both stiffer than fresh grass, although grass is tougher and more abrasive overall (Smole et al., 2004; Vincent, 1983).

Tooth Surface Area Measurements. The surface area of the lower left molars was studied. Rodent dentaries were scanned using a Skyscan1076 microcomputed tomography scanner (Skyscan Inc., Belgium). An optimization study with three of the 36 individuals identified the optimal root-contrast (relative to bone) settings to be 9µm resolution scanned with a tube voltage of 50kv, an exposure of 180mAs and a 300ms exposure time. The molar tooth roots were manually isolated from their surrounding alveolar bone using CTAn 2.1 (Skyscan Inc., Belgium), and the resulting isolated tooth slices were rendered using a smooth-surface model with a double-time cubes algorithm. The resulting stereolithography (STL) models were used to measure tooth and crown surface area in RapidForm XOR (Rapidform Inc., Sunnyvale, CA). The root surface area (RSA) for each molar tooth was quantified by manually selecting the root surface area located below the cementoenamel junction, which was readily identifiable in the STL models. Occlusal surface area (OSA) was quantified by selecting the entire surface visible when viewing the occlusal surface of the teeth. OSA variables were divided by comparable RSA variables to produce a ratio of occlusal area to root area (ORratio).

Controlling for size. In an effort to understand the role of body size in tooth root surface area, species were specifically chosen to have contrasting body sizes. Once the relationship with body size was determined, it was necessary to produce a size independent comparison of variables. As the skull was typically the only skeletal element available, its size was used as a proxy for body size. Skull size was approximated by calculating the geometric mean of five variables: foramen magnum height and width, bizygomatic breadth, basicranial length and skull length. These variables were all measured on the skulls with digital calipers. The geometric mean was squared for comparison to the surface area values (GeoSq). Root Surface Area, which had a strong body size correlation, was divided by the skull size proxy to produce a size controlled measure of root surface area (AdjRSA). A similar adjustment was made for bite force. No phylogenetic corrections were performed.

Bite Force Estimation. Bite force was estimated via cranial measures using a method from Freeman and Lemen (2008b), which relies on cross-sectional areas of the rodent incisor and has been validated with an in vivo bite force study. Using the index of a rectangular cross section's ability to resist a bending moment (Z_i), Freeman and Lemen provide a morphological measure of the incisor that is used to create a predictive model of bite force. Bite force was estimated by calculating the Z_i for the incisors of species in this study and using the regression equation provided by Freeman and Lemen (2008), which is

$$\log10(\mathbf{biteforce}) = 0.559*\log10(\mathbf{Z}_i) + 1.432$$

Because this study concerns molar morphology, the resulting incisor bite forces were transformed following Greaves (1988) to estimate the bite force at the M_1.

Muscle force = (Incisal bite Force*Moment arm of the incisor)/Moment arm of masseter

Molar bite force = (Muscle force*Moment arm masseter)/ Moment arm of molar

The bite force at the incisor (calculated from Freeman and Lemen (2008)) was used to estimate the force of the masseter, which was then used to estimate the molar bite force using moment arms measured from photographs of the rodent dentary. The molar bite force was compared between species and diet groups. It was also used to estimate the pressure at the M_1 by dividing the bite force estimate by the occlusal surface area of the M_1.

Statistical Analysis. Non-parametric tests were used to determine significance in differences in root surface area, ORratio and bite force. Kruskal-Wallis ANOVA with post-hoc Bonferroni correction for multiple testing was used to estimate the effect of diet classification. To compare the hardness categories (i.e. Grass versus Insects plus Seeds), a Mann-Whitney U test was used. Because both the independent and dependent variables are subject to error, bivariate trends were modeled using reduced major axis regression. Ratios were arcsine transformed before tests; all other values were $\log_{10}$ transformed for analysis. Analyses were carried out using PASW 18 (Polar Engineering and Consulting). Statistics are reported for the M_1. The M_2 followed all M_1 trends. The M_3 was not used in any statistical analyses.

Results

General Morphology. Figure 3-1 shows a surface rendering of 3D models of the rodent tooth rows. In all individuals, the first molar was the largest and the third molar the smallest. Root number varied from two (*O. nuttalli*) to four per tooth, with the majority having four roots.

The roots of the third molar were difficult to isolate in most cases and often oddly shaped or partially fused. Superficially, the teeth of *C. callosus* and *O. nuttalli* are very similar, even though they have different diets (Grass and Seeds respectively). Both exhibit relatively low crowns, but their root structure is different. *C. callosus* has a more substantial root presence, with nearly double the number of roots. The same can be said for *P. darwini* and *R. auritus*. Both have similar crown morphology, but again the grass eater, *R. auritus* has an increased root number over the seed eater. *R. auritus* has the shearing crest expected in a grazer, but the other grazer, *C. callosus*, has a much lower, rounded occlusal surface and lacks clear shearing crests.

RSA and Diet. Diet: Grass, Seeds, Insects — It was expected that the three food groups would have differing root surface area values due to the nature of their habitually encountered diets. Before controlling for size, there was only a marginal difference in RSA between the three diet categories ($p = 0.055$), however there was a trend for grass eaters to have the largest root surface area. Size controlled root surface area, AdjRSA, did differ very significantly among the groups ($p = 0.001$). This was apparently driven by the large AdjRSA for grass eating species (Table 3-2) while AdjRSA for insect and seed eaters was not significantly different ($p = 0.079$).

Diet: Stiffness — Chitin and shelly seeds were presumed stiff relative to grass, in the sense of requiring higher bite force. When evaluating the difference between the hard food eaters (Seeds and Insects) to the grass eating species, it was expected that the root surface area would be larger in stiff food species. However it was found that in all cases, grass eaters had the larger root surface area. This was true for the raw RSA values ($p = 0.018$) and AdjRSA ($p < 0.001$).

Occlusal Ratio. The ratio of occlusal surface to root surface area (ORratio) represents the relationship between the processing end of the tooth and the support structure. It was hypothesized that the hard food eaters would have the smallest ORratio values, meaning they would have proportionately larger roots relative to the occlusal surface than grass eaters, which would have larger occlusal surfaces. There was indeed a significant difference in ORratio between hard (Insects and Seeds) and Grass eaters ($p < 0.000$); however, the hard diet group had overall larger ORratios. Their occlusal surface was equal to approximately 40% of the root while grass eaters had ORratios nearer to 25%. There was no significant relationship between body size and ORratio ($R^2 = 0.018$, $p = 0.438$).

Bite Force. Bite force is also known to vary with body size, which was true in this sample ($R^2 = 0.743$, $p < 0.001$). In this study, seed and insect eating individuals were hypothesized to have the larger root surface area. However, differences among diet categories for estimated bite force did not reach statistical significance before and after controlling for size ($p=0.058$). The trend was for seed eaters to have the largest bite force, followed by grass and insect eaters.

The pressure at the M1 was significantly larger in *R. auritus* and *A. azarae* ($p<0.01$, Table 3-1). When grouped by diet, there was no difference in pressure between grazers and the other two categories. Seed eaters and insectivores were significantly different from one another ($p = 0.025$); however, this looks to be driven primarily by the high pressure value for *A. azarae*.

Discussion

Caveats for this study include questions about the actual mechanical properties of the foods and about the purity of the diet categories. Variation in mechanical properties of individual grass, seed and invertebrate species may account for variation within the dietary groupings. Unfortunately, specific material properties for the food usually consumed by these species are unknown. Additionally, some of the studied taxa do not feed exclusively on their primary diet category. For example, *P. darwini* eats primarily seeds, but has a seasonally variable diet including some plant material (Meserve, 1981b). It was assumed that the dominant evolutionary pressure would be the hard seed cracking, but if the signal from grass processing is in fact dominant, the occasional or seasonal consumption of plant material may have driven the relatively large root surface area in that species (Table 3-2).

There were differences in tooth root surface area for the three diet groups. However contrary to the hypothesis that those animals that process a "harder" food like seeds and chitinous insects may have a larger root surface area, the grass eating species had the largest root surface area. Additionally, the root surface area of the seed and insect eaters was essentially the same, despite the trend for estimated bite force to be larger in seed eaters than insect eaters. This may result from a processing bias. How exactly these rodents remove the shells from seeds is not recorded. If the seeds are held shelled with the front teeth, requiring a high bite force, but then the softer interior of the seed is processed with the molars, not requiring a high bite force, it may explain why the molars do not present a large root surface area. However, paw use in eating is highly variable among rodent species (Whishaw et al., 1998) and the exact eating behavior of the species studied here is unknown.

Additionally, Freeman and Lemen (2008) report that their method of bite force estimation did have varying levels of success, depending on whether or not the species was grazing or omnivorous. In their study the predicted bite force for a grazer (or omnivore) was low by an average of 9%. In this study there was no strong difference in predicted bite force for any of the three dietary groups ($p=0.058$), refuting my original hypothesis. Increasing the bite force of grazers in this study by 9% (the values given by Freeman and Lemen (2008)) removed even the hint of dietary differences in bite force ($p=0.54$ after adjustment compared to 0.058 before) indicating it is very unlikely there were differences. How then could the grass eating species present the largest root area, something that is usually associated with large, habitually encountered masticatory forces (Christiansen and Wroe, 2007; Kupczik et al., 2010; Stynder and Kupczik, 2012)?

Grass eating individuals do tend to have much higher crowns, thought to compensate for the abrasive nature of their diets (Rensberger, 1975). A larger root might be the result of increased anchoring to prevent tipping of the tooth during mastication. However, the increased root surface area is also present in grass-eater *C. callosus*, which does not exhibit a particularly high-crowned tooth. It also lacks the clear shearing crests observed in the other grass eating species. For fibrous materials such as grasses, the length of the shearing blades that are in contact with the bolus may play a role in ease of processing; without these crests it may be more difficult for effectively process grasses. It is possible that the grazing species both exhibit large roots for different reasons, one to stabilize the tooth, the other as a result of increased processing time of the grass fibers.

Large roots are often assumed to be adaptive for large peak occlusal forces, usually required to break hard foods (Kupczik and Dean, 2008). The species with the highest pressure at

the M1, *A. azarae*, was not also the species with the largest root area. Largest root area was *R. auritus*, which did have the second highest molar pressure. In general, the species subsisting on the least stiff of the three foods had the largest root surface areas. Grass is a tough material; cellulose fibers exhibit require high energy input for breakdown (Smole et al., 2004). Because a tougher item would require increased processing time and therefore longer periods of loading, the cumulative forces applied through the roots of a grass eater may be higher than those seen by a seed or insect eater. Rodents do exhibit post-acquisition mastication of food, but duration of chewing is not known for any of the studied species.

The cumulative effect of loading may be a reason for larger tooth root in *C. callosus*, *R. auritus*, and possibly *P. darwini*, without any accompanying significant difference in bite force. The effects of cumulative, rather than peak, loading are often seen on bone remodeling studies (Zioupos and Casinos, 1998), but tooth roots do not actively remodel, other than the continued apical surface cementum deposition during the life of the tooth (Diekwisch, 2001). A larger root would allow more surface area for more periodontal ligament insertions into the cementum, and this could provide more effective load dissipation. An advantage of superior load dissipation would be decreased stress on the alveolar bone, resulting in decreased likelihood of damage or bone fatigue.

While the relationship between diet, bite force and root surface area is not as straightforward in rodents as it is in carnivores, primates and bats, the ability to compare a range of diets within the same subfamily has allowed some insight into the mechanical underpinnings of root size adaptation. Based on the species observed, increased root area is a clear indication of grazing which seems to be uncoupled from the high crowns often described as adaptive for grazing, as these grass eating species do not all exhibit particularly high-crowned teeth. It would

be beneficial to study other grazers, to evaluate further the role of root size in mechanical compensation for increased temporal loading associated with processing grasses.

The final publication is available at Springer via http://dx.doi.org/10.1007/s00435-015-0262-y

Table 3-1. Rodent specimen information. Molar bite force was calculated transforming the incisal bite force from Freeman and Lemen (2008) using the Greaves (1988) method (for details see methods). The geometric mean used five cranial measurements. Pressure at the M_1 was calculated by dividing the molar bite force by the occlusal surface area of the M_1.

Species	Sex		Diet Category	Skull Size (Geometric Mean) mm^2	Estimated Molar Bite Force (N)	Adjusted Bite Force (AdjBF)	Pressure at the M_1 (Mpa)
	F	M		Mean SD	Mean SD	Mean SD	Mean SD
A. boliviensis	3	3	Insects	31.7 ± 2.2	20.6 ± 2.3	0.93 ± 0.20	10.69± 2.16
Ox. hispidus	3	3	Insects	49.8 ± 4.1	25.1 ± 7.9	1.00 ± 0.20	4.97± 1.45
C. callosus	2	4	Grass	26.5 ± 2.6	19.6 ± 3.2	1.14 ± 0.10	6.27± 0.85
R. auritus	4	2	Grass	63.0 ± 7.5	35.4 ± 7.1	1.10 ± 0.10	8.58± 2.49
P. darwinii	3	3	Seeds	51.0 ± 3.7	31.8 ± 5.9	1.28 ± 0.10	4.93± 0.54
O. nuttalli	3	3	Seeds	31.1 ± 1.9	28.6 ± 6.5	2.33 ± 0.40	5.21± 0.71

Table 3-2. Individual rodent tooth values. Statistics reported are for M1, however all tooth positions gave the same statistical result. AdjRSA is the raw RSA divided by the body size proxy squared. ORratio is the occlusal surface area divided by the root surface area.

Diet	Species	Tooth	Root Surface Area (RSA) mm^2		Size Adjusted Root Surface Area (AdjRSA)		Occlusal Surface Area (OSA) mm^2		Occlusal to Root Ratio (ORratio)
			Mean	SD	Mean	SD	Mean	SD	
Insects	A. boliviensis								
		M1	8.33	1.32	0.26	0.04	3.29	0.16	0.40
		M2	5.36	0.72	0.17	0.03	2.67	0.31	0.51
		M3	3.86	1.23	0.12	0.05	1.96	0.25	0.54
	Ox. hispidus								
		M1	12.98	2.11	0.26	0.04	5.04	0.65	0.39
		M2	9.84	1.98	0.20	0.04	4.56	0.74	0.48
		M3	5.34	0.88	0.11	0.02	2.83	0.62	0.53
Grass	C. callosus								
		M1	10.40	0.77	0.40	0.06	2.38	0.47	0.23
		M2	6.63	0.58	0.25	0.04	1.84	0.34	0.28
		M3	3.95	0.41	0.15	0.01	1.17	0.28	0.30
	R. auritus								
		M1	27.07	4.32	0.43	0.06	7.14	0.92	0.27
		M2	16.16	2.49	0.26	0.03	6.34	0.96	0.40
		M3	11.05	1.43	0.18	0.02	4.64	0.73	0.43
Seeds	P. darwinii								
		M1	21.51	3.63	0.42	0.06	6.04	0.72	0.29
		M2	13.31	4.64	0.26	0.09	4.31	0.70	0.35
		M3	7.88	1.31	0.15	0.02	2.99	0.41	0.39
	O. nuttalli								
		M1	7.15	0.87	0.23	0.02	2.67	0.27	0.38
		M2	5.75	0.71	0.18	0.02	2.48	0.30	0.43
		M3	3.78	0.32	0.12	0.01	2.07	0.32	0.55

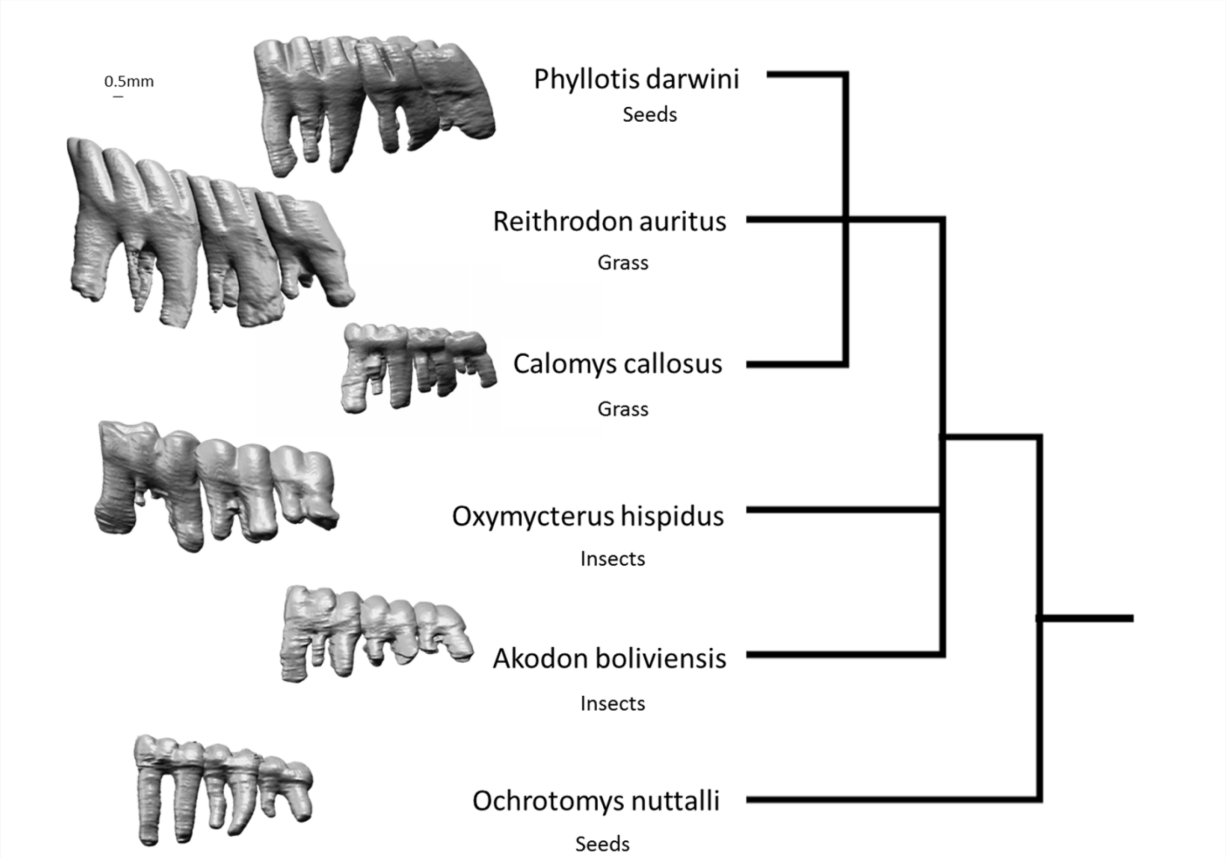

Figure 3-1. Combined phylogeny, diet, and morphology of the rodents studied, specimens scaled. Tree modified from Steppan (1995).

Chapter 4: Finite Element Analysis of Periodontal Ligament Fiber Bundle Orientation

Introduction

Finite element analysis (FEA) is commonly used in engineering applications to determine patterns of fluid flow, stress, strain, heat transfer and other problems requiring complex mathematical computations. Modeling in biomechanics offers an alternative to invasive techniques commonly used to explore the mechanics of the face (Korioth et al., 1992). An accurate and well-populated model can provide information that would otherwise be acquired with strain gages, and can be used to ask questions without animal or human testing. It is a powerful tool that is growing in popularity but is only useful if applied appropriately. Models give us the ability to investigate the biomechanical function of real structures, but also to explore the range of potential morphology. To create a useful model detailed information must be known of the structure being approximated, including the geometry, material properties and loading conditions.

The periodontal ligament (PDL) is commonly included in cranial and mandibular models created for dental and orthodontic applications, but it is often modeled as isotropic material; that is, a material with uniform properties in all orientations (Ammar et al., 2011; Cattaneo et al., 2005; Field et al., 2009; Kaipatur et al., 2014; Rees, 2001). The extent that the PDL is necessary for accurate modeling of the whole face is still under debate, but its role in distributing stresses in the micro-environment of the alveolus cannot be ignored. As remodeling of the tooth sockets is primarily due to changes in the load on tissues local to the tooth and PDL (e.g. Bozal et al.,

2013), the specific arrangement of PDL fibers may play a role in predicting how alveolar bone responds to occlusal forces in different loading scenarios. The arrangement and distribution of collagen fiber bundles varies among species (Chapter 5), but what role that variation plays in mechanical response of the alveolus to occlusal loading is unknown. The goal of this project is to build a simplified geometric model of the tooth socket, PDL and tooth, in order to identify the role PDL fiber bundle arrangement plays in tooth displacement and strain distribution in the surrounding alveolar bone.

Overview and Requirements of Modeling. Finite element analysis can be subdivided into three main processes: building the solid model geometry, constraining and loading the model, and validating the model.

*Capturing geometry***.** The construction of a model consists of creating the specimen geometry and assigning appropriate material properties. In the case of a simplified model, such as the one presented in this chapter, the geometry is created manually using software. To create a model of a specific specimen the geometry of the specimen can be digitally captured. Traditional methods include laser scanning or digitally tracing the outline of a specimen. More recently, computed tomography (CT) and magnetic resonance imaging (MRI) techniques have been used to generate the appropriate specimen geometry. CT scans are appealing because of their high resolution and the ability to import the data into finite element analysis (FEA) software, but they are not without their problems; there are complex issues involved in appropriately delineating the specimen boundaries (Ryan and van Rietbergen, 2005). Additionally, the use of detailed CT data can result in a model with geometry so complex that the computing power needed to process the model is cumbersome. In cases where true geometry would unnecessarily complicate the

question being asked of the model, simplified geometry is often used (Kumar et al., 2015; Romanyk et al., 2013). Simplified models are also valuable as tools to investigate potential morphometric space and present hypotheses of morphology based on the mechanical response to loading. Once possible morphologies have been identified via mechanical analyses, predictions of shape can be tested by analyzing existing morphologies in real specimens. Creating and refining realistic geometry is usually the most time consuming part of the process, and assumptions made at this stage can have a drastic effect on the results (Ross et al., 2005).

Once the model geometry has been established, it must be subdivided into smaller, geometrically simple areas or volumes, the "finite elements". These units of area (or volume in the case of 3D modeling) are connected at their vertices via points referred to as nodes. The collection of connected elements is called the mesh. Displacements are determined with respect to nodes. Depending on the dimensionality of the problem, there are several different shapes of elements that can be utilized. (Beaupre and Carter, 1992).

A criticism of FEA in biological settings is that it is difficult to incorporate morphological variation. It is impractical to model population-level variation. Models are generally created using idealized geometry or using scans of a single specimen, so assumptions must be made as to the representative nature of the specimen. Because generating a model can be exceedingly time consuming, usually only one specimen is modeled, and all loading scenarios are run on the same individual (Ross, 2005).

*Attributing Material Properties***.** As FEA has become more commonly used in biomechanical studies of the PDL space (Xia et al., 2013), the difficulties in modeling irregular shapes and anisotropic materials, those with directionally dependent material properties, have become more pronounced. Bone is irregularly shaped and has variable densities and elastic

moduli. PDL is a composite of anisotropic fibers in an isotropic, viscoelastic gel-like matrix. In order to create an accurate model, one must assign the appropriate material properties to each distinct tissue type being modeled; that is, bone, PDL, and tooth. A model that attempts to recreate all real physical interactions between the tooth, PDL, and bone is incredibly time consuming due to the non-symmetrical nature of the tissues and their complex material properties; that is, anisotropy and viscoelesticity in the PDL. Because of this, assumptions are commonly made to simplify the model, depending on the question being asked. In some cases isotropy is assumed and material properties are established using nanoindentation studies of comparable bone (Silva et al., 2005). Assuming isotropy and using published average values for material properties is also common (Thomason et al., 2005). Recent studies have indicated that accurate material properties are essential to a good model. Both Marinescu et al. (2005) and Richmond et al. (2005) found that different inputs for bone material properties profoundly affected the resulting strain predictions. Using literature values for PDL and bone material properties can be complicated as there are numerous reported values (Table 4-1) and many factors, like age, affect the values that are actually obtained (Fill et al., 2011). To identify reasonable PDL properties for simplified tooth geometry FEA modeling, Xia et al. (2013) attempted to anchor Young's modulus and Poisson ratio pairs for the PDL to match experimental displacement behavior. Their goal was to provide reasonable Young's modulus and Poissons ratio values for a simulated isotropic PDL material in simplified models of a single-rooted tooth.

Loading a Model. Once an appropriately detailed model has been constructed, the next step is to load and constrain it mathematically. Creating an informative loading scenario requires accurate data on the external forces acting on the specimen. Although it can be difficult to gather comprehensive data on the forces anticipated during a loading event in vivo, the resultant strains

are completely dependent on the programmed loading environment. Contraits are commonly applied to areas far away from the area of interest in the analysis. Strains measured near constrained regions are often artificially high. Marinescu et al. (2005) found that small changes in the direction of load application and constraint type had significant effects on predicted strain. While it clear that the details of construction and loading greatly affect model predictions, the relative importance of loading conditions, material properties, geometry and constraints are still under investigation (Dar et al., 2002; Marinescu et al., 2005; Panagiotopoulou et al., 2011; Papadopoulou et al., 2013; Richmond et al., 2005; Ross, 2005; Strait et al., 2005).

Validation. FEA produces a prediction of how the modeled object would react to the modeled load. In the case of a model of a specific specimen or individual, the resulting prediction should be compared to in vitro or in vivo strain data to ensure the validity of a prediction and that it lies within expected parameters. Some studies use mechanical testing on the exact specimens used in the model to generate material properties and to validate model behavior (Coleman et al., 2002; Korioth et al., 1992). When strain data are too difficult to obtain, load-displacement curves generated by in vitro specimens can be used to validate model predictions (Andersen et al., 1991; Jones et al., 2001; Meyer et al., 2010; Qian et al., 2001; Rees and Jacobsen, 1997). Models of human bone, bone from extinct animals, or very small bones, can be difficult to validate, as extensive in vivo work has not been done with humans and cannot be done with extinct organisms. In these cases, cross-species comparisons are commonly applied. In cases of idealized geometry, specific strain values cannot be validated; however, maximum strain values can be compared to existing literature to establish the relative value of the model and overall strain patterns can be compared (Kumar et al., 2015).

A History of PDL FEA. Inclusion of the PDL is common in orthodontic models and those incorporating occlusal loads, but it is usually included as a simplified, isotropic structure. What follows is a review of mathematical models of tooth and bone that attempt to include a detailed PDL. Knoell (1977) is one of the earliest modelers to consider the PDL. A three-dimensional mathematical model of a human mandible was created to investigate the biomechanical response of the tooth support region to occlusal loads. While Knoell's model did not include the PDL, it was determined that biomechanical response is highly localized to the region of tooth support; therefore, a model of the region near the applied load requires careful simulation of the surrounding anatomical structure, including the PDL. Atmaram and Mohammed (1981) created a two-dimensional mathematical model to investigate the difference between representing the PDL as a continuous structure and breaking it up into a fibrous structure, similar to its actual anatomical arrangement observed in histological sections (in the coronal plane). They determined that a fibrous PDL model yielded different alveolar stresses than the continuous PDL model.

In a three-dimensional human mandible computer model generated by Korioth et al. (1992), the periodontal region was divided into three regions, each with its own PDL properties. Material properties of the PDL vary along the root (Mandel et al., 1986). In an attempt to avoid oversimplification, Korioth et al. (1992) modeled the PDL with varying elastic moduli; however, no fibrous attachment was considered. Wilson et al. (1994) produced a model to investigate the role of orthodontic stresses in alveolar bone remodeling. Considering the PDL plays a role in bone remodeling of the tooth region, they felt it was pertinent to include PDL material properties and morphology in model construction. Similarly, in a study of orthodontic forces on teeth and surrounding tissues, Jones et al. (2001) included the PDL in their model since the PDL is the

mediator of tooth movement. Both modeled the PDL as a isotropic structure. Rees (2001) also stressed the importance of including the PDL when undertaking finite element studies of teeth; his model also included a homogenous, isotropic PDL region without fibrous consideration, as did those of Lin et al. (2006), Gonzales et al. (2009), Archangelo et al. (2012) and Atmaram and Mohammed (1981). It is generally accepted that models of the tooth and the immediate area are unreliable and inaccurate without inclusion of PDL material properties (Goel et al., 1992; Goel et al., 1990; Khera et al., 1988; 1991; Korioth and Hannam, 1994); however, as is evident, few attempt to model detailed geometry of the PDL itself.

Despite such studies, some modern models continue to be generated without inclusion of PDL material properties. Hart et al. (1992) created a mandible model investigating isometric biting and the role of missing teeth in the dissipation of stress. The tooth-bone interaction was modeled using the stiffness of cortical bone with no interface layer. The authors acknowledge that lack of a PDL in their model inhibits its capability to accurately represent the stress environment in the alveolar region. Another finite element model of the mandible without a PDL was created by Marinescu et al. (2005). Their study assumed that inclusion of the PDL in modeling was unnecessary as the teeth and PDL do not significantly contribute to the structural stiffness or strength of the mandible during non-occlusal loading. To investigate their assumption, two models were created: one edentulous with root spaces modeled as gaps and another dentate model with no PDL. After application of occlusal loads, it was found that the dentate model without PDL was overly stiff and had an inaccurate strain pattern, whereas their edentulous model produced a more reasonable strain pattern. Finally, as a case study in their review of modeling practices, Richmond et al. (2005) included a finite element model lacking a PDL. While their model was primarily concerned with muscle forces, the study did contain

occlusal restraints and loads, indicating that results may not have been accurate due to oversimplification of dental structures. This is especially pertinent to their model of the palate as it is intimately related to dental alveolar morphology.

Overall it seems that the field-specific areas of cranial and mandibular finite element literature have chosen to deal with the inclusion of the PDL differently. Orthodontic literature includes PDL, but often in a simplified, homogenous manner, while comparative and fossil-based models often choose to leave the structure out completely. PDL fiber bundle organization has not yet been successfully modeled (Panagiotopoulou et al., 2015). This is partly because a detailed understanding of PDL fiber bundle orientation is not known for most species being modeled, but also because the inclusion of a detailed variable structure such as the PDL greatly increases the complexity of a model. While it may be valid to conclude that models of non-occlusal forces should not need to include the PDL, as the effect of the PDL seems to be limited to the alveolar region and its contribution to alveolar bone strain is the result of occlusal loading. It would, however, be an oversimplification to model detailed tooth and alveolar bone behavior without anticipating the complex structural context of in vivo loads.

Predictions. The goal of this project is to identify the role of detailed PDL collagen fiber arrangement as it relates to strain distribution in the alveolar bone in an idealized three-dimensional tooth and socket geometrical model. If fiber direction does strongly affect strain distribution in a simplified tooth model, the case for its inclusion in a more detailed and complex model is supported. In this experiment, an idealized tooth socket (Figures 4-1, 4-2) is populated with a tooth root and a fibrous PDL. In the horizontal plane, both models rely on an overlapping spoke arrangement, commonly attributed to the PDL and seen in *N. vison* (Chapter 5) (Sloan and

Carter, 1995). The angle of the PDL is varied in two ways in the coronal plane: a highly acute angle (30°) that might be expected in an obligate carnivore with a primarily vertical bite, and a less-acute angle (60°), as might be expected in an herbivore with a strong horizontal bite component. While these initial arrangements are what would be logically expected from a mechanical perspective, They also resemble the angulations found in Chapter 5, 37±9° in a carnivore, *N. vison*, and 59±12° in an herbivore, *O. cuniculus*.

Two load cases are used to test bone strain response: a primarily vertical load application in line with the axis of the tooth (simulating the carnivore bite), and a load applied at a 45° angle with respect to the axis of the tooth (simulating the herbivore bite). Each PDL fiber arrangement model is evaluated under both loading conditions, and resulting bone strain distribution and tooth displacement are compared and used to generate predictions regarding PDL fiber bundle arrangement for species that habitually encounter these types of occlusal loads. These model predictions are then compared to a summary of results from Chapter 5. The goal is to identify the mechanical relevance, if any, of PDL collagen fiber bundle arrangement in mastication.

Methods

Model geometry. The solid model of the tooth and bone were generated within ANSYS Design Modeler (Workbench version 14.5.7, Cannonsburg, PA). Tooth geometry was based on a histological analysis of a first mandibular premolar of an adult *N. vison* specimen. As shown in Figure 4-1, the tooth model was simplified to be a cone with hemispherical ends. Based on dimensions from the mink premolar, the crown diameter was modeled as 1 mm, and the root diameter as 0.87 mm. The taper angle between the crown and root was modeled as 30° off the tooth centerline axis. Overall tooth length was modeled as 6 mm. The PDL space, distance

between the tooth and bone, was modeled as 0.11 mm. The alveolar bone was modeled as a cylinder 4 mm in diameter simply to provide enough material outboard of the tooth to provide reasonable stiffness.

Finite element model setup. The tooth was meshed using the high-order 3D 20-node solid element (SOLID186). To improve model run time, the tooth mesh was intentionally created to be very coarse since resolving stress or strain values in the tooth was not an objective of the model. The bone was meshed using the high-order 3D 10-node solid element (SOLID187). The mesh throughout the bulk of the bone is coarse; however, the mesh was refined at each PDL attachment point in order to resolve strains at these locations. The PDL bundles were modeled using LINK180 elements. The LINK180 element is a uniaxial tension-only element with three degrees of freedom at each node: translations in the nodal x, y, and z directions. As in a pin-jointed structure, no bending of the element is considered. To simulate the tension-only option for the LINK180 element, a nonlinear iterative solution approach was necessary with the large deflection option turned on. The bottom surface of the bone was constrained with a FIXED condition, locking all 6-degrees of freedom. In each model, the intrusive load was applied to the entire hemispherical tooth crown surface.

Material Properties. Alveolar bone, dentin and PDL were each modeled as homogeneous isotropic materials (Jones et al., 2001; Pietrzak et al., 2002). The alveolar bone Young's Modulus was set as 25GPa and the Poisson's ratio was set as 0.29 (Ho et al., 2010). The tooth Young's Modulus was set as 12GPa and the Poisson's ratio was set as 0.28 (Ho et al., 2010). The LINK180 element, used to model the PDL, was defined by two nodes, the cross-

sectional area and the Young's Modulus. The LINK180 element allows a change in cross-sectional area as a function of axial elongation. By default, the cross-sectional area changes such that the volume of the element is preserved, even after deformation, thereby simulating a material with a Poisson's ratio equal to 0.5. The Young's Modulus of the PDL was set at 1.0 MPa (Chiba et al., 1990; Komatsu et al., 1998; Pini et al., 2004).

Anchoring/model simplification. The number of PDL fiber bundles in the horizontal plane was modeled after the histological investigation of the first mandibular premolar of the same adult *N. vison* specimen. Average PDL bundle diameter was measured to be 100 microns. Thirty-six tendon bundles were observed on average around the tooth in horizontal section, and 12 PDL bundles were observed on average along the middle 2/3 of the tooth in the coronal view. To reduce the model complexity, the number of individual PDL attachment couples was reduced by a factor of 16 (9 in the horizontal instead of 36 and 3 in the coronal instead of 12). To compensate for the reduced number of attachments, the PDL stiffness was increased by the same factor of 16 in order to maintain an overall average PDL system stiffness.

In reality, PDL attachments to both the tooth and bone splay out, presumably to help spread the load and reduce the resulting tooth and bone strain. The model does not capture this geometry accurately, and therefore peak strains at the bone and tooth are over-predicted. To negate this effect, average surface strain inside a .05 mm radius from each PDL attachment point is reported. Additionally, PDL stiffness is likely higher in reality than what is modeled due to the increasing cross-sectional area of the fibers near the tooth and bone attachments where the PDL fibers splay out. This geometry effect is not captured in the model; the fibers are simplified

to have constant circular cross-sections. The resulting modeled tooth will displace more for a given load than would be expected in nature.

Due to this inaccuracy in PDL stiffness, the applied load was selected such that the tooth would never contact the bone under either the axial or lateral load nor in either the 30 or 60 degree PDL angle configurations. A 1N load was originally targeted, but rather than scale up PDL stiffness, the load was reduced to .354 N, which corresponds to .25N in the Z-axis and .25N in the X-axis for the lateral load case. The alveolar bone was restricted from movement in all planes using its external edge.

Lastly, the proteoglycan matrix that surrounds the PDL was not modeled. This was omitted for three reasons: The focus on this model is comparing the differences in tooth displacement and strain distributions with variable load direction and PDL attachment angle; matrix properties are considered to be homogenous, and therefore would not change between load and geometry cases; and accurate material properties for only the matrix are not readily available in existing literature due to the difficulty separating the PDL fibers while keeping the matrix material intact.

Load and ligament geometry cases. Two models were created to compare PDL fiber bundle angle orientation. In the coronal plane, cervical and apical rows of fiber bundles were maintained at a 90° angle for both models, but the PDL fiber bundles in the mid-region of the tooth were modeled at 30° from the tooth axis in one model and 60° in the other (Fig 4-1). In both models, the PDL fiber bundles in the coronal plane were kept in an evenly spaced spoke arrangement (Fig. 4-2). Two load cases were applied to each model. The two load cases were extreme examples of occlusal loads of *N. vison* (purely axial) and *O. cuniculus* (a horizontal

component). The total applied load in each model was 0.354 N, which corresponds to .25N in the Z-axis and .25N in the X-axis for the lateral load case.

Strain results from the four total models were normalized to the highest strain value in each model. Strains in the horizontal plane were calculated at Row 2 (Fig. 4-1) and compared between models for an analysis of strain distribution. Overall displacement of the tooth was calculated and broken down into its vertical and horizontal components for a comparison of displacement patterns between the four model load cases.

Results

Displacement. Vertical displacement is 12% less under axial loading in the 30° fiber angle model (Table 4-2). The 60° fibers are more horizontal and therefore proportionally less stiff in the Y-axis direction compared to the 30° fibers; however, the lack of stiffness due to attachment angle is largely counteracted by the fact that these fibers begin twice as stiff as the 30 fibers due to their shorter lengths.

In the lateral loading scenario, the 30° fiber model undergoes more total displacement than the 60° fiber model. The nature of the tooth movement is similar in both cases; there is almost no z-axis translation. The majority of the z-axis load results in rotation of the tooth around the x-axis (Figure 4-3). In the 60° fiber model, the center of rotation is more coronal, resulting in a slightly larger apex displacement and greatly reduced crown displacement when compared to the 30° fiber model (Table 4-2, Fig. 4-3). The vertical displacement in both fiber conditions is very similar. Again, even though the 30° fibers should be better oriented to resist vertical displacement, they are less stiff overall (due to their increased length) than the 60° fibers, resulting in similar vertical displacement magnitudes between the two models.

Strain Distribution: horizontal plane. Bone strains were calculated at the first row of angled PDL fiber bundle insertions (Row 2 in Fig. 4-1). Under axial loading in both the 30° and 60° fiber models, the strain is fairly evenly distributed radially around the tooth, although the strain values are slightly larger in the 60° fiber model. In the axial load conditions they should, theoretically, be identically distributed around the tooth, as we modeled the tooth symmetrically. However there is up to a 25% difference in strains. This may be the result of uneven load application across the course mesh of the tooth crown producing a slightly off axis load, or an artifact of our method for sampling strain values in the alveolar bone. Overall, we assume that the differences in strain seen around the tooth socket are the result of error in using a simplified model and we assume that the normalized differences in strain observed under axial loading are outside the sensitivity of this model. Under lateral loading, looking at the tooth in the coronal plane, from the perspective of Figure 4-1 (horizontal plane), the bone strains in fiber attachments on the right side (B, A, I in Fig. 4-2), which are in tension, are very high. They are smaller 90° relative to the applied load (Table 4-3) and smallest on the left side (E, F, Fig. 4-2,), where the tendons go into compression and provide no support. The observed differences in strain are much larger than the variation in strain observed in the axial load condition.

Discussion

Limitations. As this is a simplified geometry model, there are many significant limitations to applying this model to in vivo tooth behavior. The goal of this model is not to reflect real world scenarios exactly, especially since it is unknown if these fiber angle and load

combinations actually exist. The goal is to predict morphology of PDL fiber bundles in relationship to habitual occlusal loading, to be applied to histological investigations in Chapter 5.

Displacement. Under vertical loading, overall displacement is 12.5% less in the 30° model. This would suggest that, if displacement is the limiting factor, a tooth subjected to primarily axial loads should exhibit predominantly acute fibers. The 60° model results in less overall displacement under lateral loading, which again, was expected. Again, if displacement is the limiting factor in horizontal loading, one would expect to see horizontal component chewers exhibit more obtuse fiber bundles.

*Results from histology***.** These predictions are supported by findings in Chapter 5; *N. vision*, a vertical chewer had significantly more acute PDL fiber bundles than either the *M. musculus* and *O. cuniculus*, which both have a more horizontal component to their bite.

Strain Distribution: horizontal plane. Under horizontal loading, bone strain at the PDL bundle attachments on the compression side of the tooth were near zero. However, this model only addressed loading in one direction. In the in vivo load case, the horizontal component of the bite in some species is somewhat reciprocating. The ligaments that go into compression during the primary phase of the bite stroke would then go into tension on the return phase of the stroke. So while compression side bone sees near zero strain in this model, on the return chewing stroke it is likely the ligament bundles would be in tension and result in similar bone strains as the tension side in this model. For this reason, the orientation and density of PDL fiber bundles in line with the horizontal component of the load should be similar on both sides of tooth. Fiber attachments normal to the horizontal load component would continue to see less bone strain

during both phases of the bite. In horizontal chewers, *M. musculus* and *O. cuniculus*, fiber organization might be expected to differ between quadrants of the tooth relative to the horizontal component of the bite. Those fibers in line with loading are likely to be straight and densely packed, while those normal to the load may be sparser and more angled towards the direction of applied load. In the vertical load condition, strain is more evenly distributed around the tooth, which would likely result in a more consistent fiber organization when comparing the quadrants of the tooth.

Results from histology. The organizational component of this hypothesis is supported by findings in Chapter 5. During biting in *N. vison*, the tight TMJ restricts biting motion to a primarily up-down rotational movement around a bicondylar axis (Dyce et al., 2009). This species exhibits uniform fiber distribution around the perimeter of the tooth with an organization similar to the crossed spoke arrangement commonly attributed to the PDL. *O. cuniculus*, which has a strong bucco-lingual bite component (there is an anterior motion as well, but this is not reciprocal) (Ardran et al., 1958), has crossed fibers predominantly in the posterior region of the molar and direct connections in the other three regions. *M. musculus*, which has a strong antero-posterior bite component bite (there is also a small lingual component) (Weijs and Dantuma, 1975), exhibits predominantly direct fibers in the A-P orientation; however, these differences in distribution of PDL fiber bundle organization are not statistically significant (Chapter 5, Table 5-4).

Concluding Remarks. Mathematical modeling has value in biomechanical studies, and the specific value of this simplified model lies in exploring imaginary morphospace. In this case, a generalized single-rooted tooth was used to make predictions about PDL fiber bundle

organization under two types of habitual loading. Although simplified geometry and loading were used, the a priori PDL fiber morphological hypotheses were generally correct. Fiber angle in the vertically chewing species was more acute than in those with a horizontal bite component and fiber organization was different between the vertical and horizontal chewers; *N. vison* exhibited a crossed PFL fiber bundle and the others a more direct attachment pattern.

While the hypotheses of interest in this study were relating to PDL fiber bundle organization, this type of model could also be used to investigate PDL collagen fiber density. Additionally, finite element models like this could also be used to make predictions of bone morphology based on loading history. A model more densely populated with PDL fibers coupled with mathematical bone remodeling theory could provide insight into how the alveolar socket may remodel under different loading regimes (Beaupré et al., 1990; Goel et al., 1995; Hart et al., 1984; Weinans et al., 1992). Work of this type is being done for clinical problems, investigating tooth implant failure (Lin et al., 2010a; Lin et al., 2010b). In order to provide interesting insight into the evolutionary morphology of the tooth socket, the same type of bone remodeling estimation methodology could be applied to a simplified model.

Table 4-1. Experimentally determined properties of the tooth-bone interface. Modified from Fill (2011) and Herring (2012).

	Modulus†	Specimens	Test	Reference
Alveolar bone	0.2-9.6 GPa (E_r)	Human mandible, molar alveolus	Nanoindentation wet	Ho et al. 2010
	9.0-15.8 GPa (E)	Colobine monkey mandibular alveoli	Microindentation, dry	Daegling et al., 2011
	10.7-12.7 GPa (E_r)	Dog mandibular alveoli	Nanoindentation wet	Huja et al., 2007
	8.4-12.1 GPa (E_r)	Dog maxillary alveoli	Nanoindentation wet	Huja et al., 2007
Peridontal Ligament	0.45-1.34 MPa (E)	Rat incisor sections	Intrusion	Chiba et al., 1990
	1-6 MPa (E), varying regionally	Mouse incisor sections	Extrusion	Komatsu et al., 1998
	1.4 Mpa (E)	Human	Extrusion	Yamanda and Evans 1970
	3.8 MPa (E)	Human, all teeth	Intrusion	Atkinson and Ralph, 1977
	3 MPa	Human premolar sections	Intrusion	Mandel at al., 1986
	0.22 ± 0.06 MPa (G*)	Pig incisor sections	Dynamic shear	Tanaka et al., 2006
	0.14 – 0.19 MPa (G*)	Pig molar sections	Dynamic shear at 2 Hz, varying regionally	Tanaka et al., 2007
	1-8 MPa (E)	Cow incisor and molar sections	Transverse tension	Pini et al., 2004
	5-19 Ma (E) depending on strain rate	Cow molar sections	Dynamic tension	Sanctuary et al., 2005
	0.012 MPa (G)	Pig premolar	Intrusion, optical	Natali et al., 2007
Dentin	10-25 GPa (Er)	Human molar	Nanoindentation	Ho et al., 2010
	17-50 GPa (E), higher for intertubular	Human molar	Viscoelastic imaging	Balooch et al., 2004
	21-27 GPa (E)	Bovine incisor	Nanoindentation	Inoue et al., 2009

† E, elastic modulus; E_r, reduced elastic modulus; G, tangent shear stiffness, G*, complex dynamic shear modulus.

Table 4-2. Root apex displacement under two loading regimes for each fiber angle. Negative vertical values indicate intrusion of the tooth into the socket. Under horizontal load, the displacement was measured at both the tooth crown and root apex. Negative horizontal values indicate motion towards the lateral component of the applied load.

	Axial Load		Lateral Load		
PDL Bundle Angle	Plane	Displacement (mm)	Plane	Apex Displacement (mm)	Crown Displacement (mm)
30°	Vertical	-0.021	Vertical	-0.022	-0.037
	Horizontal	-	Horizontal	0.019	-0.087
60°	Vertical	-0.024	Vertical	-0.025	-0.036
	Horizontal	-	Horizontal	0.025	-0.062

Table 4-3. Normalized strain distribution around a horizontal section of the tooth socket. Strains are compared at the first row of angled PDL fiber attachments (see Fig. 2 for reported strain locations). Results are shown for the 30° and 60° PDL fiber bundle models under both loading regimes.

	30°		60°	
Location	Axial	Lateral	Axial	Lateral
A	100%	100%	98%	100%
B	89%	82%	88%	82%
C	100%	67%	100%	56%
D	97%	44%	96%	18%
E	86%	30%	74%	0%
F	90%	33%	77%	0%
G	97%	48%	99%	21%
H	85%	63%	81%	52%
I	76%	68%	71%	62%

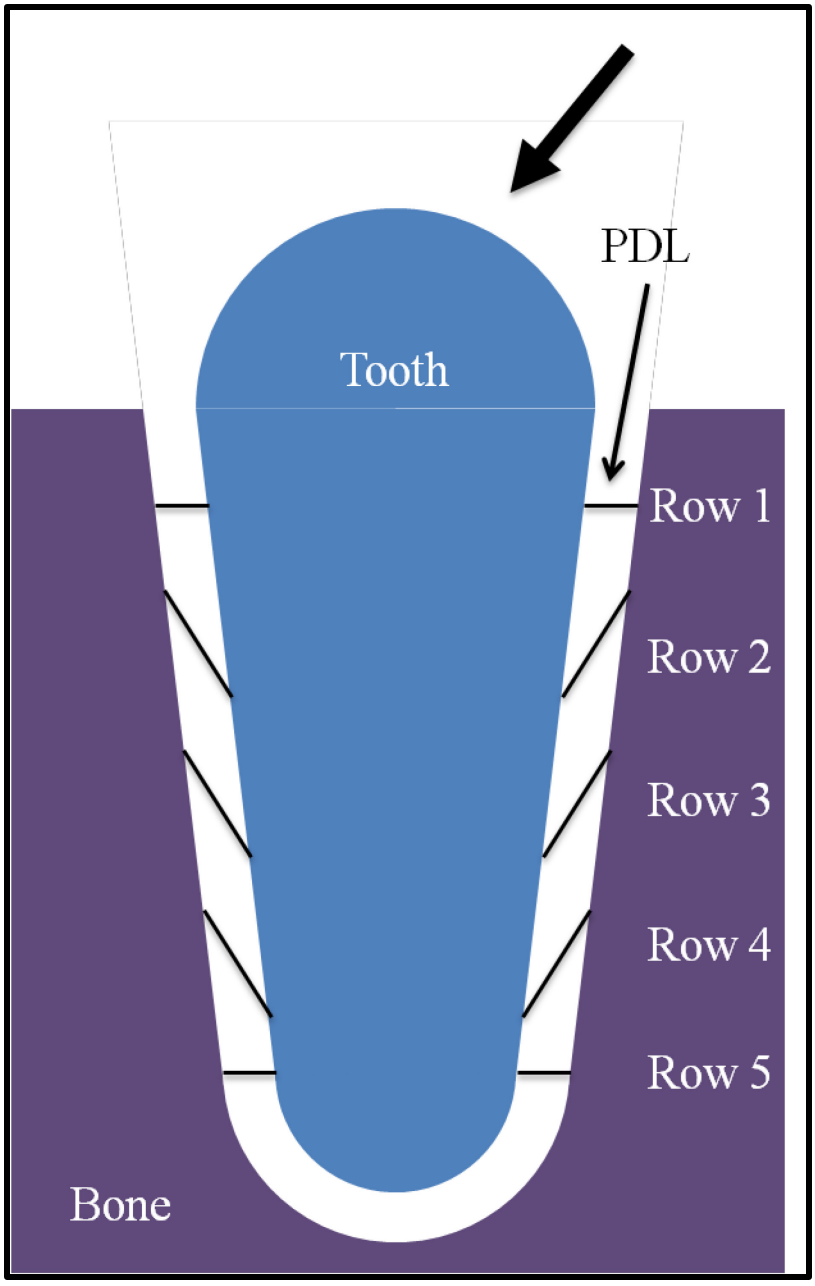

Figure 4-1. Diagram of the FEA model in the coronal plane. Fibers in the cervical and axial region were maintained at 90° for both models. The 30° model consisted of fibers in the mid-region of the tooth, rows 2-4, at 30° relative to the tooth; the 60° model has those same fibers at 60°. Direction of the lateral loading scenario is indicated by the arrow.

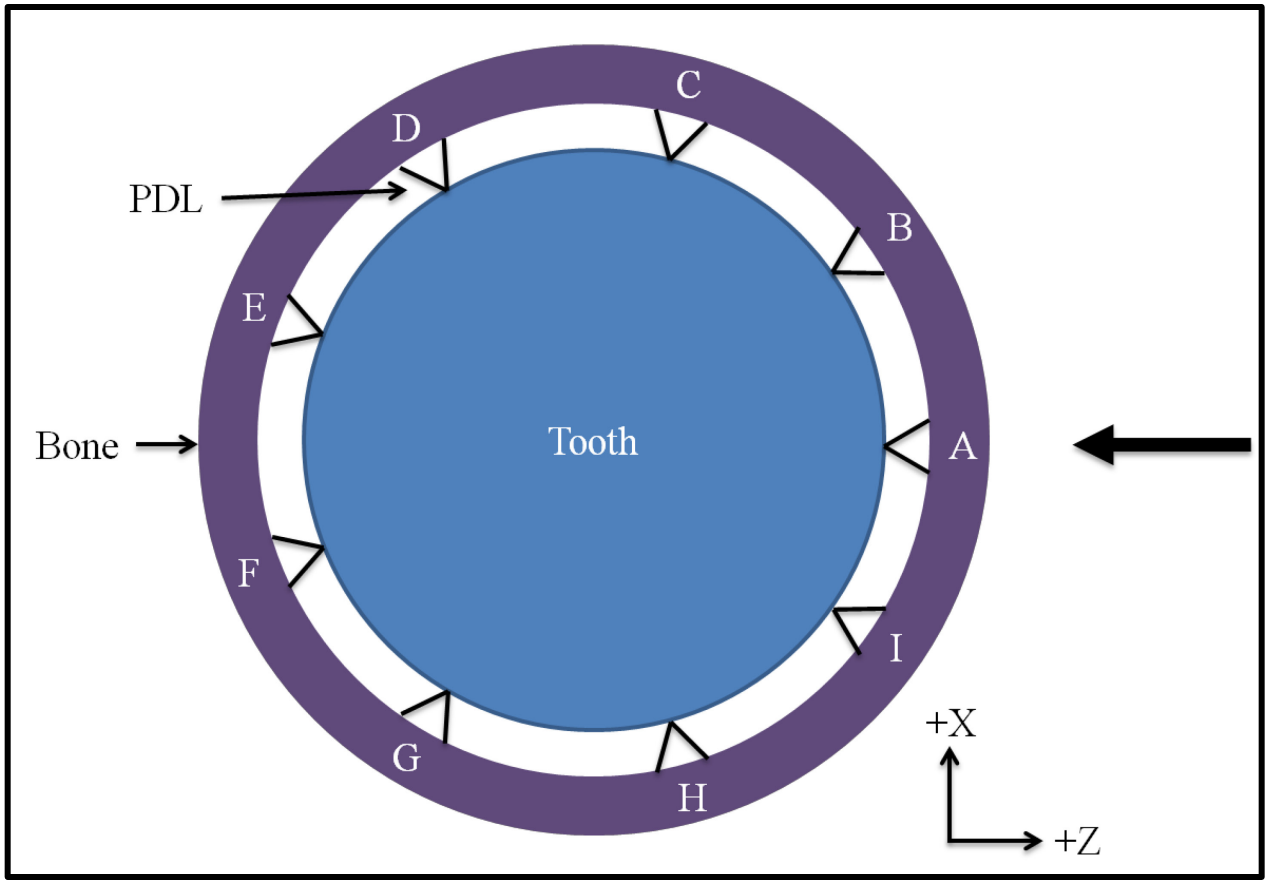

Figure 4-2. Diagram of the FEA model in the horizontal plane. Fiber bundles in both the 30° and 60° model were kept in the same arrangement in the horizontal plane. The fibers are a uniformly spaced spoke arrangement. The number and organization of fiber bundles is based on histological investigations of the *Neovison vison* first mandibular premolar. The horizontal direction of the lateral loading scenario is indicated by the arrow.

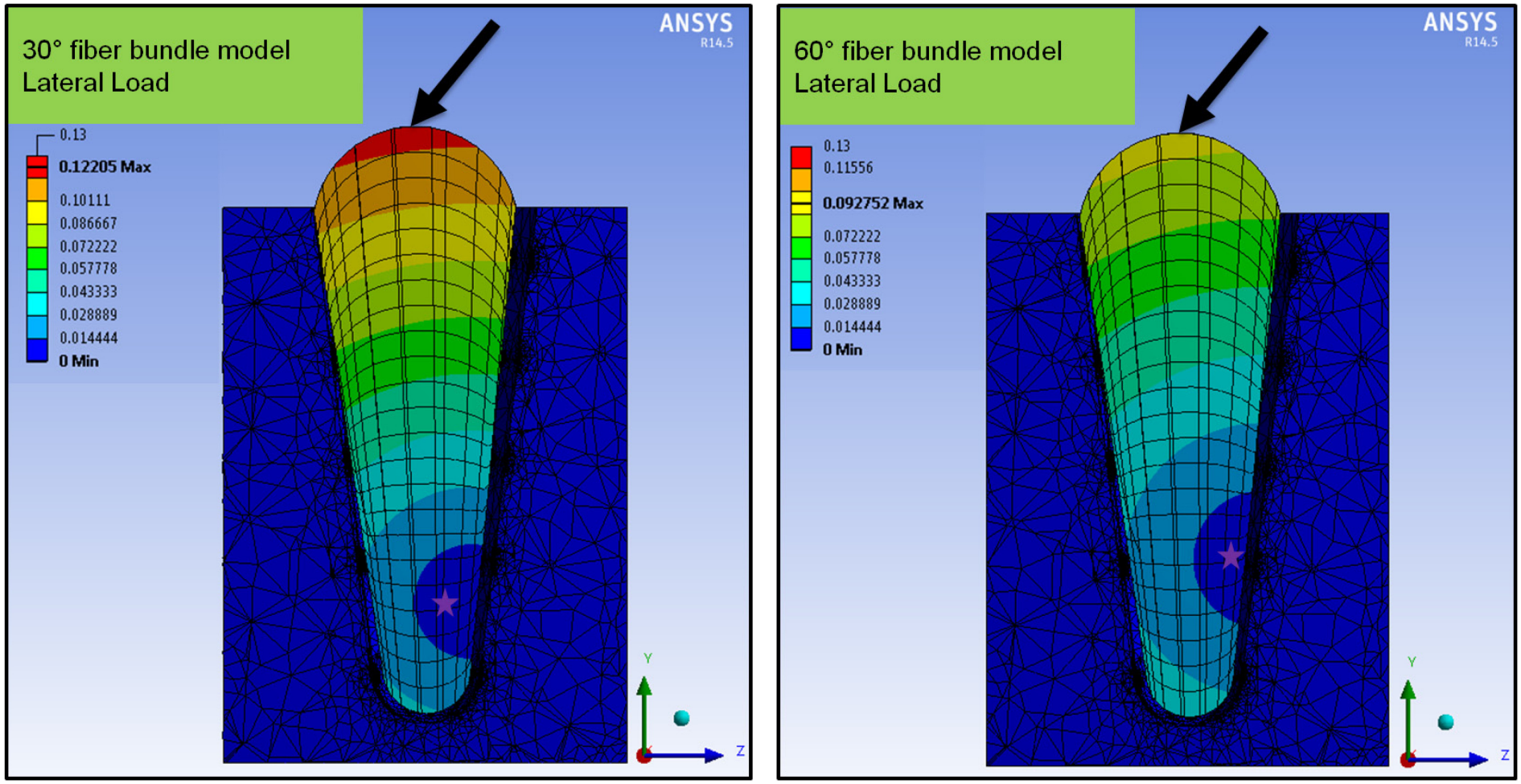

Figure 4-3. Rotational movement of the tooth under horizontal loading. The area of least motion (indicated by the star) moves up the tooth as fiber angle increases. Angle of applied load is indicated by black arrow. Scale shows absolute displacement in mm.

Chapter 5: The Comparative Periodontium

Introduction

Many orthodontic and restorative dentistry research studies are carried out on non-human animals. It is known that the chewing behavior and temporomandibular joint (TMJ) of commonly studied species may not closely mimic those of humans (Herring, 2003). It is unclear how much variation there is in periodontal ligament (PDL) morphology among the different species used in animal research and how those differences may be related to biomechanical function. The PDL is a connective tissue that links the tooth to the surrounding alveolar bone, and its morphology is relatively understudied, especially in a comparative sense. Much research has been done on isolated species to establish material properties of the periodontium (see Chapter 1). However, the morphology of the PDL has not been studied in a systematically comparative way. Detailed PDL architecture is not known outside of humans, two notable exceptions being the horse (Staszyk and Hagen, 2004; Staszyk et al., 2006) and rat (Carter and Sloan, 1994; Komatsu et al., 2002; Komatsu and Viidik, 1996) but even those two studies do not evaluate the PDL from more than one plane. A lack of information regarding PDL morphological attributes, or a misunderstanding of its morphology, may result in the choice of improper animal models.

Animal models will always play a large role in oral research but one must determine whether a given model is appropriate for a project based upon a detailed understanding of the anatomy. The goal of this study is to gain increased insight into the arrangement of PDL fibers within the PDL space for three species that are commonly used as research animals: the mink, an

obligate carnivore; the rabbit, an herbivore and the mouse, an omnivore (Figure 5-1). The PDL is very important for maintaining proper occlusion and alveolar bone volume. Its disruption, for example in cases of severe periodontitis, can lead to catastrophic tooth and bone loss; in the case of dental implants the lack of PDL can result in alveolar bone loss and loss of the implant itself. Animal models are often used to investigate these responses, a clearer understanding of the variety in initial PDL morphology may help inform future studies.

The Mink. The American Mink (*Neovison vison*) is native to North America but is found worldwide due to its popularity as a farm commodity (Bonesi and Palazon, 2007; Mason et al., 2001). The mink used in this project were farm raised and most likely subsisted on beef by-products, tripe, fish, liver, and cereal (Hartsough and Burger, 1965), although the exact diet is unknown. Farm-raised *N. vison* are somewhat larger and heavier than wild *N. vison* but are not different in the context of the biomechanics of their bite (Scapino, 1976). A *N. vison*'s diet in the wild primarily consists of small mammals, frogs, invertebrates and fish. *N.vison* are also known to consume birds and the eggs of birds (Brzezinski, 2008; Brzeziński and Romanowski, 1996; Brzezinski and Żurowksi, 1992). *N.vison* have been observed to eat animals near to their own body size, or larger, although it is not clear if this a seasonal necessity or common behavior (Korschgen, 1958). Unlike large carnivores that commonly bolt large chunks of food, *N.vison* thoroughly masticates what is eaten (Korschgen, 1958). When eating large items, the head is seen to bend to the side, and the premolars and carnassial are used to pick up the food; forepaws are not used to aid this process (Valentin, 1996).

Masticatory muscles in carnivores are highly developed, and their scissor-like bite aids in separation of flesh from bone in their prey. The TMJ is elongated mediolaterally and nearly

circular in cross-section (Valentin, 1996). During biting, the tight TMJ restricts biting motion to a primarily up-down rotational movement (Dyce et al., 2009). While the translational aspect of the *N. vison* bite is very constrained, they do have a moveable symphysis, which allows for some adjustment of carnassial contact when the canines are not in contact (Scapino, 1981; Valentin, 1996). They also have a very strong maxilla and mandible and exhibit rather large muscles, which results in very strong occlusion at the carnassial (Christiansen and Wroe, 2007; Greaves, 1983). The constrained TMJ arrangement combined with strong muscles of mastication allows *N.vison* to be capable of a wide, rapid and powerful opening of the jaws (Scapino, 1976).

The Rabbit. European rabbits (*Oryctolagus cuniculus*) have been introduced by humans widely around the world. In the wild, *O. cuniculus* are generalized herbivores; they subsist on a diverse diet of grasses, leaves, tree bark, roots and buds. They can also be a crop nuisance, eating lettuce, root vegetables, and grains (Macdonald and Norris, 2001; Nowak, 1999). They practice coprophagy as a method to extract essential nutrients out of a low nutritional value diet (Macdonald and Norris, 2001). The New Zealand white rabbits used in this study were farm-bred and lab-raised, primarily on a standard laboratory rabbit diet.

O. cuniculus have jaws specialized for an herbivorous diet. Similar to ruminants, rabbits have increased jaw mobility in the transverse plane, allowed by a specialized TMJ morphology (Herring, 2003). The rabbit has an antero-posterior component to the bite, but with a rounded condyle, they also demonstrate lateral movement (Herring, 2003). The lateral component of the bite is observed during the closing phase (Ardran et al., 1958; Morimoto et al., 1985). The mandibular symphysis in rabbits is un-fused but immobile, and they exhibit one-sided chewing (Ardran et al., 1958; Herring, 2003). Unilateral chewing combined with a non-moveable

symphysis allows a horizontal force to be produced by the masticatory musculature (Smith and Savage, 1959; Weijs, 1975). Efficient grinding is also achieved through the inclined plane formed by the rabbit molar teeth, which controls the direction of the power stroke (Herring, 1995).

The Mouse. The mouse (*Mus musculus*) is native to Western Europe, southwestern Asia, Africa and the Americas. *M. musculus* are commonly found in association with human settlement. Although omnivorous, they do primarily feed on plant material (Nowak, 1999) and the evolution of the characteristic mouse dentition and myomorphic masticatory muscle arrangement is thought to be the result of the selection pressures of a vegetarian diet (Landry, 1970). They exhibit coprophagy, similar to other non-ruminant herbivores (Macdonald and Norris, 2001). The laboratory mice in this project were captive bred and consumed a standard laboratory rodent diet. When eating, food is generally held in the forepaws and ingested via the anterior part of the oral cavity. The bolus is then transported to the posterior part of the mouth with small-amplitude jaw movements and then is chewed with large-amplitude jaw movements (Kobayashi et al., 2002).

The mouse TMJ design is highly specialized for extensive protrusive movements, much more so than the rabbit. The mandibular condyle travels in a trough-like articular (glenoid) fossa. The power stroke is in the protrusive direction and exhibits only a minor medial component. During the chewing cycle, the jaw moves forward in the initial opening phase where it is protruded. Then the mandible is retruded to its most posterior position in the jaw-closing phase (Koga et al., 2001). Inclined tooth rows guide the gliding power stroke; a slight transverse rotation increases grinding efficiency and utilizes the protrusive components of the bite (Weijs

and Dantuma, 1975). The rami spread apart during biting, and a moveable symphysis facilitates simultaneous chewing on both sides of the mouth (Weijs, 1975; Weijs and Dantuma, 1975).

Predictions. The collagen fibers in the PDL are arranged into bundles. The angle between these bundles and the attachment surface of the tooth is readily identifiable under magnification. In humans, this angle is about 30º (Raspanti et al., 2000), in rats it averages 61º (Komatsu and Viidik, 1996) and in cows it approximates 50º (Pini et al., 2004). In the herbivore and omnivore (*O. cuniculus* and *M. musculus*), I hypothesize that the mechanical demands of a horizontal component to the bite force will optimize structurally using a more lateral PDL bundle arrangement; i.e, a relatively obtuse angle similar to the rat or bovine. I expect that *N.vison* PDL bundles should exhibit a relatively steep angle, perhaps less than 30°, due to the majority of force on the tooth being vertical. These predictions are the result of the mathematical model constructed in previous work (Fig. 4-1, Chapter 4).

PDL organization in the horizontal plane is primarily thought to universally have a crossed fiber arrangement (Fig. 5-3), which is observed in humans (Sloan and Carter, 1995). However, results from the mathematical model in Chapter 4 indicate that fibers normal to loading in the horizontal load condition are relatively un-strained, while those in-line with the load are highly strained. It is expected therefore that the species with a strong horizontal component to their bite, *O. cuniculus* and *M. musculus*, will predominantly have fibers in line with the direction of load application (transverse for *O. cuniculus* and antero-posterior for *M. musculus*), in lieu of a crossed fiber orientation (Fig. 5-3).

In addition to testing hypotheses regarding bundle angle and organization, more general information will be gathered, including PDL space width in two planes and individual PDL

bundle widths. All of these data are intended to further our understanding of PDL morphology in a comparative sense.

Methods

Specimens. Euthanized wild-type *M. musculus* specimens (n=8) were obtained using the University of Washington Department of Comparative Medicine rodent exchange service (http://depts.washington.edu/compmed). *N. vison* (n = 10) used in this project were preserved laboratory specimens (Carolina Biological Supply, Item 228250). *O. cuniculus* specimens (n = 11) are the control rabbits from a previous experiment (Rafferty et al., 2012). No live animals were specifically harvested for this project. Rabbits were all female, 6-9 months of age. Sex and age were unknown for the mink and mouse specimens, but all were adult. Mandibles were fixed in a 10% formalin solution and then decalcified in a 10% formic acid solution. The left or right mandible for each animal was randomly designated for coronal or horizontal sectioning, resulting in equal numbers for each case. The specimens were then paraffin embedded and sectioned at 10μm.

For analysis of the horizontal plane, serial sections of the middle third of the length of the first molar roots were analyzed. In the coronal plane, molar sections that included the pulp canal were used for analysis. In specimens with a multi-rooted first molar the anterior root was used. All sections were Sirius red stained (Junqueira et al., 1979) and photographed under polarized light at 10x magnification for *N. vison* and *O. cuniculus*, 20x for *M. musculus*.

PDL angle measurements were taken on only on coronal sections, using the long-axis of the tooth as the reference plane. PDL width measurements were taken in both the coronal and horizontal plane and were obtained by measuring the smallest distance between the cementum

and alveolar bone. PDL bundles were defined as clusters of fibers with clear black background space on either side; bundle width was measured at the mid-point of the bundle length as it crossed the PDL space (Fig. 5-5). Bundle width and PDL space width did not vary significantly in the two planes (t-test, $P>0.05$ in all cases), so the data taken from the two planes were combined to produced average values for each specimen. PDL space width around the tooth was measured in four directions: anterior, posterior, buccal and lingual, in the horizontal sections. A normalized PDL variable was also computed (space width/root diameter*100) to establish the relationship between tooth size and PDL space width. When necessary for measurements, photographs were stitched together to create whole-tooth panoramas using AutoPano Giga (V2.0.1 Kolor). All measurements were taken using ImageJ (NIH).

Statistical Methods. PDL width and bundle width were each compared among species using ANOVAs and post hoc Tukey's HSD tests. The four measurements of PDL width in the horizontal plane were compared, within each species, also using an ANOVA with post-hoc Tukey's HSD tests. The four directions were then combined to represent the two planes of movement: antero-posterior (A-P) and bucco-lingual (B-L); these were compared using student's T-tests. A Boneferroni correction was used in all post-hoc testing.

PDL bundle organization was classified into one of three categories: Crossed, where the fibers took a more angled approach and were often overlapping each other (Fig. 5-11), Direct, where the PDL fibers were approximately in line with the anatomical quadrant arranged primarily A-P or B-L (Fig. 5-13), or Undefined, where individual fibers could not be discerned, or their orientation was unclear (Fig. 5-13). As a result of damage during thin sectioning, some specimens were unclassifiable in one or more quadrants. In the case of obvious tearing or folding

of the structures in question individual quadrants were excluded from the analysis, but any intact measurable quadrant was included. A Chi-square test was used to determine if fiber organization classification varied among the quadrants in each species, and to establish whether or not overall fiber organization pattern was different among the three species. Analyses were carried out using PASW 18 (Polar Engineering and Consulting).

Results

Overall morphology. Overall, *N. vison* and *M. musculus* teeth exhibit similar PDL space shape in the coronal plane (Figs. 5-4, 5-5, 5-6, 5-7) with the PDL space continually widening from the tooth crown to the root apex. In contrast, the width of the PDL space of *O. cuniculus* was generally consistent along the length of the tooth (Figure 5-8, 5-9). Bundled PDL fibers were seen in all three species, but the width of those bundles was highly variable (Figs. 5-5, 5-7, 5-9, Table 5-1).

In the horizontal plane, the PDL architecture was very different in *N. vison*, compared to the two herbivores. In *N. vison*, the bundles exhibited an overlapping spoke or basket weave pattern similar to what has been described in the literature for humans (Sloan and Carter, 1995) (Figs. 5-10, 5-11). *M. musculus*, however, exhibited more of a direct tooth-to-bone connection with most individuals showing strong organization of the PDL in the A-P direction and less so in the B-L direction, with very little overlapping of fiber bundles (Figs. 5-12, 5-13). *O. cuniculus* showed a mix of *M. musculus* and *N. vison* patterns, with a direct connection around most of the tooth but a more complex woven pattern along the posterior side of the molar (Figs. 5-14, 5-15).

PDL Width. PDL width did not vary significantly among species (P = 0.203). Normalizing the PDL width by the molar root size of each specimen, however highlighted significant differences in relative PDL width ($p < 0.001$) The *N. vison* PDL is 6% the width of the tooth, the *O. cuniculus* is 10% and the *M. musculus*, 22% (Table 5-2).

PDL Space Width Distribution. *N. vison* showed no difference in PDL space width among the four anatomical directions ($p = 0.66$). *M. musculus* did show a significant difference; the lingual region had the thinnest PDL space (Table 5-2). To investigate the specific question of directional jaw movement, the width measurements were averaged into two groups: Antero-posterior (A-P) and Bucco-lingual (B-L). In this analysis, *N. vison* still showed no significant difference ($p = 0.20$), although there was a tendency for A-P widths to be greater (A-P = 0.21mm B-L = 0.19mm). The mouse showed no significant difference when the regions were grouped, losing the statistical significance of the smaller lingual quadrant ($p = 0.09$).

The regions of the *O. cuniculus* PDL space were more difficult to compare due to the lobed nature of the evergrowing tooth (Figure 5-14), PDL space was measured at the long axis of each lobe and averaged to produce buccal and lingual measurements. An ANOVA indicated differences among the four anatomical directions ($p = 0.01$). Post-hoc t-testing indicated a wider PDL in the B-L orientation compared to A-P ($p = 0.012$), primarily due to the lingual side being much wider when compared to the posterior side ($p= 0.002$, Table 5-2).

PDL Bundles. In *N. vison*, the PDL was generally less overtly bundled in the coronal plane than in the other two species, with larger stretches of continuous PDL (Figure 5-5, 5-7, 5-9). When bundles were observed, they were often quite wide in the coronal plane, very wide

compared to the two herbivore species ($p < 0.001$, Table 5-1) which both had more clearly distinct bundling patterns in both planes. In the case of the *O. cuniculus*, bundles were distinct; however close to the tooth, they merged into a thick vertically-oriented layer. In all cases, there was very large variation in bundle width, with complete overlap in widths between all species; however, the *N. vison* demonstrated the highest variability (Fig. 5-16).

Bundle angle was significantly different in the three species ($p < 0.001$, Table 5-1). Post-hoc testing indicates that all three species were actually significantly different from each other ($p = 0.025$).

Bundle organization classification was different among the three species (Table 5-3, $p = < 0.001$). *N. vison* overwhelmingly presented crossed PDL bundles, while *M. musculus* and *O. cuniculus* had a more mixed type of organization. In general *O. cuniculus* showed crossed fibers predominantly in the posterior region of the molar and direct connections in the other three regions. The mouse exhibited predominantly direct fibers in the A-P orientation; however these differences in distribution of PDL fiber bundle organization were not statistically significant (Table 5-4).

Discussion

N. vison. The relatively acute PDL angle seen in *N. vison* was predicted successfully (Table 5-1). The basket weave pattern seen in the PDL fiber bundles of *N. vison* may provide an advantage to resisting rotational forces (Sloan and Carter, 1995); the scissor-like bite and tall crown of the *N. vison* molar may result in considerable torsion of the tooth root. The crossed arrangement enables the collagen fibers to be under tension, (hence load bearing) value (Gordon, 1978; 1984) for any given torsional load.

Irregular distribution of PDL space is seen in the horizontal plane of *O. cuniculus* and *M. musculus*, but not in *N. vison*. *N. vison* also shows the smallest absolute PDL width. This is surprising because the *N. vison* tooth is approximately three times the size of the corresponding *M. musculus* tooth. The width of the PDL space does not seem scale with body or tooth size (Table 5-1). It is interesting that the *N. vison*, which are known for their large bite force relative to body size (Radinsky, 1981), has the narrowest PDL space in the mid-region of the tooth. Because the PDL space allows tooth mobility (Bondevik, 1984) the narrowness implies that horizontal movement is limited in *N. vison*. Perhaps the strong rapid bite of *N. vison* (Greaves, 1983) would be impeded by a highly moveable tooth in the horizontal plane. A too-mobile tooth might result in tip-to-tip crown contact when biting, which would be highly likely to cause tooth damage. A narrow PDL might help to maintain tooth stability in lateral directions, while retaining vertical mobility to the extent available at the apex of the tooth.

PDL bundles in the coronal plane vary widely in *N. vison* (Table 5-1, Fig. 5-16). In some regions, the PDL is nearly continuous. This implies a larger relative ligamentous component compared to the other species. Since the mechanical function of the PDL is to distribute occlusal force to the alveolar bone, perhaps the increased fiber content of large bundles is advantageous to load distribution. Although PDL fiber density was not measured in this study, that would be an interesting avenue for future work.

M. musculus. It was confirmed that *M. musculus* has a more obtuse fiber angle in the coronal plane than the mink. The predictions of horizontal PDL fiber organization hold true in this species. However, it does not have as obtuse an angle as *O. cuniculus*. In the case of *M. musculus*, rotation of the tooth does not seem to be an issue, as the PDL fibers are arranged

essentially perpendicular to the tooth surface in the A-P plane. This would seem to indicate that the forces seen at the tooth root are primarily in line with the chewing stroke, with no strong rotational component. The continuous molar tooth row and multi-rooted tooth may itself restrict rotation around the root axis. Studies of the horse periodontium also show this direct fiber arrangement although directionality is unclear (Staszyk and Hagen, 2004).

It would appear that the *M. musculus* PDL space is quite large compared to the tooth size, compared to *O.* cuniculus, and especially to *N. vison*. PDL space width is known to change due to age (Leong et al., 2012), diet hardness (McCulloch et al., 2000; Niver et al., 2011), disease (Auluck, 2014) and orthodontic loading (King et al., 1991; Verna et al., 1999). Of these diet hardness only is relevant here. Considering the small size of the jaw in mice, rodent pellets are probably rather hard. Further, the horizontal component of the chewing behavior may lead to an enlarged PDL space, meaning that the directionality of chewing has some effect on PDL width. The widest areas of the *M. musculus* PDL space did seem to correlate with the primary A-P chewing direction. A wider PDL space, in general, may be advantageous to effectively distribute the occlusal force, or alternatively, the movement of teeth during chewing enlarges the space in the direction of movement.

O. cuniculus. Although not essential to the hypothesis, *M. musculus* and *O. cuniculus* were expected to have a similar PDL angle; however, *O. cuniculus* exhibits a more obtuse angle (Table 1). Since *O. cuniculus* are strict herbivores, as opposed to *M. musculus*'s omnivory, rabbits presumably more regularly rely on the strong lateral component to their bite with less importance for vertical loads. A more flexible diet in *M. musculus* may result in variable

chewing patterns, but the consistent grinding of *O. cuniculus* is reflected in more horizontally oriented PDL fibers.

O. cuniculus PDL exhibits a complex arrangement that was highly variable among individuals, most likely due to the lobed nature of the molar and the fact that these molars are ever-growing. The arrangement of the PDL fibers in the *O. cuniculus* seems to be strongly influenced by hypselodonty (See also Chapter 6). The lobed nature of the tooth may result in complex mechanical situations, an idea supported by the observation of a mix of fiber arrangement types in the horizontal plane. A basket weave architecture in the posterior region of the molar may indicate some rotational forces at the root. Buccally and lingually, direct fiber arrangements were observed, as expected, but there were also direct fibers anteriorly. Those three regions also showed wider PDL space than the posterior region, suggesting these are the major directions of mobility.

Although PDL fiber density was not directly measured in this study, all species seem to have a high density of fibers inserting on the tooth, but for the *O. cuniculus*, the insertion into bone is neatly organized into sparse, distinct bundles (Fig. 5-9).

Limitations and future work. Serial histology is very time consuming and destructive. The enamel layer running the length of the *O. cuniculus* root was particularly confounding, especially during sectioning. During the decalcification process, enamel is removed, leaving a gap between tissues in the specimens. This gap would sometimes result in shifting of the tooth during sectioning. For those reasons, the sample size here is small. The sample size is made even smaller by the goal to evaluate the PDL in both the horizontal and coronal plane. The sagittal plane is not addressed here, since it would have resulted in further splitting of the sample.

In future work, it would be interesting to see any differences in the sagittal versus coronal plane between *O. cuniculus* and *M. musculus*.

Standard polarized histology is a two-dimensional methodology. A three-dimensional approach to PDL architecture investigation would be ideal. Serial histological sections can be integrated to create a three-dimensional representation of the specimen, but the methodology is complicated and not always successful (Ourselin et al., 2001). Confocal microscopy of thick sections can also be done, but this is still destructive and limited to slices less than a mm in thickness. The PDL has been visualized using micro-computed tomography (microCT), and as CT resolution and computing power increase, this technology may make non-destructive analysis of PDL morphology a viable option (Naveh et al., 2013).

Overall, this study raises some questions about the relationship between periodontal ligament space width and PDL fiber density. Further investigation into this question is required as it cannot be answered with the current sampling. Ideally, PDL space width should be compared among several obligate carnivores to determine if the narrow PDL space in the *N. vison* is an attribute of carnivore chewing behavior or a species specific trait. In the future, an attempt to quantify PDL fiber density along the entire tooth root may provide insight into the narrowness of the *N. vison* PDL.

Future work into the relationship between PDL width, bite force and diet would address some of the differences in PDL morphology seen in these species. A further comparison of different herbivores, both small and large bodied, would allow insight into overarching patterns of PDL architecture. Also, development of a non-destructive method of morphological analysis would greatly expand the range of specimens available and reduce the manpower required to carry out studies such as these.

Conclusions. The architecture of the PDL in the coronal and horizontal plane observed here is supported by work in Chapter 4. PDL bundle angle was different among the species studied, with the carnivore demonstrating the steepest bundle angle, as predicted. *M. musculus* and *O. cuniculus* were not predicted to differ in angle, but in fact, *O. cuniculus* demonstrated a more obtuse angle. PDL fiber bundle organization in the horizontal plane also varied among species, with *N. vison* exhibiting primarily crossed fibers while the other two species had more direct fibers.

Table 5-1 . Average values and standard deviation for bundle width and angle in the coronal plane. See methods and Fig. 5-5 for description of bundle width definition and measurement. Significance for one-way ANOVA reported.

Species	PDL Bundle Width (mm)	PDL Bundle Angle	N
Mouse	0.09 ± 0.01	49.1 ± 6.77	5
Mink	0.14 ± 0.03	37.4 ± 8.53	5
Rabbit	0.05 ± 0.02	58.6 ± 12.32	6
P-value	< 0.001	< 0.001	

Table 5-2. Average values and standard deviation for PDL width in the four anatomical quadrants and species averages. Measurements are in mm. Significance for one-way ANOVA are shown in italics. Normalized PDL width is the PDL space width divided by the root diameter.

Species	N	Anterior	Posterior	Buccal	Lingual	Quadrant ANOVA P-value	PDL Space Width (mm)	Normalized PDL Width (%)
Mouse	5	0.18 ± 0.04	0.18 ± 0.04	0.18 ± 0.05	0.12 ± 0.03	*0.02*	0.19 ±0.04	22 ± 5
Mink	6	0.20 ± 0.05	0.23 ± 0.08	0.19 ± 0.07	0.18 ± 0.05	*0.66*	0.16 ±0.02	6 ± 1
Rabbit	5	0.13 ± 0.02	0.09 ±0 .02	0.13 ± 0.03	0.17 ± 0.05	*0.01*	0.19 ±0.01	10 ± 2
P-value		*0.02*	*0.001*	*0.03*	*0.07*		*0.203*	*<0.001*

Table 5-3. Response table for overall species difference in PDL bundle organization category. Observations from all anatomical quadrants were summed to produce species observations. X^2 significance is reported in italics.

PDL Category	Mink	Rabbit	Mouse
Crossed	18	11	4
Direct	2	13	9
Undefined	0	4	7

$p < 0.005$

Table 5-4. Response table for PDL bundle organization category in the four anatomical quadrants for each species. X^2 significance for each species is reported in italics.

Mink	PDL Category	Anterior	Posterior	Buccal	Lingual
p = 0.5	Crossed	5	5	4	4
	Direct	0	0	1	1
	Undefined	0	0	0	0
Rabbit					
p = 0.6	Crossed	2	5	2	2
	Direct	4	1	4	4
	Undefined	1	1	1	1
Mouse					
p = 0.08	Crossed	0	1	2	1
	Direct	4	4	0	1
	Undefined	1	0	4	2

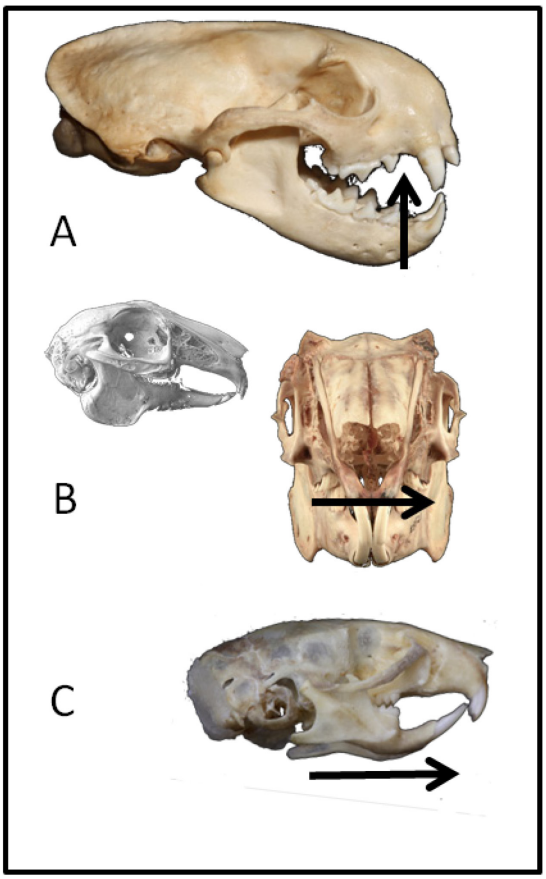

Figure 5-1. Comparison of skull morphology and primary chewing direction in the three study taxa. A) left lateral view of *N. vison*, B) left lateral and anterior view of *O. cuniculus* and C) left lateral view of *M. musculus*. Arrows indicate primary chewing direction.

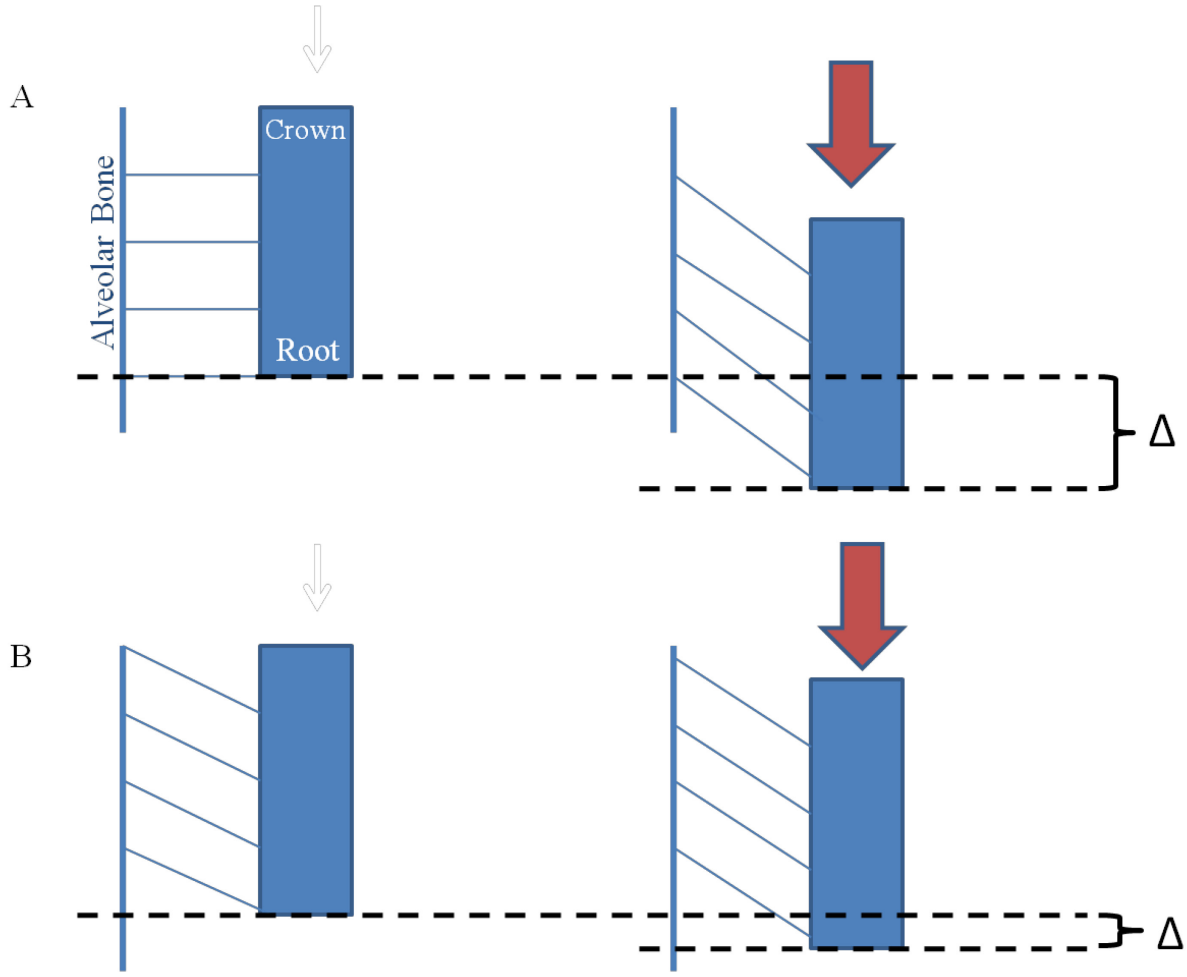

Figure 5-2. Predictions for PDL fiber bundle orientation in the coronal plane. Scenario A, an obtuse fiber angle (90° in this exaggerated case) may optimize strain levels in a primarily horizontal load, however vertical support is less, as indicated by the larger displacement of the tooth is much greater than a more acute fiber angle (Scenario B). Based on estimated tooth displacements in Chapter 4, the vertical chewer, *N. vison*, is expected to have a more acute PDL fiber angle while the horizontal chewers (*O. cuniculus* and *M. musculus*) will exhibit a more obtuse fiber angle.

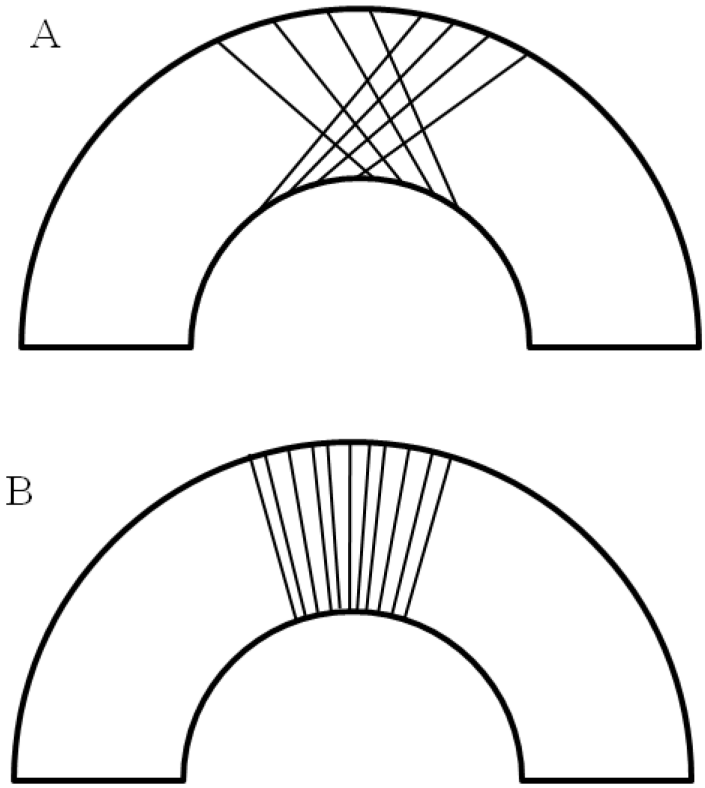

Figure 5-3. Predictions for PDL fiber orientation in the horizontal plane. A) commonly described PDL fiber orientation (Sloan and Carter, 1995). Arrangement of fibers assures that in primarily axial loading most fibers will be in tension, resulting in an evenly distributed load. B) a more direct, rather than crossed fiber orientation, expected in horizontal chewers, where mathematical modeling (Chapter 4) predicts little to no PDL fiber loading except in-line with the load application. Predictions for this experiment are that the mink PDL will be best described by A, while the mouse and rabbit will be more like B. However direct fiber orientation should be observed in different quadrants for the two horizontal chewers: A-P for mouse and B-L for rabbit.

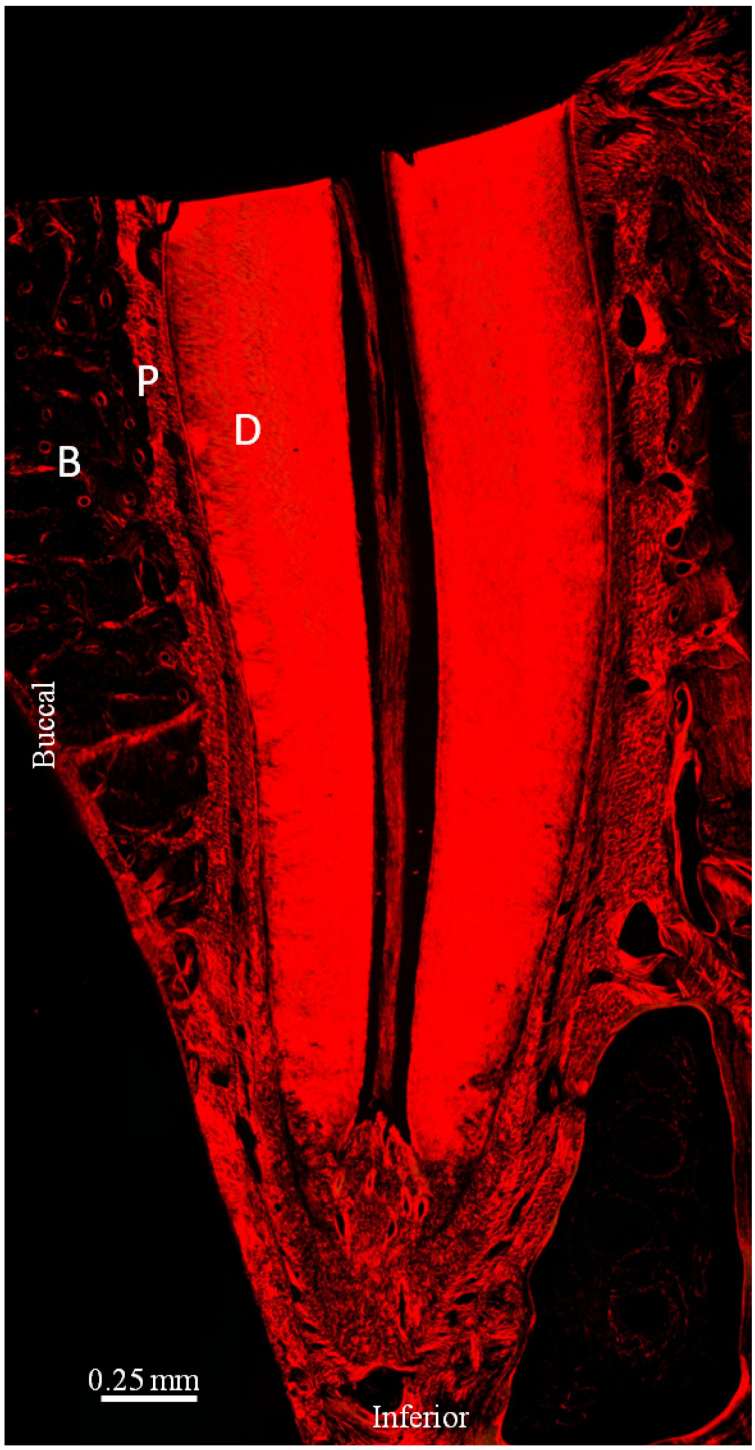

Figure 5-4. An overview of tooth root and PDL morphology in the coronal section in the mid-first molar region of *N. vison*. B) Alveolar bone, P) Periodontal ligament space, D) Dentin. Image is a panorama composed of individual photographs at 10x.

Figure 5-5.Detailed image of PDL fiber arrangement in the coronal plane for *N. vison*, 10x. Large variation in bundle width was commonly seen within a single specimen. Bundles are identified by brackets. In general bundle definition was groups of fibers, with clear black background on either side. Bundle thickness was measured at the middle of the PDL space, indicated by white line. B) Alveolar Bone, P) Periodontal ligament space, D) Dentin.

Figure 5-6. An overview of tooth root and PDL morphology in the coronal section in the mid-first molar region of *M. musculus*. B) Alveolar bone, P) Periodontal ligament space, D) Dentin. Image is a panorama composed of individual photographs at 20x.

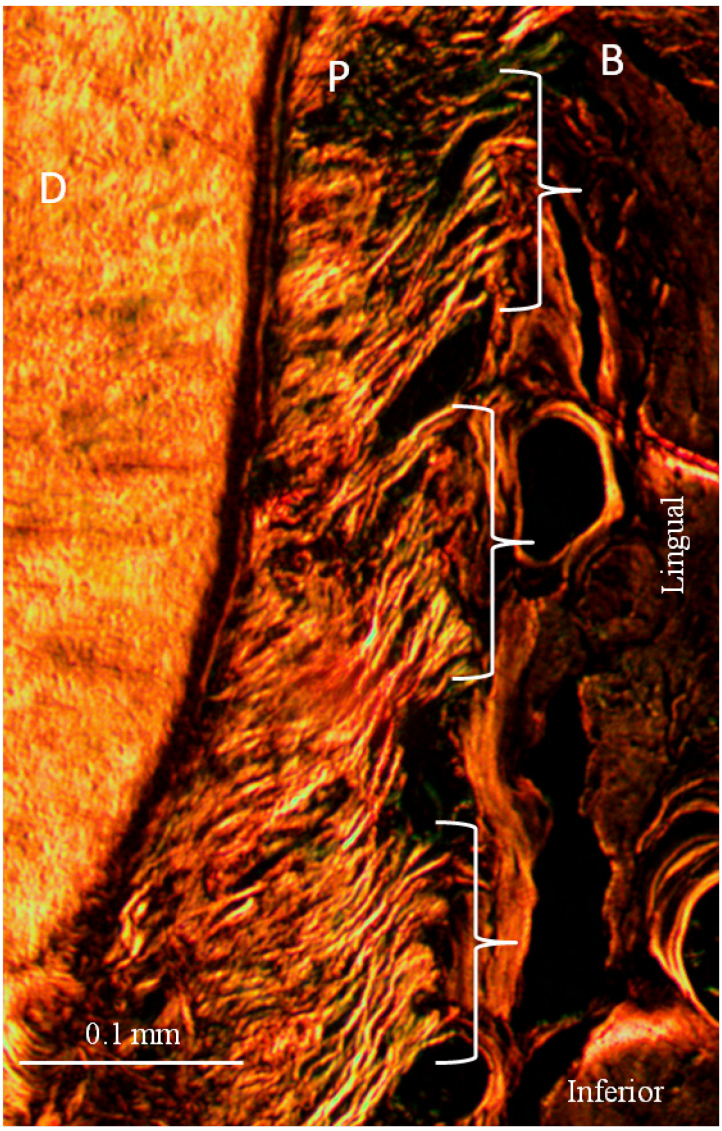

Figure 5-7. Detailed image of PDL fiber arrangement in the coronal plane for *M. musculus*, 20x. Uniformly sized, distinct PDL bundles were commonly observed, indicated by brackets. B) Alveolar bone, P) Periodontal ligament space, D) Dentin.

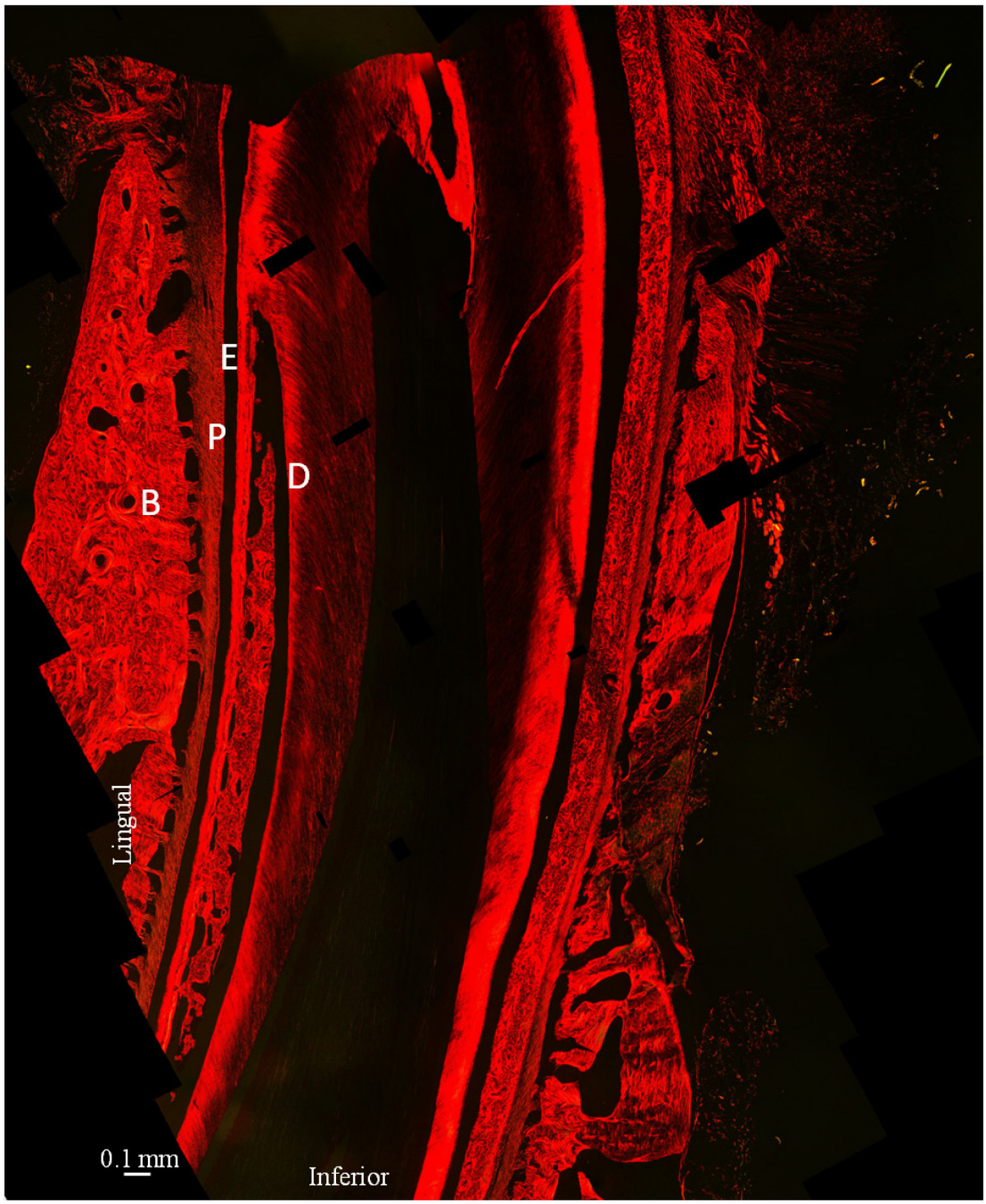

Figure 5-8. An overview of tooth root and PDL morphology in the coronal plane in the mid-first molar region of *O. cuniculus*. B) Alveolar bone, P) Periodontal ligament space, E) Enamel space D) Dentin. Image is panorama composed of individual photographs at 10x, black square voids are and artifact of unphotographed regions revealed during panorama creation.

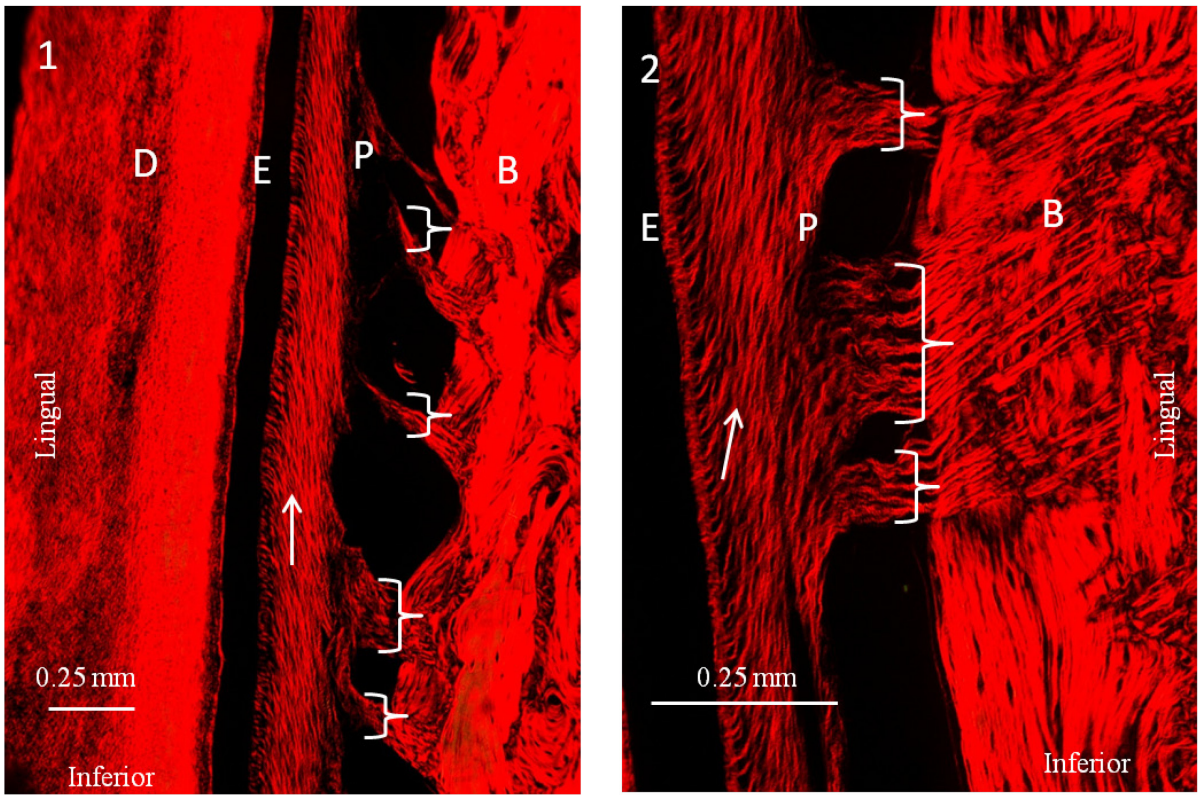

Figure 5-9. Detailed image of PDL fiber arrangement in the coronal plane for *O. cuniculus.* 1) Specimen 6685 left, 10x. 2) Specimen 6684 right, 20x. A relatively wide PDL space is observed with an obvious region of superior-inferiorly oriented PDL fibers, indicated by arrows. Additionally, small distinct PDL bundles are observed crossing the space to insert in the alveolar bone, indicated by brackets. B) Alveolar bone, P) Periodontal ligament space, E) Enamel space D) Dentin.

Figure 5-10. An overview of PDL morphology in the horizontal plane in the mid-first molar region of *N. vison*. B) Alveolar bone, P) Periodontal ligament space, D) Dentin. Image is panorama composed of individual photographs at 10x.

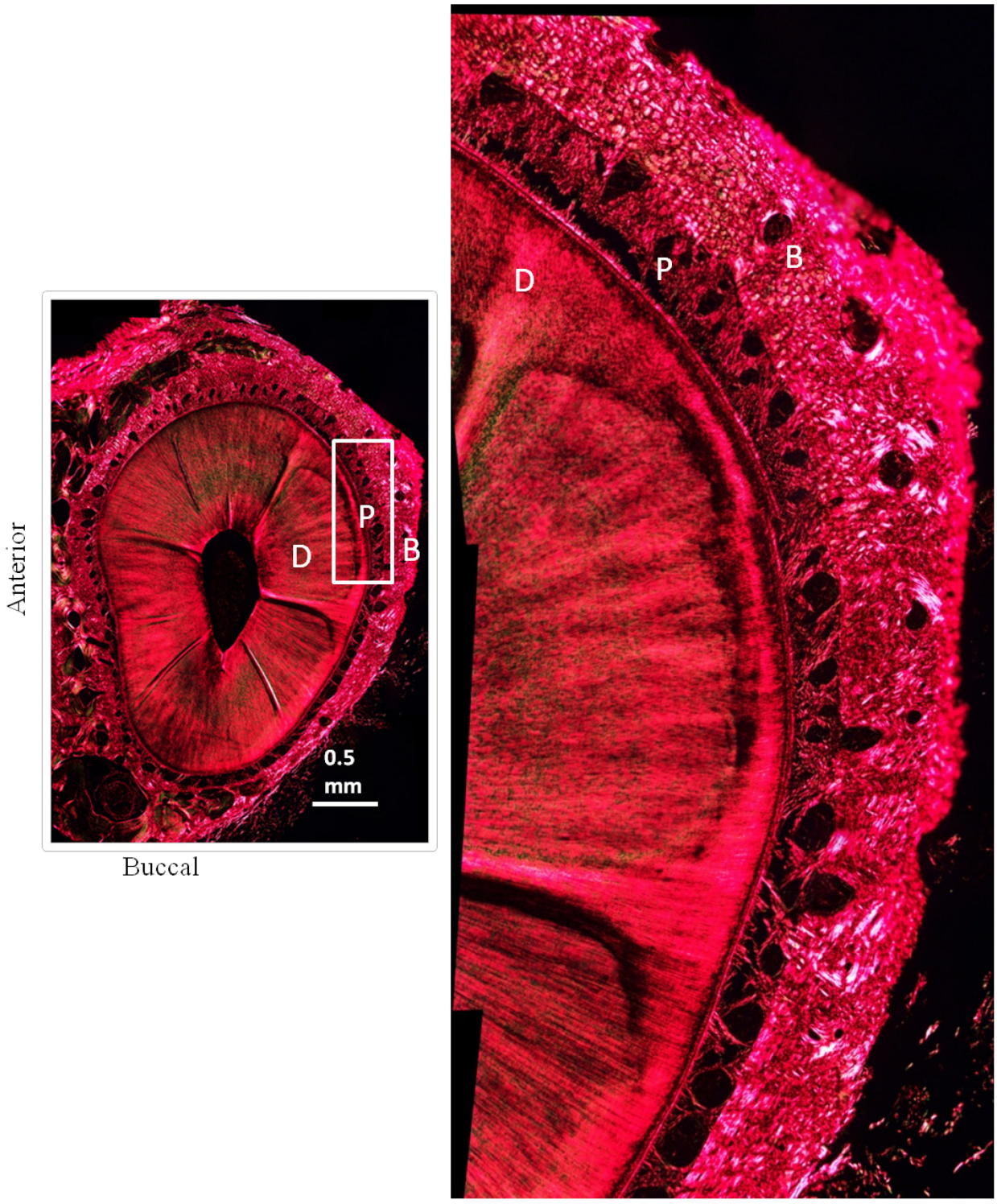

Figure 5-11. Detailed image of PDL fiber arrangement in the horizontal plane of *N. vison.* The white box indicates location of detailed image. Crossed PDL bundles were the predominant PDL fiber pattern, observed around the entire tooth in all anatomical quadrants.

Figure 5-12. An overview of PDL morphology in the horizontal plane in the mid-first molar region of *M. musculus*. B) Alveolar bone, P) Periodontal ligament space, D) Dentin. Image is panorama composed of individual photographs at 20x.

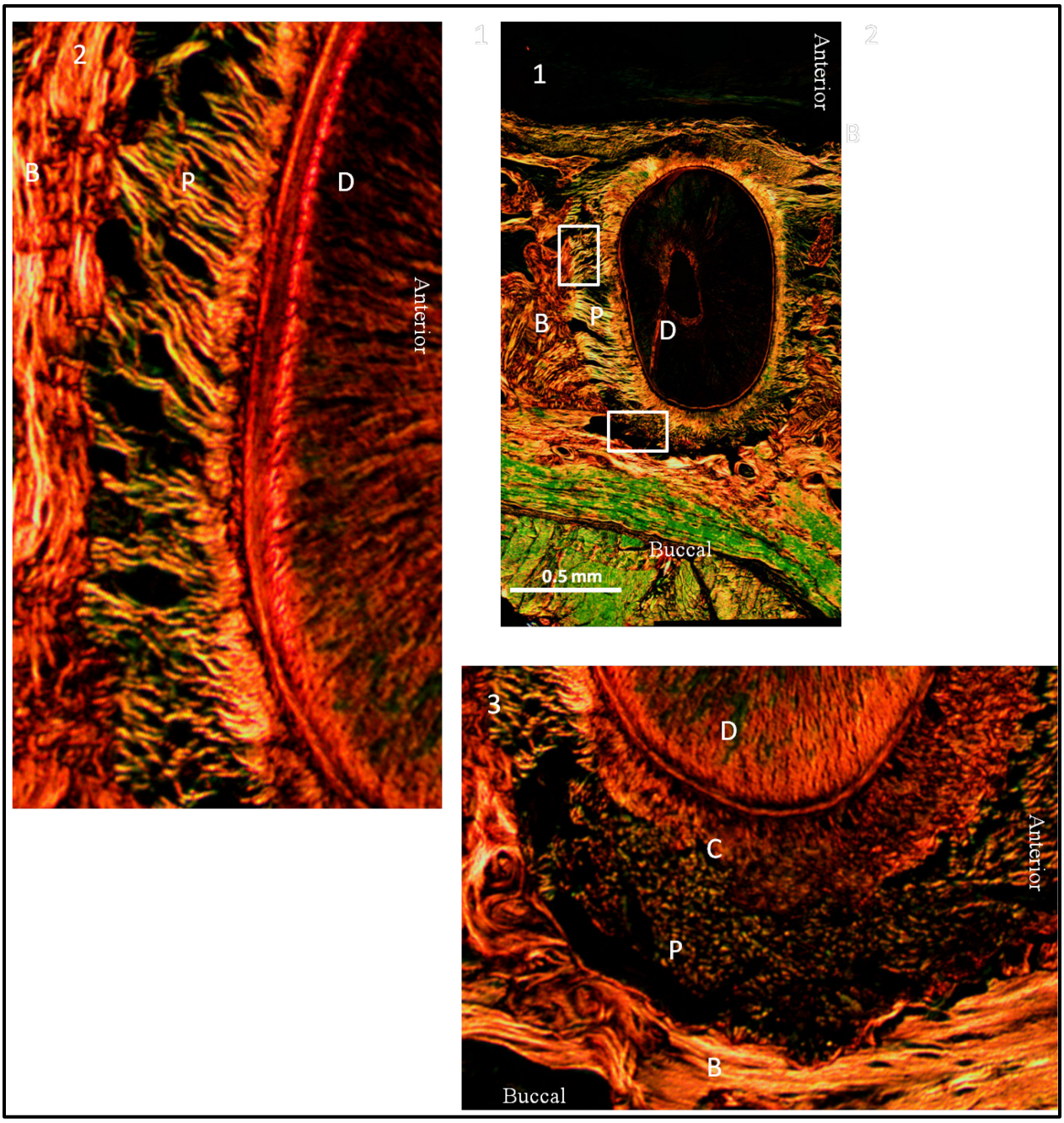

Figure 5-13. Details of *M. musculus* PDL morphology in the horizontal plane. 20x. 1) An overview of the mouse tooth orientation in the horizontal plane. 2) A direct anterior-posterior orientation was commonly observed. 3) The buccal and lingual sides were predominantly characterized by an undefined fiber organization and a thick cementum layer. B) Alveolar bone, P) Periodontal ligament space, C) Cementum, D) Dentin.

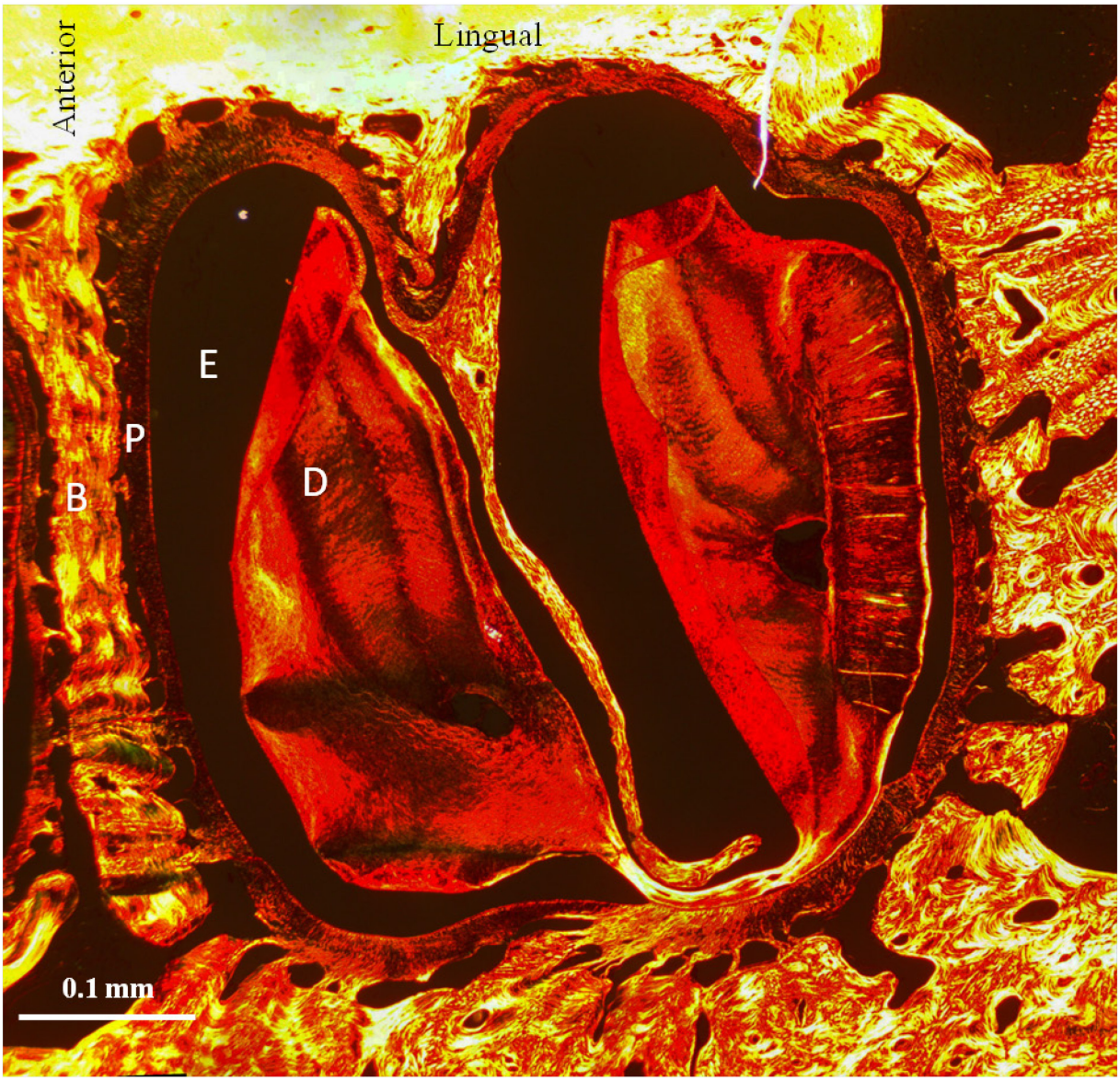

Figure 5-14. An overview of PDL morphology in the horizontal plane in the mid-first molar regions of *O. cuniculus*. B) Alveolar bone, P) Periodontal ligament space, E) Enamel space D) Dentin. Image is a panorama composed of individual photographs at 10x.

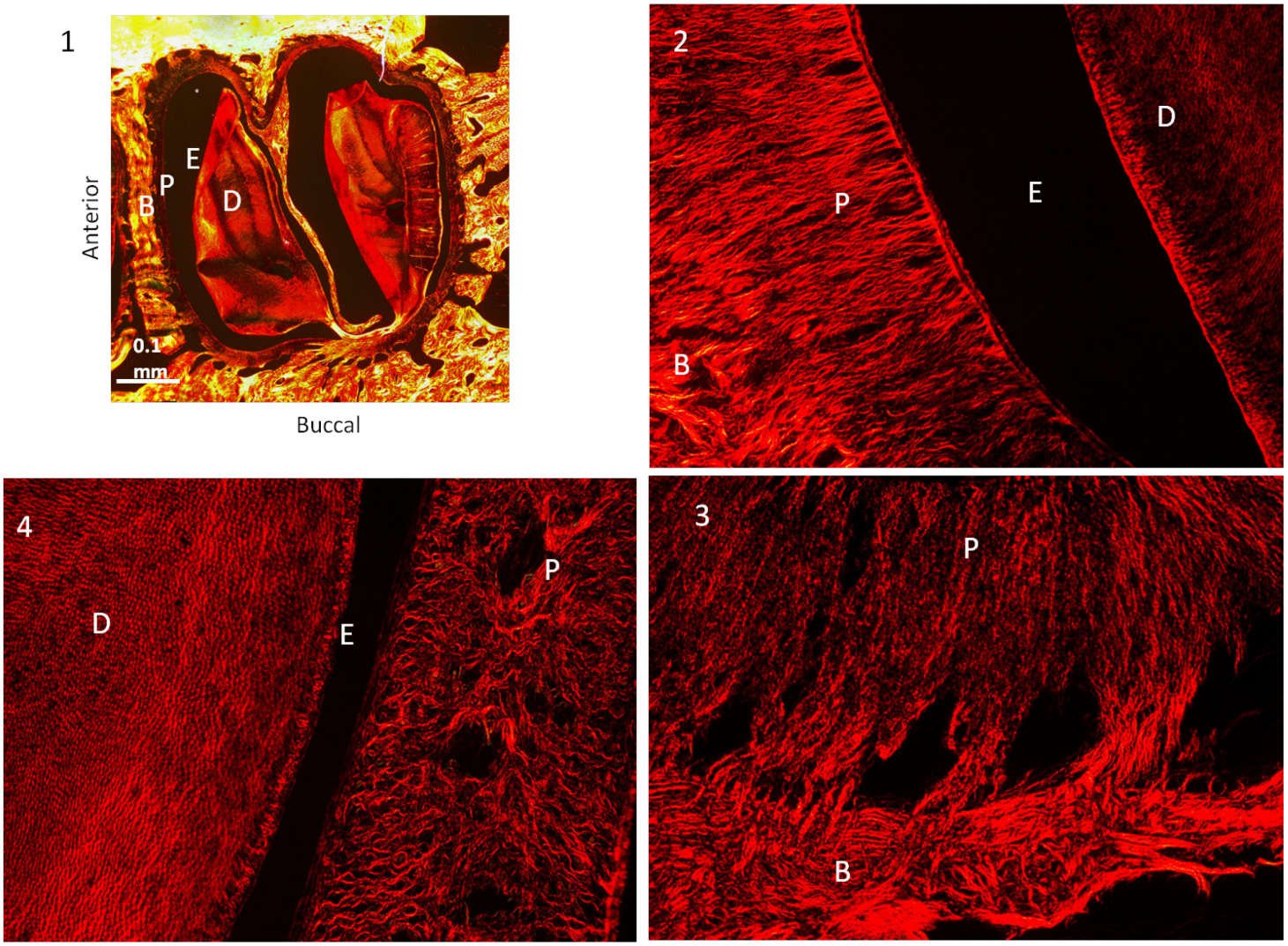

Figure 5-15. Details of PDL morphology in the horizontal plane of *O. cuniculus* 1) Overview of tooth orientation of *O. cuniculus*. Three types of PDL fiber arrangement were commonly seen. 2) Direct anterior-posterior orientation or 3) Direct buccal-lingual fiber orientation or 4) Crossed pattern. B) Alveolar bone, P) Periodontal ligament space, E) Enamel space D) Dentin.

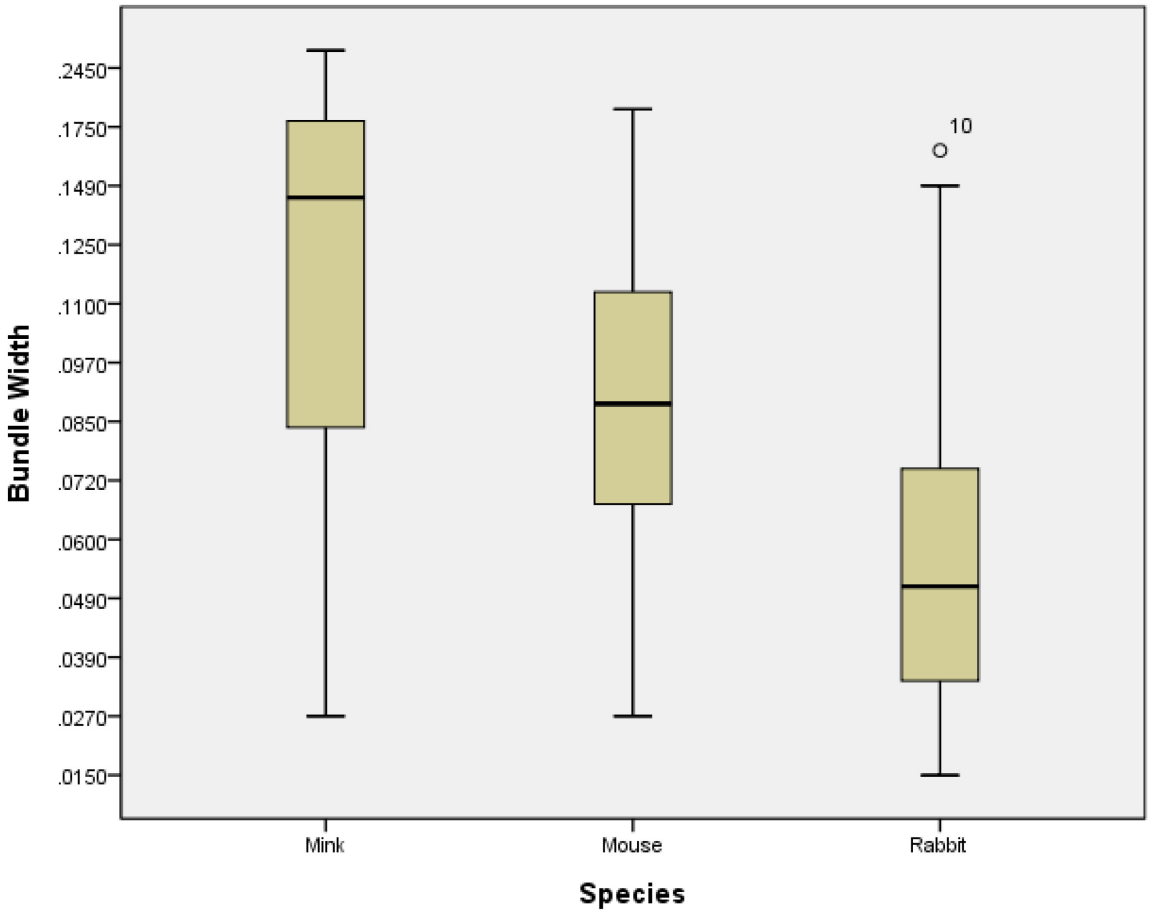

Figure 5-16. Distribution and variation of bundle width measurements for each species. There is overlap in values for all species, but in general the mink has the largest bundle width and the rabbit the smallest. Values were obtained by measuring the width of each bundle visible in a quadrant (see methods for further details).

Chapter 6: The Effect of Reduced Loading on PDL Morphology

Introduction

Reduction of bite force is a common treatment for severe bruxism, and reduction of masticatory muscle mass is an increasingly popular cosmetic treatment. Both are achieved with botulinum toxin (BTX) injections to the muscles of mastication. A rabbit model was used to address the effects of bite force reduction via BTX injection on the morphology of the periodontal ligament (PDL). The PDL is primarily composed of two structural elements: the complex network of collagen fibers spanning the gap between cementum and bone, and the proteoglycan molecules that fill in the space of the collagen matrix. Together, these elements of the PDL cushion and re-distribute the load produced during occlusion (Beertsen et al., 2000; Melcher and Eastoe, 1969). The rate of collagen turnover is very high in the PDL and is regulated via loading (Sodek, 1977; Sodek, 1989). Strains that result from the action of the muscles of mastication are the impetus for both PDL and bone remodeling. A reduction in bite force would lead to the reduced loading of the alveolar complex, and bone loss has been observed in the rabbits used for this study, at both the condyles and in the alveolar region (Rafferty et al., 2012). Here, we address the effects of reduced loading on the morphology and composition of the PDL using the same rabbit model.

Remodeling of the PDL is driven by the character of the load: whether it is in tension or compression and the magnitude of perceived forces (Cattaneo et al., 2009; Kawarizadeh et al., 2004; Masella and Meister, 2006). Overall, a reduction in loading results in a reduction in the

PDL (McCulloch et al., 2000). In mice, a soft diet led to thinning of the PDL space and decreased collagen birefringence (Niver et al., 2011). In the reduced bite force rabbits of this study, a reduction in the percent of collagen present in the PDL is expected, as is a reduction in the area of the PDL space.

In addition to overall volume, the morphology of the PDL is also affected by loading. Similar to the remodeling behavior suggested for trabecular bone (Bertram and Swartz, 1991), PDL collagen fibers seem to be arranged in line with peak tension loads (Komatsu and Viidik, 1996). Niver et al. (2011) also found decreased organization of PDL in response to a soft diet. If PDL fibers become disorganized as a result of reduced loading, an increase in the fractal dimension of the PDL space is expected. The fractal dimension is a measure of complexity; it describes the amount of space and self-similarity of a structure. In ruptured tendons, fractal dimension increased as healing, that is reorganization of fibers, progressed (Frisch et al., 2012). As PDL fibers become disorganized, that is less stringently bundled, the fractal complexity of that structure would increase. However, if fibers are lost, the fractal dimension would decrease.

The PDL inserts into the alveolar bone; so remodeling of the PDL as a result of bite force reduction may result in morphological changes to the alveolar wall. Indeed, an increase in force on the tooth via orthodontic intervention in rats resulted in increased complexity, as measured by the fractal dimension, of the tooth-bone interface (Wagle et al., 2005). This increase in complexity is most likely due to increased PDL-bone connections on the tension side. A reduction in loading may result in a loss of those same type of connections, resulting in a smoother, less complex PDL-bone interface.

If the PDL reflects both directionality and magnitude of loading that difference should be seen when comparing unaltered rabbits to those whose bite force has been experimentally

reduced. Individuals with reduced bite force are expected to exhibit reduced complexity of the PDL-bone interface, smaller PDL area and collagen content, and reduced complexity of the PDL itself due to the loss of collagen content.

Methods

This study relies on samples taken in the course of a pre-existing, completed experiment. In a study by Rafferty et al. (2012), female New Zealand white rabbits received randomized unilateral injections of botulinum toxin (BTX) in the masseter, resulting in muscle paralysis and reduced bite force. Controls were achieved with sham injections (saline). The goal of that study was to evaluate bite force, muscle loss and bone loss in the alveolar and mandibular condyle region, as well as recovery from the injection. Rafferty et al. compared individuals at 4 weeks and 12 weeks post-injection. This study utilizes the alveolar region of 12 individuals (6 Botox, 6 saline) culled at 4 weeks post-injection. Individuals at four weeks post injection were chosen (over 12 weeks post-injection) because the maximum reduction of stimulated bite force was found at week 3, and as such, the most changes in the PDL are expected in the four-week post-injection specimens. As the PDL has a high turnover rate, it is expected that any changes in PDL morphology would have disappeared by the 12-week recovery point.

Sections of the rabbit mandible containing the third molar were isolated and decalcified in a 10% formic acid solution. The left and right sides were randomly assigned to either horizontal or coronal sectioning, and 7μm thick sections of the mid-region of the third molar were taken in the respective planes and stained with Sirius Red. Sirius Red enhances collagen birefringence; under polarized light detailed morphology of the collagen fibers could be easily observed (Retamoso et al., 2009; Rich and Whittaker, 2005; Roush et al., 1988). Serial photographs were taken of the sections at 10x magnification and stitched together using

AutoPano Giga 2.0.1 (Kolor) to create a complete rendering of the tooth socket in the horizontal and coronal planes (Figure 6-1A).

Although 12 individuals were collected, not all individuals could be used for each analysis. The number of specimens used is reported in the description of each analysis. Four lines of inquiry were followed:

PDL-Bone interface: (n = 9). The rendering of the whole socket was used to create an outline of the bone-PDL interface. This black and white outline was analyzed for complexity via fractal dimension. (ImageJ, Fraclac) (Fig. 6-1B, C).

PDL Complexity: (n = 11). Once the whole socket was reconstructed, the collagen mesh of the PDL was isolated and converted to greyscale (ImageJ). Greyscale images were used to measure the fractal dimension of the PDL collagen network, indicating the overall complexity of the PDL (ImageJ, FracLac) (Fig. 6-1D)

Collagen Content: (n = 11). Uniform, 0.25mm square, regions of the PDL were isolated at the four cardinal anatomical directions (anterior, posterior, buccal and lingual) and converted to 8-bit black and white images (Adobe Photoshop). The percent of white pixels (collagen) was calculated and averaged for each specimen (Fig. 6-1E).

PDL Space Area: (n = 9). The area of the region that defines the inner boundary of the PDL space was measured by outlining the PDL-Cementum interface (ImageJ). To calculate the area of the PDL space, the area of the inner boundary was subtracted from the area of the outer boundary. The perimeter of both the inner and outer boundaries were also measured.

Statistical Methods. Individuals who received BTX injections were considered the reduced bite force group; saline injections were the controls. Initial analysis indicated no

difference in any of the measured variables between the injected and non-injected sides of either group. When possible, both sides were measured and pooled to create an average value for each individual. Differences between the reduced bite force values and the saline injected controls were compared using non-parametric tests. Comparison of the four quadrants of PDL collagen were done with an ANOVA. Analyses were carried out using PASW 18 (Polar Engineering and Consulting).

Results

Morphological Description. There were no striking morphological differences between the control and reduced bite force animals.

Coronal Plane: PDL fiber bundles were readily visible. Distinct fiber bundles could be seen inserting into the alveolar bone. On the tooth side of the PDL space, distinct bundles were not common. Instead there was a wide band of primarily horizontal fibers that inserted into the dentin (Fig. 6-2). On average, the fiber bundles inserted at a 62±10º angle relative to the alveolar bone in the plane of the section.

Horizontal Plane: Rabbit molars present enamel down the length of the tooth. As such, decalcification in the middle region of the tooth was often incomplete, resulting in faulty sections. Additionally, the large enamel space present after decalcification often resulted in movement of the tooth during the staining processes. Due to the difficulty in sectioning, teeth in this plane were most often damaged. A common example of this damage due to shifted tooth dentin can be seen in Figure 6-3. Although the tooth was shifted, the PDL space was generally intact. There was a high degree of variation in PDL morphology in the horizontal plane. The lobed nature of the rabbit molar results in a very complex alveolar socket. In general, the lingual

side of the PDL space had the thinnest PDL. The space between the two lobes of the molar was often filled with bone, but it was lacking PDL within the groove. Clear bundles can be seen inserting into the alveolar bone around the entire socket, however their location, density, number and thickness was highly variable among specimens.

PDL-Bone Interface. A measurement of the complexity of the tooth-bone interface was achieved by taking the fractal dimension of the outline of the alveolar bone as it contacted the PDL. The fractal dimension of these outlines were strikingly similar, with no statistical difference ($p = 0.23$, Table 6-1)

PDL Complexity. PDL complexity was approximated by taking the fractal dimension of a grayscale reduction of the PDL space. No difference was found in PDL complexity between the reduced and normal bite force groups ($p = 0.17$, Table 6-1).

Collagen Content . First, to determine whether collagen content varied in the four quadrants, an ANOVA compared the areas within the reduced and normal bite force groups. There was no difference in collagen content among the quadrants (Saline, $p = 0.895$; Reduced, $p = 0.276$). Due to the lack of difference, all quadrants were then pooled for an individual to produce average collagen content per specimen. These values were averaged to produce a reduced and normal bite force collagen percentage (Table 6-1). There was no difference in collagen content between the normal and reduced bite force groups ($p = 0.49$).

PDL Space Area. The area of PDL space was very similar between the two groups (p = 0.52, Table 6-2). However, the inner perimeter was different between the two groups, with the reduced bite force group having a larger perimeter by approximately 2mm (p = 0.048, Table 6-2). While the outer dimension did trend larger in the reduced bite force group, the difference did not reach significance (p=0.52).

Discussion

The expected changes in PDL shape and size, as a result of reduced loading, were not seen. There was no reduction in PDL area or collagen content, nor was the complexity of either the PDL or bone affected. The first possible reason for this is that there was no change in the PDL due to changes in loading. Alternatively, the PDL may have recovered from any potential loss by the time these specimens were harvested. Bite force reduction was observed via muscle stimulation (Rafferty et al., 2012). The peak loss of bite force was seen at week 3. However, recovery begins at that point as bite force begins to return to normal levels. Collagen turnover in the PDL is very high. It is possible that changes that may have resulted from the peak loss in bite force were missed by the 4-week rabbits and that the recovery in bite force that had begun and was enough to cause full recovery of any PDL lost in the earlier period. This would account for no difference in PDL collagen content, or organization.

Additionally while bone loss occurred on both sides, it was greater on the injected side. However, I did not consider injected sides separately because there was no difference between the side in the initial data analysis. The rabbit's teeth are sloped such that once the bite begins; the direction is maintained regardless of force applied (Michaeli et al., 1980; Schwartz et al., 1989). Such a strong maintenance of chewing direction and modality would likely result in bite

force being well distributed between the molar rows, justifying grouping the sides. However, if the PDL was less affected on the uninjected side, the study could have missed an effect on the injected side. Although it is not known what percentage of loading decrease is required to incite PDL collagen loss, if the lower PDL remodeling threshold was not reached, no PDL remodeling could be expected to take place.

The only evidence that remodeling may have taken place is the change in inner PDL boundary in the reduced bite force groups. An increase in the inner boundary is presumed to be the result of cementum deposition, which is a normal process. All rabbits were of the same age, therefore the same baseline rate of cementum deposition would be expected. The fact that the inner PDL boundary is larger in reduced bite force rabbits would indicate a faster deposition rate in those individuals. This may be an indicator of PDL remodeling. While no studies of cementum deposition in remodeling are apparent, this phenomenon has been observed in tooth eruption. Teeth in rodents induced to super-eruption resulted in a 3x increase in cementum deposition (Luan et al., 2007). The PDL space in those rodents was maintained, while surrounding alveolar bone was lost. In the case of these rabbits, the PDL space was maintained and, while alveolar bone perimeter was not significantly different, the reduced bite force individuals did trend towards an outer perimeter increase of the same magnitude as seen in the inner dimension, approximately 2mm.

Taken together, results seem to indicate that if there was increased PDL remodeling activity in the reduced bite force individuals, it was lost by the 4^{th} week. These specimens were primarily collected to observe changes in bone, which has a much slower turnover rate than that of PDL. Given that PDL turnover rates have been observed as quickly as 1 day (Sodek, 1977; Sodek, 1989) and that the minimum loading threshold required to maintain PDL is relatively

unknown, the likelihood that we missed the brief window into PDL loss is high. However, it is likely that eruption was affected (as was demonstrated in the incisors of the same animal (Navarrete et al., 2013)). Ideally, future work would also rely on natural, rather than stimulated, bite force measurements. It would be interesting to see how loss of masticatory force on one side of the jaw would result in natural bite force seen at both sides of the molar row. Additionally, if recovery of any loss of the PDL does occur at such a high rate, collection of specimens much closer to the peak loss in bite force would be ideal.

Table 6-1. Comparison of PDL characteristics in normal and reduced loading cases. Average and (±S.D.) and number of individuals (N). The p-value of non-parametric comparison of means between the groups is reported.

	Bite Force Category				
	Normal	N	Reduced	N	P Value
Percent Collagen	22.65 ± 1.89	5	22.69 ± 2.74	6	0.49
Fractal Dimension of PDL	1.72 ± 0.03	5	1.70 ± 0.04	6	0.17
Fractal Dimension of PDL-Bone interface	1.12 ± 0.02	4	1.12 ± 0.02	5	0.23

Table 6-2. PDL perimeter measurements and PDL area measurements for all studied species. Individual values as well as group averages and standard deviations are reported. Statistical results are reported in text.

Specimen Number	Bite Force Category	PDL Area (mm2)	Inner Perimeter (mm)	Outer Perimeter (mm)
4038	Normal	1.69	20.23	29.87
5223	Normal	1.36	20.68	29.03
6831	Normal	1.66	21.51	32.14
8232	Normal	1.78	20.85	31.11
Average		1.62	20.82	30.54
Standard Deviation		0.18	0.53	1.37
4037	Reduced	1.94	21.60	30.26
5218	Reduced	1.81	21.78	33.76
5219	Reduced	1.93	23.22	34.61
6832	Reduced	1.16	25.29	31.42
6833	Reduced	1.20	23.63	30.10
Average		1.61	23.10	32.03
Standard Deviation		0.39	1.51	2.05

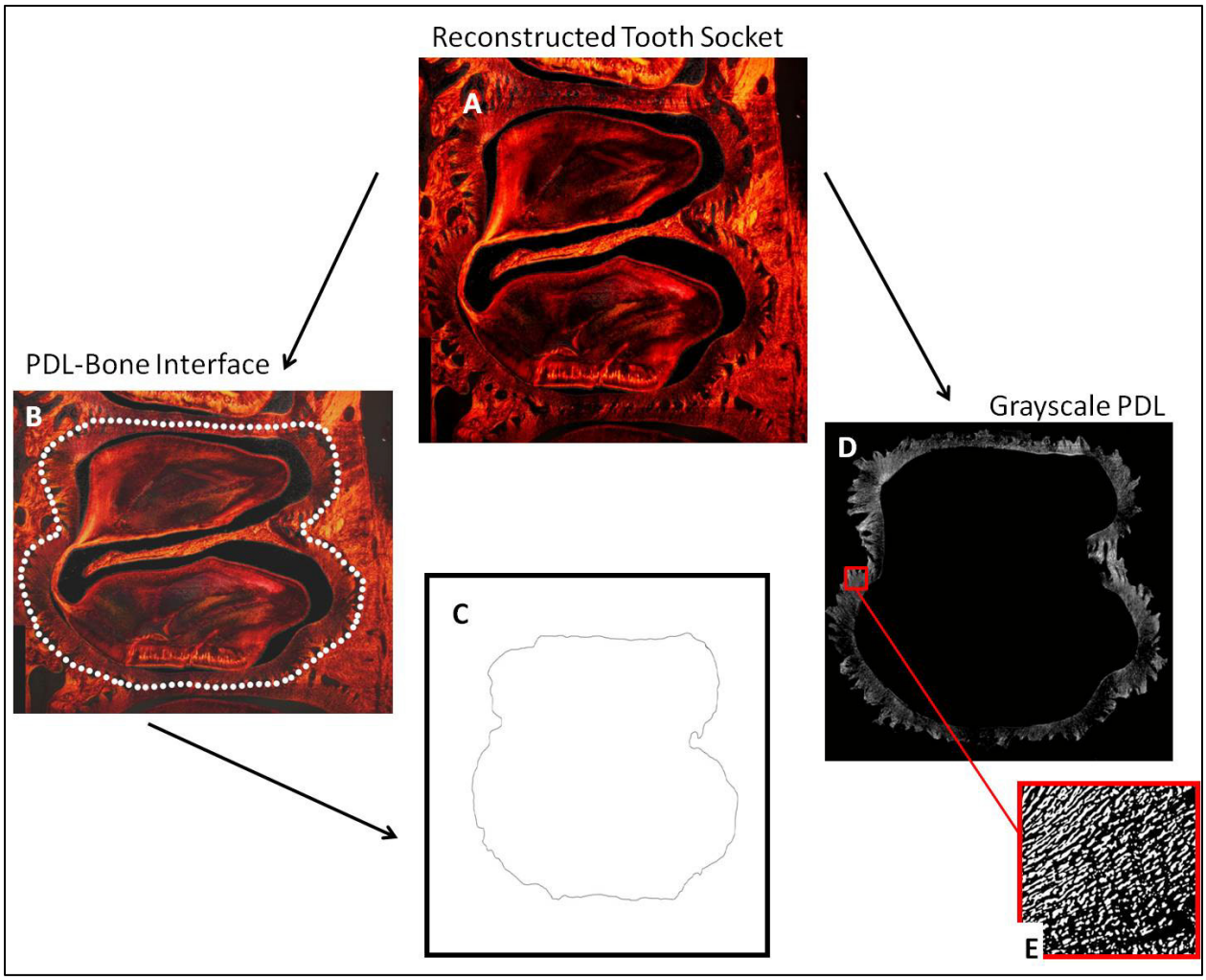

Figure 6-1. Diagram of work-flow for parsing of digital images for the four PDL analyses. Serial photographs of the horizontally sectioned third molar were stitched together to create a reconstructed tooth socket (A). The topography of the PDL-Bone interface was identified (B) resulting in a black and white line representation of the border (C) which was used to determine the complexity of the interface. To measure the complexity of the PDL collagen network, the PDL was isolated and converted to grayscale for analysis of the fractal dimension (D). Uniform, 0.5mm square, regions of the PDL were isolated at the four cardinal anatomical directions (anterior, posterior, buccal and lingual) and converted to 8-bit black and white images (E). The percent of white pixels (collagen) was calculated and averaged for each specimen to estimate collagen content within the PDL space.

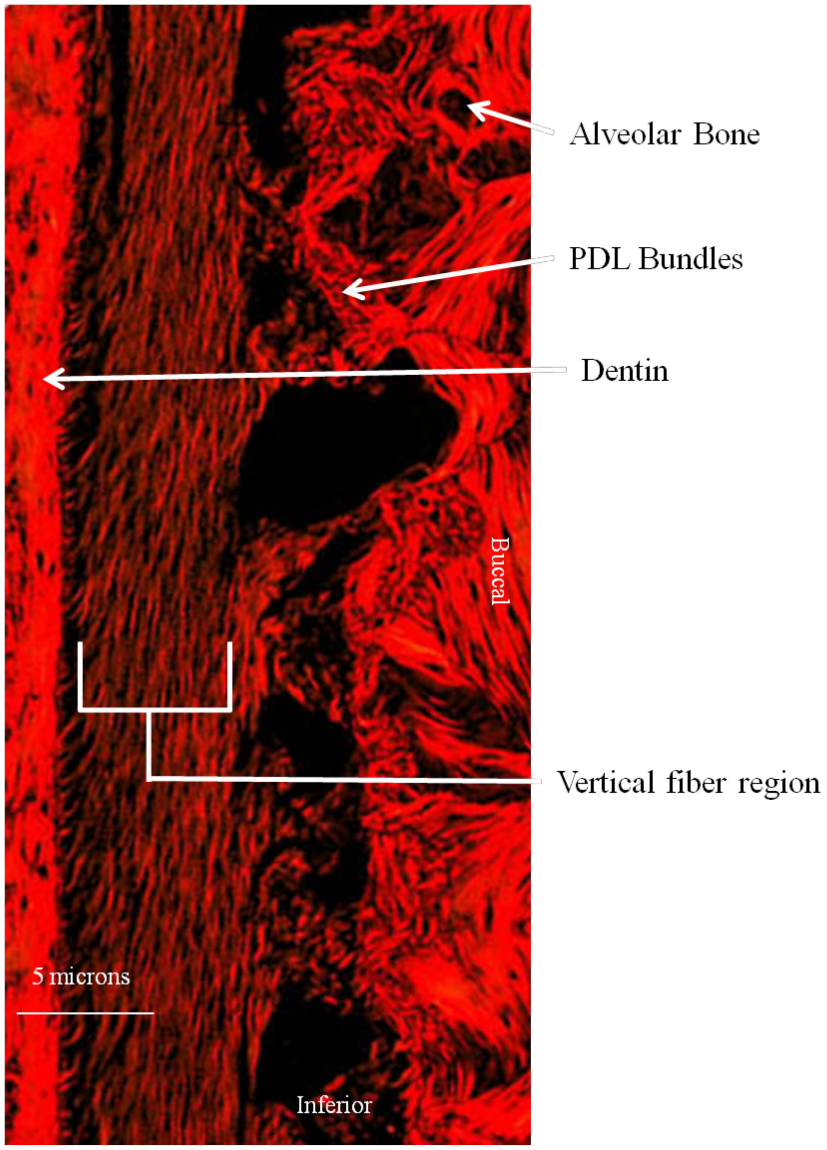

Figure 6-2. Detailed image of *O. cuniculus* PDL organization in the coronal plane. Specimen 6688. Sirius Red stain under circularly polarized light, 10x. A distinct vertical PDL region is apparent, as well as alveolar bone bundles.

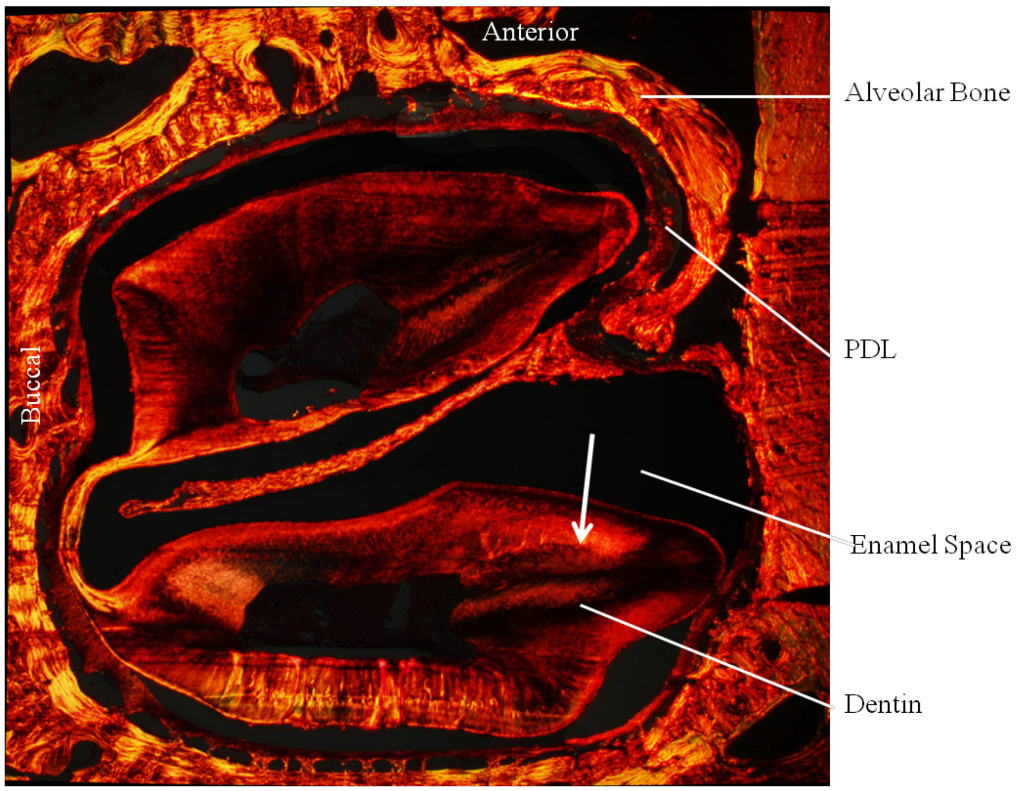

Figure 6-3. An example of tooth displacement within the decalcified enamel space. Specimen 5218. Sirius Red stain under circularly polarized light. Post-sectioning shifting of the tooth within the enamel space can be observed, direction of movement is indicated by the white arrow. This type of damage was commonly observed during tissue processing for this species, PDL measurements were not hindered by the tooth movement.

Chapter 7: Conclusions and Future Work

Summary of Results

Tooth Root Morphology. The relationship between tooth roots and diet is relatively unexplored, although a logical relationship between harder diets and increased root surface area is suggested. Two studies were done to address the interaction between tooth root morphology, diet and bite force in small mammals. In bats there was a clear relationship between food hardness and root surface area, and while this study was not large enough to tease apart the relationship between crown and root morphology, it applied modern tools to identify areas of future work. Much plasticity in bat feeding behavior has been identified in terms of both niche partitioning and seasonal variation. Limitations to behavioral plasticity could be identified with a detailed understanding of the mechanical potential of the root as well as the crown. In contrast, no strong relationship was found between estimated bite force and tooth root surface area in rodents. The mechanics of grass-eating seemed to have a stronger effect on tooth root surface area than bite force. In general, these studies show that MicroCT successfully allows the non-destructive quantification of previously difficult-to-access tooth morphology. This method shows the potential for studies of tooth roots to provide valuable dietary, behavioral and ecological information in small mammals.

Model Predictions and Comparative Histology. The study of root morphology by microCT inevitably ignores the PDL fibrous component, yet this is also a critical aspect chewing mechanics. Therefore, a simplified single-rooted tooth geometry was used to make predictions of

the functional significance of PDL fiber bundle organization under two types of habitual loading. The resulting PDL fiber morphological hypotheses were subsequently tested using a histological analysis.

The finite element model indicated that under vertical loading, overall displacement was lower when PDL fiber bundles were acutely angled. If displacement is the limiting factor, a tooth that is subjected primarily to axial loads should exhibit predominantly acute fibers. However, under lateral loading, the obtuse PDL fiber bundle model resulted in less overall displacement. If displacement is the limiting factor in lateral loading, one would expect to see lateral component chewers exhibit more obtuse fiber bundles. These predictions were supported by histological findings, that *N. vision*, a vertical chewer, had significantly more acute PDL fiber bundles than either *M. musculus* and *O. cuniculus*, which both have a more lateral component to their bite.

Under lateral loading, bone strain at the PDL bundle attachments on the compression side of the root was near zero. As a result, fiber organization in horizontal chewers would be expected to differ between quadrants of the tooth relative to the lateral component of the bite, whereas for the vertical load condition, a more even distribution of strain around the tooth would lead to an expectation of a more consistent fiber organization when comparing the quadrants of the tooth.

The architectural hypotheses generated by FEA were generally supported by histological findings, although statistical significance was not achieved. During biting in *N. vison* the tight TMJ restricts biting motion to a primarily axial rotational movement (Dyce et al., 2009), this species had relatively acute fibers and exhibited uniform fiber distribution around the perimeter of the root, similar to the crossed spoke arrangement commonly attributed to the PDL. *O. cuniculus*, which has a antero-lingual bite component (Ardran et al., 1958), had directly connected fibers in every quadrant except the relatively unloaded posterior region of the root. *M.*

musculus, has a strong poster-anterior power stroke, similar to that found in rats (Weijs and Dantuma, 1975), and exhibited predominantly direct fibers in the A-P orientation, but not in the B-L quadrants.

Reduced loading effect on PDL morphology. An unanswered question is whether PDL architecture can be modified in response to altered diet. A rabbit model was used to investigate the effects of reduced loading on the morphology and composition of the PDL. This is not a change in diet hardness per se, but it was assumed that the animals could not bite with normal force. The expected changes in PDL shape and size, as a result of reduced loading, were not seen. There was no reduction in PDL area or collagen content, nor was the complexity of either the PDL or bone affected. This could indicate that PDL morphology cannot adapt to changed circumstances or that the change in loading was not sufficient to trigger adaptation. Alternatively, the PDL may have recovered from the potential loss by the time these specimens were harvested. Bite force reduction was observed via muscle stimulation (Rafferty et al., 2012), but had begun to recover by week 3. Collagen turnover in the PDL is very high. When rabbits were harvested at week 4, changes that may have resulted from loss in bite force might already have been reversed.

Future work

Further investigation into the relationship between bite force and root surface area would provide added value to paleontological investigations. Paired with detailed understanding of chewing behavior, studies of roots would improve our understanding of the functional morphology of feeding. Information regarding the potential versus actual bite force of many

species is lacking. Adding to the bite force literature would greatly improve future work in this area. An ideal combination would be to film normal chewing behavior and then, using a force transducer to take bite force measurements. These types of studies on animals in the wild are always difficult, but inroads could be made in this problem by initially by improving our understanding of chewing behavior and PDL morphology in commonly used laboratory animals.

In addition to looking at root surface area, microCT would also be useful in getting a picture of detailed PDL architecture, at least in larger animals. While some work has been done in rats (Ho et al., 2010; Leong et al., 2012; Naveh et al., 2013; Niver et al., 2011) too few species have been closely studied in terms of PDL microstructure to allow comparative questions to be addressed.

If a broader understanding of PDL morphology is desired, fiber architecture must be examined. However, a less destructive and time-consuming method than tissue histology must be developed. Additionally, a 3D approach would allow one to integrate root morphology and PDL morphology. This is a multi-part and challenging issue, but a thorough microCT study plus bite force measurement, fiber architecture, and a biomechanical analysis of chewing stroke would have the potential to inform paleontological work as well as have clinical applications.

List of References

Agnarsson I, Zambrana-Torrelio CM, Flores-Saldana NP, May-Collado LJ. 2011. A Time-Calibrated Species-Level Phylogeny of Bats (Chiroptera, Mammalia). PLoS Curr 3:RRN1212.

Aguirre LF, Herrel A, Van Damme R, Matthysen E. 2002. Ecomorphological Analysis of Trophic Niche Partitioning in a Tropical Savannah Bat Community. Proc R Soc Lond B Biol Sci 269(1497):1271-1278.

Aguirre LF, Herrel A, Van Damme R, Matthysen E. 2003. The Implications of Food Hardness for Diet in Bats. Funct Ecol 17(2):201-212.

Ammar HH, Ngan P, Crout RJ, Mucino VH, Mukdadi OM. 2011. Three-Dimensional Modeling and Finite Element Analysis in Treatment Planning for Orthodontic Tooth Movement. Am J Orthod Dentofacial Orthop 139(1):59-71.

Andersen KL, Pedersen EH, Melsen B. 1991. Material Parameters and Stress Profiles within the Periodontal Ligament. Am J Orthod Dentofacial Orthop 99(5):427-440.

Apajalahti S, Sorsa T, Railavo S, Ingman T. 2003. The in Vivo Levels of Matrix Metalloproteinase-1 and-8 in Gingival Crevicular Fluid During Initial Orthodontic Tooth Movement. J Dent Res 82(12):1018-1022.

Archangelo CM, Rocha EP, Pereira JA, Martin Junior M, Anchieta RB, Freitas Júnior AC. 2012. Periodontal Ligament Influence on the Stress Distribution in a Removable Partial Denture Supported by Implant: A Finite Element Analysis. J Appl Oral Sci 20(3):362-368.

Ardran GM, Kemp FH, Ride DL. 1958. A Radiographic Analysis of Mastication and Swallowing in the Domestic Rabbit, *Oryctolagus cuniculus*. J Zool 130(2):257-274.

Atkinson H, Ralph W. 1977. In Vitro Strength of the Human Periodontal Ligament. J Dent Res 56(1):48-52.

Atmaram G, Mohammed H. 1981. Estimation of Physiologic Stress with a Natural Tooth Considering Fiberous Pdl Structure. J Dent Res 60(5):873-877.

August PV. 1981. Fig Fruit Consumption and Seed Dispersal by *Artibeus jamaicensis* in the Llanos of Venezuela. Biotropica 13(2):70-76.

Auluck A. 2014. Widening of Periodontal Ligament Space and Mandibular Resorption in Patients with Systemic Sclerosis. Dento Maxillo Facial Rad 36(7):441-452.

Ayala SC, D'Alessandro A. 1973. Insect Feeding Behavior of Some Colombian Fruit-Eating Bats. J Mammal 54(1):266-267.

Balooch G, Marshall GW, Marshall SJ, Warren OL, Asif SAS, Balooch M. 2004. Evaluation of a New Modulus Mapping Technique to Investigate Microstructural Features of Human Teeth. J Biomech 37(8):1223-1232.

Barlow JC. 1969. Observations on the Biology of Rodents in Uraguay. Life Sci Contr, Royal ontario Museum 75:1-59.

Bartold M, Narayanan A. 1998. Biology of the Periodontal Tissues. Chicago: Quintessence Publishing.

Beaupré G, Orr T, Carter D. 1990. An Approach for Time-Dependent Bone Modeling and Remodeling—Theoretical Development. J Orthop Res 8(5):651-661.

Beaupre GS, Carter DR. 1992. Finite Element Analysis in Biomechanics. In: Biewener M, editor. Biomechanics: Structures and Systems, a Practical Approach. Oxford: IRC Press at Oxford University Press. p 149-174.
Beertsen W. 1975. Migration of Fibroblasts in the Periodontal Ligament of the Mouse Incisor as Revealed by Autoradiography. Arch Oral Biol 20(10):659-666.
Beertsen W, McCulloch CA, Sodek J. 2000. The Peridontal Ligament: A Unique, Multifunctional Connective Tissue. Periodontol 2000 13(1):20-40.
Bell GP, Bartholomew GA, Nagy KA. 1986. The Roles of Energetics, Water Economy, Foraging Behavior, and Geothermal Refugia in the Distribution of the Bat, *Macrotus californicus*. J Comp Physiol, B 156(3):441-450.
Berkovitz BKB, Weaver ME, Shore RC, Moxham BJ. 1981. Fibril Diameters in the Extracellular-Matrix of the Periodontal Connective Tissues of the Rat. Connect Tissue Res 8(2):127-132.
Bertram J, Swartz S. 1991. The 'Law of Bone Transformation': A Case of Crying Wolff? Biol Rev Camb Philos Soc 66(3):245-273.
Bondevik O. 1984. Tissue Changes in the Rat Molar Periodontium Following Alteration of Normal Occlusal Forces. Eur J Orthod 6(1):205-212.
Bonesi L, Palazon S. 2007. The American Mink in Europe: Status, Impacts, and Control. Biol Conserv 134(4):470-483.
Bozal CB, Sanchez LM, Mandalunis PM, Ubios Á. 2013. Histomorphometric Study and Three-Dimensional Reconstruction of the Osteocyte Lacuno-Canalicular Network One Hour after Applying Tensile and Compressive Forces. Cells Tissues Organs 197(6):474-483.
Bradshaw GVR. 1961. A Life History Study of the California Leaf-Nosed Bat, *Macrotus californicus*: University of Arizona.
Brzezinski M. 2008. Food Habits of the American Mink *Mustela vison* in the Mazurian Lakeland, Northeastern Poland. Mamm Biol 73(3):177-188.
Brzeziński M, Romanowski J. 1996. American Mink. Poland: Low.
Brzezinski M, Żurowksi W. 1992. Spring Diet of the American Mink *Mustela vison* in the Mazurian and Brodnica Lakelands, Northern Poland. Acta Theriol 37(1-2):193-198.
Carter DH, Sloan P. 1994. The Fibrous Architecture of the Rat Periodontal Ligament in Cryosections Examined by Scanning Electron Microscopy. Arch Oral Biol 39(11):949-953.
Carvalho F, da Cruz-Neto AP, Zocche JJ. 2008. AmpliaçãO Da DistribuiçãO E Descrição Da Dieta De Mimon Bennettii (Phyllostomidae, Phyllostominae) No Sul Do Brasil. Chiroptera Neotrop 14(2):403-408.
Carvalho RS, Scott JE, Suga DM, Yen EH. 1994. Stimulation of Signal Transduction Pathways in Osteoblasts by Mechanical Strain Potentiated by Parathyroid Hormone. J Bone Miner Res 9(7):999-1011.
Cathelineau G, Yardin M. 1982. The Relationship between Tooth Vibratory Sensation and Periodontal Disease. J Periodontol 53(11):704-707.
Cattaneo P, Dalstra M, Melsen B. 2005. The Finite Element Method: A Tool to Study Orthodontic Tooth Movement. J Dent Res 84(5):428-433.
Cattaneo PM, Dalstra M, Melsen B. 2009. Strains in Periodontal Ligament and Alveolar Bone Associated with Orthodontic Tooth Movement Analyzed by Finite Element. Orthod Craniofac Res 12(2):120-128.

Chiba M, Yamane A, Ohshima S, Komatsu K. 1990. In Vitro Measurement of Regional Differences in the Mechanical Properties of the Periodontal Ligament in the Rat Mandibular Incisor. Arch Oral Biol 35(2):153-161.
Christiansen P, Wroe S. 2007. Bite Forces and Evolutionary Adaptations to Feeding Ecology in Carnivores. Ecology 88(2):347-358.
Coleman JC, Hart RT, Owan I, Tankano Y, Burr DB. 2002. Characerization of Dynamic Three-Dimensional Strain Fields in the Canine Radius. J Biomech 35:1677-1683.
Curtis A, Seehar G. 1978. The Control of Cell Division by Tension or Diffusion. Nature 274(5666):52-53.
Daegling DJ, Granatosky MC, McGraw WS, Rapoff AJ. 2011. Reduced Stiffness of Alveolar Bone in the Colobine Mandible. Am J Phys Anthropol 144(3):421-431.
Dalby PL. 1975. Biology of Pampa Rodents. Michigan State Univ Mus Publ, Biol Ser 5:149-272.
Dalby PL, Mares MA. 1974. Notes on the Distribution of the Coney Rat, *Reithrodon auritus*, in Northwestern Argentina. Amer Midl Nat 92:205-206.
Daly C, Nicholls J, Kydd W, Nansen P. 1974. The Response of the Human Periodontal Ligament to Torsional Loading—I. Experimental Methods. J Biomech 7(6):517-522.
Dar FH, Meakin JR, Aspden RM. 2002. Statistical Methods in Finite Element Analysis. J Biomech 35(9):1155-1161.
Dávalos LM, Cirranello AL, Geisler JH, Simmons NB. 2012. Understanding Phylogenetic Incongruence: Lessons from Phyllostomid Bats. Biol Rev (Camb) 87(4):991-1024.
de Araujo RMS, Oba Y, Kuroda S, Tanaka E, Moriyama K. 2014. Rhoe Regulates Actin Cytoskeleton Organization in Human Periodontal Ligament Cells under Mechanical Stress. Arch Oral Biol 59(2):187-192.
Dechmann DKN, Santana SE, Dumont ER. 2009. Roost Making in Bats-Adaptations for Excavating Active Termite Nests. J Mammal 90(6):1461-1468.
Diekwisch TGH. 2001. The Developmental Biology of Cementum. Int J Dev Biol 45:695-706.
Druzinsky RE. 1995. Incisal Biting in the Mountain Beaver (Aplodontia Rufa) and Woodchuck (*Marmota monax*). J Morphol 226(1):79-101.
Dumont ER, Kunz T, Fenton M. 2003. Bats and Fruit: An Ecomorphological Approach. In: Kunz TH, Fenton MB, editors. Bat Ecology. Chicago: University of Chicago Press. p 398-429.
Dumont ER, O'neal R. 2004. Food Hardness and Feeding Behavior in Old World Fruit Bats (Pteropodidae). J Mammal 85(1):8-14.
Dyce KM, Sack WO, Wensing CJG. 2009. Textbook of Veterinary Anatomy. St. Louis: Elsevier Health Sciences.
Edel A, Wills D. 1975. A Method of Studying the Effects of Reduced Alveolar Support on the Sensibility to Axial Force on the Incisor Teeth in Humans. J Clin Periodontol 2(4):218-225.
Evans AR, Sanson GD. 2005a. Biomechanical Properties of Insects in Relation to Insectivory: Cuticle Thickness as an Indicator of Insect 'Hardness' and 'Intractability'. Aust J Zool 53(1):9-19.
Evans AR, Sanson GD. 2005b. Correspondence between Tooth Shape and Dietary Biomechanical Properties in Insectivorous Microchiropterans. Evol Ecol Res 7(3):453-478.

Evans AR, Sanson GD. 2006. Spatial and Functional Modeling of Carnivore and Insectivore Molariform Teeth. J Morphol 267(6):649-662.
Fenton MB, Whitaker Jr JO, Vonhof MJ, Waterman JM, Pedro WA, Aguiar L, Baumgarten JE, Bouchard S, Faria DM, Portfors CV. 1999. The Diet of Bats from Southeastern Brazil: The Relation to Echolocation and Foraging Behaviour. Rev Bras Zool 16(4):1081-1085.
Field C, Ichim I, Swain MV, Chan E, Darendeliler MA, Li W, Li Q. 2009. Mechanical Responses to Orthodontic Loading: A 3-Dimensional Finite Element Multi-Tooth Model. Am J Orthod Dentofacial Orthop 135(2):174-181.
Fill TS, Carey JP, Toogood RW, Major PW. 2011. Experimentally Determined Mechanical Properties of, and Models for, the Periodontal Ligament: Critical Review of Current Literature. J Dent Biomech:312980.
Fleming TH. 1991. The Relationship between Body Size, Diet, and Habitat Use in Frugivorous Bats, Genus Carollia (Phyllostomidae). J Mammal 72(3):493-501.
Freeman PW. 1979. Specialized Insectivory: Beetle-Eating and Moth-Eating Molossid Bats. J Mammal 60(3):467-479.
Freeman PW. 1995. Nectarivorous Feeding Mechanisms in Bats. Biol J Linn Soc Lond(56):439-463.
Freeman PW, Lemen CA. 2008a. Measuring Bite Force in Small Mammals with a Piezo-Resistive Sensor. J Mammal 89(2):513-517.
Freeman PW, Lemen CA. 2008b. A Simple Morphological Predictor of Bite Force in Rodents. J Zool 275(4):418-422.
Freeman PW, Lemen CA. 2010. Simple Predictors of Bite Force in Bats: The Good, the Better and the Better Still. J Zool 284(4):284-290.
Frisch KE, Duenwald-Kuehl SE, Kobayashi H, Chamberlain CS, Lakes RS, Vanderby Jr R. 2012. Quantification of Collagen Organization Using Fractal Dimensions and Fourier Transforms. Acta Histochem 114(2):140-144.
Gardner AL. 1977. Feeding Habits. In: Baker RJ, Jones JK, Carter DC, editors. Biology of Bats of the New World Family Phyllostomatidae. Lubbock: Texas Tech Press. p 293-350.
Goel VK, Khera SC, Gurusami S, Chen R. 1992. Effect of Cavity Depth on Stresses in a Restored Tooth. J Prosthet Dent 67(2):174.
Goel VK, Khera SC, Sing K. 1990. Clinical Implications of the Response of Enamel and Dentin to Masticatory Loads. J Prosthet Dent 64(4):174.
Goel VK, Ramirez SA, Kong W, Gilbertson LG. 1995. Cancellous Bone Young's Modulus Variation within the Vertebral Body of a Ligamentous Lumbar Spine--Application of Bone Adaptive Remodeling Concepts. J Biomech Eng 117(3):266-271.
Gonzales C, Hotokezaka H, Arai Y, Ninomiya T, Tominaga J, Jang I, Hotokezaka Y, Tanaka M, Yoshida N. 2009. An in Vivo 3d Micro-Ct Evaluation of Tooth Movement after the Application of Different Force Magnitudes in Rat Molar. Angle Orthod 79(4):703-714.
Gordon J. 1978. Structures: Or Why Things Don't Fall Down. Cambridge: Da Capo Press.
Gordon J. 1984. The New Science of Strong Materials or Why You Don't Fall through the Floor. Princeton: Princeton University Press.
Grant D, Bernik S. 1972. Formation of the Periodontal Ligament. J Periodontol 43(1):17-27.
Grant D, Bernik S, Dreizen S. 1972. A Comparative Study of Periodontal Ligament Development in Teeth with and without Predecessors in Marmosets. J Periodontol 43(3):162-169.
Greaves W. 1983. A Functional Analysis of Carnassial Biting. Biol J Linn Soc 20(4):353-363.

Greaves WS. 1988. The Maximum Average Bite Force for a Given Jaw Length. J Zool 214(2):295-306.
Hall ER. 1981. The Mammals of North America. 2nd. New York: Wiley & Sons.
Hannam AG. 1982. The Neuro Physiology of Normal and Abnormal Mandiubular Motion. J Dent Res 61(SPEC. ISSUE):175.
Hart R, Davy D, Heiple K. 1984. Mathematical Modeling and Numerical Solutions for Functionally Dependent Bone Remodeling. Calcif Tissue Int 36(1):S104-S109.
Hart R, Hennebel V, Thongpreda N, Van Buskirk W, Anderson R. 1992. Modeling the Biomechanics of the Mandible: A Three-Dimensional Finite Element Study. J Biomech 25(3):261-286.
Hartsough G, Burger D. 1965. Encephalopathy of Mink: I. Epizootiologic and Clinical Observations. J Infect Dis 115(4):387-392.
Herrel A, De Smet A, Aguirre LF, Aerts P. 2008. Morphological and Mechanical Determinants of Bite Force in Bats: Do Muscles Matter? J Exp Biol 211(1):86-91.
Herring S. 1995. Animal Models of Temporomandibular Disorders: How to Choose. In: Sessle BJ, Bryant PS, Dionne RA, editors. Temporomandibular Disorders and Related Pain Conditions. Seattle: IASP Press. p 323-328.
Herring S. 2003. TMJ Anatomy and Animal Models. J Musculoskelet Neuron Interact 3(4):391.
Herring SW. 2007. Masticatory Muscles and the Skull: A Comparative Perspective. Arch Oral Biol 52(4):296-299.
Herring SW. 2012. Biomechanics of Teeth in Bone: Function, Movement, and Prosthetic Rehabilitation. In: McCauley LK, Sommerman MJ, editors. Mineralized Tissues in Oral and Craniofacial Sceince Biological Principles and Clincal Correlates. p 255.
Hiiemae KM. 1978. Mammalian Mastication: A Review of the Activity of the Jaw Muscles and Movements They Produce in Chewing. In: Butler PM, Joysey KA, editors. Development, Function and Evolution of Teeth. London: Academic Press.
Hiiemae KM. 1984. Functional Apects of Primate Jaw Morphology. In: Chivers DJ, Wood BA, Bilsborough A, editors. Food Acquisition and Processing in Primates. New York: Plenum Press. p 257-281.
Hiiemae KM. 2000. Feeding in Mammals. In: Schwenk K, editor. Feeding: Form, Function and Evolution in Tetrapod Vertebrates. San Diego: Academic Press. p 441-448.
Hillam DG. 1973. Stresses in the Periodontal Ligament. J Periodontal Res 8(1):51-56.
Ho SP, Kurylo MP, Fong TK, Lee SS, Wagner HD, Ryder MI, Marshall GW. 2010. The Biomechanical Characteristics of the Bone-Periodontal Ligament-Cementum Complex. Biomaterials 31(25):6635-6646.
Huang Y, Ohaski Y, Kurisu K. 1991. Distribution of Type I and Type Iii Collagen in the Developing Periodontal Ligament of Mice. Matrix 11(1):25-35.
Huja S, Fernandez S, Hill K, Gulati P. 2007. Indentation Modulus of the Alveolar Process in Dogs. J Dent Res 86(3):237-241.
Ingman T, Apajalahti S, Mäntylä P, Savolainen P, Sorsa T. 2005. Matrix Metalloproteinase-1 and -8 in Gingival Crevicular Fluid During Orthodontic Tooth Movement: A Pilot Study During 1 Month of Follow-up after Fixed Appliance Activation. Eur J Orthod 27(2):202-207.
Inoue T, Saito M, Yamamoto M, Debari K, Kou K, Nishimura F, Miyazaki T. 2009. Comparison of Nanohardness between Coronal and Radicular Intertubular Dentin. Dent Mater J 28(3):295-300.

Jespen A. 1963. Root Surface Measurement and a Method for X-Ray Determination of Root Surface Area. Acta Odontol Scand 21(1):35-46.
Jones DB, Nolte H, Scholubbers J-G, Veltel D. 1991. Biomechanical Signal Transduction of Mechanical Strain in Osteoblast-Like Cells. Biomaterials 12(2):101-110.
Jones M, Hickman J, Middleton J, Knox J, Volp C. 2001. A Validated Finite Element Method Study of Orthodontic Tooth Movement in the Human Subject. J Orthod 28(1):29-38.
Junqueira LCU, Bignolas G, Brentani RR. 1979. Picrosirius Staining Plus Polarization Microscopy, a Specific Method for Collagen Detection in Tissue Sections. Histochem J 11(4):447-455.
Kaipatur N, Wu Y, Adeeb S, Stevenson T, Major P, Doschak M. 2014. A Novel Rat Model of Orthodontic Tooth Movement Using Temporary Skeletal Anchorage Devices: 3d Finite Element Analysis and in Vivo Validation. Int J Dent 2014:1-11.
Karring T, Nyman S, Gottlow J, Laurell L. 1993. Development of the the Biological Concept of Guided Tissue Regeneration Animal and Human Studies. Periodontol 2000 1(1):2635.
Kato R, Ishihara Y, Kawanabe N, Sumiyoshi K, Yoshikawa Y, Nakamura M, Imai Y, Yanagita T, Fukushima H, Kamioka H. 2013. Gap-Junction-Mediated Communication in Human Periodontal Ligament Cells. J Dent Res 92(7):635-640.
Kawarizadeh A, Bourauel C, Zhang D, Gotz W, Jager A. 2004. Correlation of Stress and Strain Profiles and the Distribution of Osteoclastic Cells Induced by Orthodontic Loading in Rat. Eur J Oral Sci 112(2):140-147.
Keene HJ. 1991. On Heterochrony in Heterodonty: A Review of Some Problems in Tooth Morphogenesis and Evolution. Am J Phys Anthropol 34(S13):251-282.
Khera SC, Goel VK, Chen R, Gurusami S. 1988. A Three Dimensional Finite Element Model. Oper Dent 13:128.
Khera SC, Goel VK, Chen R, Gurusami S. 1991. Parameters of Mod Cavity Preperations: A 3d Fem Study, Part Ii. Oper Dent 16:42.
King G, Keeling S, Wronski T. 1991. Histomorphometric Study of Alveolar Bone Turnover in Orthodontic Tooth Movement. Bone 12(6):401-409.
Klein-Nulend J, Roelofsen J, Sterck JG, Semeins CM, Burger EH. 1995. Mechanical Loading Stimulates the Release of Transforming Growth Factor-B Activity by Cultured Mouse Calvariae and Periosteal Cells. J Cell Physiol 163(1):115-119.
Kloehn SJ. 1938. Significance of Root Form as Determined by Occlusal Stress. The Angle Orthodontist 8(3):213-220.
Knoell A. 1977. A Mathematical Model of an in Vitro Human Mandible. J Biomech 10:169-166.
Kobayashi M, Masuda Y, Kishino M, Ishida T, Maeda N, Morimoto T. 2002. Characteristics of Mastication in the Anodontic Mouse. J Dent Res 81(9):594-597.
Koga Y, Yoshida N, Kobayashi K, Okayasu I, Yamada Y. 2001. Development of a Three-Dimensional Jaw-Tracking System Implanted in the Freely Moving Mouse. Med Eng Phys 23(3):201-206.
Komatsu K, Chiba M. 1993. The Effect of Velocity of Loading on the Biomechanical Responses of the Periodontal Ligament in Transverse Sections of the Rat Molar in Vitro. Arch Oral Biol 38(5):369-375.
Komatsu K, Mosekilde L, Viidik A, Chiba M. 2002. Polarized Light Microscopic Analyses of Collagen Fibers in the Rat Inscisor Periodontal Ligament in Relation to Areas, Regions and Ages. Anat Rec 268(4):381-387.

Komatsu K, Viidik A. 1996. Changes in the Fibre Arrangement of the Rat Incisor Periodontal Ligament in Relation to Various Loading Levels *in Vitro*. Arch Oral Biol 41(2):147-159.
Komatsu K, Yamazaki Y, Yamaguchi S, Chiba M. 1998. Comparison of Biomchanical Properties of the Incisor Peridontal Ligament among Different Species. Anat Rec 250(4):408-417.
Korioth T, Romilly D, Hannam A. 1992. Three-Dimensional Finite Element Stress Analysis of the Dentate Human Mandible. Am J Phys Anthropol 88(1):69-96.
Korioth TW, Hannam AG. 1994. Deformation of the Human Mandible During Simulated Tooth Clenching. J Dent Res 73(1):56.
Korschgen LJ. 1958. December Food Habits of Mink in Missouri. J Mammal 39(4):521-527.
Kovacs I. 1979. The Surface Characterisitics of Tooth Roots and Their Biomechanical Importance. Ossa Int J of Sk Res 6:181-192.
Krieger E, Hornikel S, Wehrbein H. 2013. Age-Related Changes of Fibroblast Density in the Human Periodontal Ligament. Head Face Med 9:22.
Kumar A, Mamgain DP, Jaiswal H, Patil PP. 2015. Modal Analysis of Hand-Arm Vibration (Humerus Bone) for Biodynamic Response Using Varying Boundary Conditions Based on FEA. Intelligent Computing, Communication and Devices: Springer. p 169-176.
Kupczik K, Dean MC. 2008. Comparative Observations on the Tooth Root Morphology of *Gigantopithecus blacki*. J Hum Evol 54(2):196-204.
Kupczik K, Hublin JJ. 2010. Mandibular Molar Root Morphology in Neanderthals and Late Pleistocene and Recent Homo Sapiens. J Hum Evol 59(5):525-541.
Kupczik K, Le Cabec A, Hublin JJ. 2010. Comparative Morphology of Incisor and Molar Roots in Neanderthals, Middle Pleistocene Homo and Homo Sapiens. Am J Phys Anthropol 50(Suppl):148.
Kupczik K, Olejniczak AJ, Skinner MM, Hublin JJ. 2009. Molar Crown and Root Size Relationship in Anthropoid Primates. Frontiers in Oral Biology 13:16-22.
Kupczik K, Spoor F, Dean MC. 2003. Tooth Root Morphology and Masticatory Muscle Force Pattern in Humans and Nonhuman Primates. Am J Phys Anthropol 36(Suppl.):134.
Kupczik K, Stynder DD. 2012. Tooth Root Morphology as an Indicator for Dietary Specialization in Carnivores (Mammalia: Carnivora). Biol J Linn Soc 105(2):456-471.
Landry SJ. 1970. The Rodentia as Omnivores. The Quarterly Review of Biology 45(4):351-372.
Le Cabec A, Gunz P, Kupczik K, Braga J, Hublin JJ. 2013. Anterior Tooth Root Morphology and Size in Neanderthals: Taxonomic and Functional Implications. J Hum Evol 64(3):169-193.
Leong NL, Hurng JM, Djomehri SI, Gansky SA, Ryder MI, Ho SP. 2012. Age-Related Adaptation of Bone-PDL-Tooth Complex: *Rattus norvegicus* as a Model System. PLoS ONE 7(4):e35980.
Leung D, Glagov S, Mathews MB. 1976. Cyclic Stretching Stimulates Synthesis of Matrix Components by Arterial Smooth Muscle Cells in Vitro. Science 191(4226):475-477.
Lin C-L, Lin Y-H, Chang S-H. 2010a. Multi-Factorial Analysis of Variables Influencing the Bone Loss of an Implant Placed in the Maxilla: Prediction Using Fea and Sed Bone Remodeling Algorithm. J Biomech 43(4):644-651.
Lin CL, Wang JC, Kuo YC. 2006. Numerical Simulation on the Biomechanical Interactions of Tooth/Implant-Supported System under Various Occlusal Forces with Rigid/Non-Rigid Connections. J Biomech 39(3):453-463.

Lin D, Li Q, Li W, Duckmanton N, Swain M. 2010b. Mandibular Bone Remodeling Induced by Dental Implant. J Biomech 43(2):287-293.
Luan X, Ito Y, Holliday S, Walker C, Daniel J, Galang TM, Fukui T, Yamane A, Begole E, Evans C. 2007. Extracellular Matrix-Mediated Tissue Remodeling Following Axial Movement of Teeth. J Histochem Cytochem 55(2):127-140.
Lucas P. 2004. Dental Functional Morphology. Cambridge: Cambridge University Press.
Lucas P, Constantino PJ, Wood BA, Lawn B. 2008. Dental Enamel as a Dietary Indicator in Mammals. Bioessays 30(4):374-385.
Lund J, Lamarre Y. 1973. The Importance of Positive Feedback from Periodontal Pressoreceptors During Voluntary Isometric Contraction of Jaw-Closing Muscles in Man. J Biol Buccale 1(4):345-351.
Macdonald DW, Norris S. 2001. The Encyclopedia of Mammals. New York: Facts on File, Incorporated.
Maglio VJ. 1973. Origin and Evolution of the Elephantidae. Transactions of fhe American Philosophical Society(63):1-149.
Mandel U, Dalgaard P, Viidik A. 1986. A Biomechanical Study of the Human Periodontal Ligament. J Biomech 19(8):637-645.
Marinescu R, Daegling D, Rapoff A. 2005. Finite-Element Modeling of the Anthropoid Mandible: The Effects of Altered Boundary Constraints. Anat Rec 283A(2):300-309.
Martin R, Burr DB, Sharkey N. 1998. Skeletal Tissue Mechanics. New York: Springer-Verlag.
Martin T. 1993. Early Rodent Incisor Enamel Evolution: Phylogenetic Implications. J Mamm Evol 1(4):227-254.
Masella RS, Meister M. 2006. Current Concepts in the Biology of Orthodontic Tooth Movement. Am J Orthod Dentofacial Orthop 129(4):458-468.
Mason GJ, Cooper J, Clarebrough C. 2001. Frustrations of Fur-Farmed Mink. Nature 410(6824):35-36.
Matsuo M, Takahashi K. 2002. Scanning Electron Microscopic Observation of Microvasculature in Periodontium. Microsc Res Tech 56(1):3-14.
McCulloch C, Lekic P, McKee M. 2000. Role of Physical Forces in Regulating the Form and Function of the Periodontal Ligament. Periodontol 2000 24(1):56-72.
Melcher AH, Eastoe JE. 1969. The Connective Tissues of the Periodontium. In: Melcher A, Bowen W, editors. Biology of the Periodontium. London: Academic Press. p 291.
Mello MAR, Schittini GM, Selig P, Bergallo HG. 2004. Seasonal Variation in the Diet of the Bat *Carollia perspicillata* (Chiroptera: Phyllostomidae) in an Atlantic Forest Area in Southeastern Brazil. Mammalia mamm 68(1):49-55.
Meserve PL. 1981a. Resource Patitioning in a Chilean Semi-Arid Small Mammal Community. J Anim Ecol 50(3):745-757.
Meserve PL. 1981b. Trophic Relationships among Small Mammals in a Chilean Semiarid Thorn Scrub Community. J Mammal 62(2):304-314.
Meyer BN, Chen J, Katona TR. 2010. Does the Center of Resistance Depend on the Direction of Tooth Movement? Am J Orthod Dentofacial Orthop 137(3):354-361.
Michaeli Y, Hirschfeld Z, Weinreb M. 1980. The Cheek Teeth of the Rabbit: Morphology, Histology and Development. Cells Tissues Organs 106(2):223-239.
Milton K. 1981. Food Choice and Diegestive Strategies of Two Sympatric Primate Species. Am Nat 117(4):496-505.

Mitchell DL, West JD. 1975. Attempted Orthodontic Movement in the Presence of Suspected Ankylosis. Am J Orthod 68(4):404-411.
Morimoto T, Inoue T, Nakamura T, Kawamura Y. 1985. Characteristics of Rhythmic Jaw Movements of the Rabbit. Arch Oral Biol 30(9):673-677.
Moss-Salentjin L, Hendricks-Klyvert M. 1990. Dental and Oral Tissues. Philadelphia: Lea & Febiger.
Moxham B, Evans I. 1995. The Effects of Aging Upon the Connective Tissues of the Periodontal Ligament. Connect Tissue Res 33(1-3):31-35.
Nahm D-S, Kim H-J, Mah J, Baek S-H. 2004. In Vitro Expression of Matrix Metalloproteinase-1, Tissue Inhibitor of Metalloproteinase-1 and Transforming Growth Factor-ß1 in Human Periodontal Ligament Fibroblasts. Eur J Orthod 26(2):129-135.
Natali AN, Carniel EL, Pavan PG, Bourauel C, Ziegler A, Keilig L. 2007. Experimental-Numerical Analysis of Minipig's Multi-Rooted Teeth. J Biomech 40(8):1701-1708.
Navarrete AL, Rafferty KL, Liu ZJ, Ye W, Greenlee GM, Herring SW. 2013. Botulinum Neurotoxin Type a in the Masseter Muscle: Effects on Incisor Eruption in Rabbits. Am J Orthod Dentofacial Orthop 143(4):499-506.
Naveh GR, Brumfeld V, Shahar R, Weiner S. 2013. Tooth Periodontal Ligament: Direct 3d Microct Visualization of the Collagen Network and How the Network Changes When the Tooth Is Loaded. J Struct Biol 181(2):108-115.
Nikolai R, Schweiker J. 1972. Investigation of Root-Periodontium Interface Stresses and Displacements for Orthodontic Application. Experimental Mechanics:406-414.
Nikolai RJ. 1996. Rigid-Body Kinematics and Single-Tooth Displacements. Am J Orthod Dentofacial Orthop 110(1):88-92.
Niver EL, Leong N, Greene J, Curtis D, Ryder MI, Ho SP. 2011. Reduced Functional Loads Alter the Physical Characteristics of the Bone–Periodontal Ligament–Cementum Complex. J Periodontal Res 46(6):730-741.
Nogueira MR, Perracchi AL. 2003. Fig-Seed Predation by 2 Species of Chiroderms: Discovery of a New Feeding Stratgey in Bats. J Mammal 84(1):225-233.
Nowak RM. 1999. Walker's Mammals of the World. Baltimore: The Johns Hopkins University Press.
Ourselin S, Roche A, Subsol G, Pennec X, Ayache N. 2001. Reconstructing a 3d Structure from Serial Histological Sections. Image Vision Comput 19(1):25-31.
Oxberry BA. 1975. An Anatomical, Histochemical, and Autoradiographic Study of the Ever-Growing Molar Dentition of Microtus with Comments on the Role of Structure in Growth and Eruption. J Morphol 147(3):337-353.
Panagiotopoulou O, Kupczik K, Cobb SN. 2011. The Mechanical Function of the Periodontal Ligament in the Macaque Mandible: A Validation and Sensitivity Study Using Finite Element Analysis. J Anat 218(1):75-86.
Panagiotopoulou O, Kupczik K, Cobb SN. 2015. The Mechanical Function of the Periodontal Ligament in the Macaque Mandible: A Validation and Sensitivity Study Using Finite Element Analysis (Retraction of Vol 218, Pg 75, 2011). J Anat 226(5):498-498.
Papadopoulou K, Hasan I, Keilig L, Reimann S, Eliades T, Jäger A, Deschner J, Bourauel C. 2013. Biomechanical Time Dependency of the Periodontal Ligament: A Combined Experimental and Numerical Approach. Eur J Orthod 35(6):811-818.
Parfitt GJ. 1960. Measurement of the Physiological Mobility of Individual Teeth in an Axial Direction. J Dent Res 39(3):608-618.

Pearson OP. 1988. Biology and Feeding Dynamics of a South American Herbivorous Rodent, Reithrodon. Stud Neotrop Fauna Environ 23(1):25-39.
Phillips CJ, Oxberry B. 1972. Comparative Histology of Molar Dentitions of Microtus and Clethrionomys, with Comments on Dental Evolution in Microtine Rodents. J Mammal 53(1):1-20.
Pietrzak G, Curnier A, Botsis J, Scherrer S, Wiskott A, Belser U. 2002. A Nonlinear Elastic Model of the Periodontal Ligament and Its Numerical Calibration for the Study of Tooth Mobility. Comput Methods Biomech Biomed Eng 5(2):91-100.
Pilbeam D, Badgley C, Barry JC, Morgan ME, Behrensmeyer AK. 2008. Ecological Changes in Miocene Mammalian Record Show Impact of Prolonged Cliamatic Forcing. Proc Natl Acad Sci USA 105:12145-12149.
Pini M, Wiskott H, Scherrer S, Botsis J, Belser U. 2002. Mechanical Characterization of Bovine Periodontal Ligament. J Periodontal Res 37(4):237-244.
Pini M, Zysset P, Botsis J, Contro R. 2004. Tensile and Compressive Behaviour of the Bovine Periodontal Ligament. J Biomech 37(1):111-119.
Pizzimenti JJ, Salle R. 1981. Factors Influencing the Distributional Abundance of Two Trophic Guilds of Peruvian Cricetid Rodents. Biol J Linn Soc 15(4):339-354.
Qian H, Chen J, Katona TR. 2001. The Influence of PDL Principal Fibers in a 3-Dimensional Analysis of Orthodontic Tooth Movement. Am J Orthod Dentofacial Orthop 120(3):272-279.
Radinsky L. 1967. Relative Brain Size: A New Measure. Science 155(3764):836-838.
Radinsky LB. 1981. Evolution of Skull Shape in Carnivores: 1. Representative Modern Carnivores. Biol J Linn Soc 15(4):369-388.
Rafferty KL, Liu ZJ, Ye W, Navarrete AL, Nguyen TT, Salamati A, Herring SW. 2012. Botulinum Toxin in Masticatory Muscles: Short-and Long-Term Effects on Muscle, Bone, and Craniofacial Function in Adult Rabbits. Bone 50(3):651-662.
Ralph W. 1982. Tensile Behaviour of the Periodontal Ligament. J Periodontal Res 17(4):423-426.
Raspanti M, Cesari C, De Pasquale V, Ottani V, Strocchi R, Zucchelli G, Ruggeri A. 2000. A Histological and Electron-Microscopic Study of the Architecture and Ultrastucture of Human Periodontal Tissues. Arch Oral Biol 45(3):185-192.
Redlich M, Reichenberg E, Harari D, Zaks B, Shoshan S, Palmon A. 2001. The Effect of Mechanical Force on Mrna Levels of Collagenase, Collagen Type I, and Tissue Inhibitors of Metalloproteinases in Gingivae of Dogs. J Dent Res 80(12):2080-2084.
Reeder SA, Carroll DS, Edwards CW, Kilpatrick CW, Bradley RD. 2006. Neotomine–Peromyscine Rodent Systematics Based on Combined Analyses of Nuclear and Mitochondrial DNA Sequences. Mol Phylogenet Evol 40(1):251-258.
Rees JS. 2001. An Investigation into the Importance of the Periodontal Ligament and Alveolar Bone as Supporting Structures in Finite Element Studies. J Oral Rehabil 28(5):425-432.
Rees JS, Jacobsen PH. 1997. Elastic Modulus of the Periodontal Ligament. Biomaterials 18(14):995-999.
Rensberger JM. 1975. Function in the Cheek Tooth Evolution of Some Hypsodont Geomyoid Rodents. J Paleontol 49(1):10-22.
Retamoso LB, Da Cunha TDA, Knop LAH, Shintcovsk RL, Tanaka OM. 2009. Organization and Quantification of the Collagen Fibers in Bone Formation During Orthodontic Tooth Movement. Micron 40(8):827-830.

Rich L, Whittaker P. 2005. Collagen and Picrosirius Red Staining: A Polarized Light Assessment of Fibrillar Hue and Spatial Distribution. Braz J Morphol Sci 22(2):97-104.
Richmond B, Wright B, Grosse I, Dechow P, Ross C, Spencer M, Strait D. 2005. Finite Element Analysis in Functional Morphology. Anat Rec 238A(2):258-274.
Rippin J. 1976. Collagen Turnover in the Periodontal Ligament under Normal and Altered Functional Forces. J Periodontal Res 11(2):101-107.
Roberts W, Goodwin Jr W, Heiner S. 1981. Cellular Response to Orthodontic Force. Dent Clin North Am 25(1):3-17.
Roberts WE. 1999. Bone Dynamics of Osseointegration, Ankylosis, and Tooth Movement. J Indiana Dent Assoc 78(3):24-32.
Romanyk DL, Collins CR, Lagravere MO, Toogood RW, Major PW, Carey JP. 2013. Role of the Midpalatal Suture in FEA Simulations of Maxillary Expansion Treatment for Adolescents: A Review. International Orthodontics 11(2):119-138.
Ross C. 2005. Finite Element Analysis in Vertebrate Biomechanics. Anat Rec 283A(2):253-258.
Ross C, Patel B, Slice D, Strait D, Dechow P, Richmond B, Spencer M. 2005. Modeling Masticatory Muscle Force in Finite Element Analysis: Sensitivity Analysis Using Prinicpal Coordinates Analysis. Anat Rec 283A(2):288-299.
Roush JK, Breur GJ, Wilson JW. 1988. Picrosirius Red Staining of Dental Structures. Stain Technol 63(6):363-367.
Ryan TM, van Rietbergen B. 2005. Mechanical Significance of Femoral Head Trabecular Bone Structure in *Loris* and *Galago* Evaluated Using Micromechanical Finite Element Models. Am J Phys Anthropol 126(1):82-96.
Sabat P, Bozinovic F. 2000. Digestive Plasticity and the Cost of Acclimation to Dietary Chemistry in the Omnivorous Leaf-Eared Mouse *Phyllotis darwini*. J Comp Physiol B 170(5-6):411-417.
Saito M, Saito S, Ngan PW, Shanfeld J, Davidovitch Z. 1991a. Interleukin 1 Beta and Prostaglandin E Are Involved in the Response of Periodontal Cells to Mechanical Stress in Vivo and in Vitro. Am J Orthod Dentofacial Orthop 99(3):226-240.
Saito S, Ngan P, Rosol T, Saito M, Shimizu H, Shinjo N, Shanfeld J, Davidovitch Z. 1991b. Involvement of Pge Synthesis in the Effect of Intermittent Pressure and Interleukin-1β on Bone Resorption. J Dent Res 70(1):27-33.
Sanctuary CS, Wiskott H, Justiz J, Botsis J, Belser U. 2005. In Vitro Time-Dependent Response of Periodontal Ligament to Mechanical Loading. J Appl Physiol 99(6):2369-2378.
Santana SE, Dumont ER. 2011. Do Roost-Excavating Bats Have Stronger Skulls? Biol J Linn Soc 102(1):1-10.
Santana SE, Dumont ER, Davis JL. 2010. Mechanics of Bite Force Production and Its Relationship to Diet in Bats. Funct Ecol 24(4):776-784.
Santana SE, Geipel I, Dumont ER, Kalka MB, Kalko EK. 2011a. All You Can Eat: High Performance Capacity and Plasticity in the Common Big-Eared Bat, Micronycteris Microtis (Chiroptera: Phyllostomidae). PLoS ONE 6(12):e28584.
Santana SE, Grosse IR, Dumont ER. 2012. Dietary Hardness, Loading Behavior, and the Evolution of Skull Form in Bats. Evolution 66(8):2587-2598.
Santana SE, Strait S, Dumont ER. 2011b. The Better to Eat You With: Functional Correlates of Tooth Structure in Bats. Funct Ecol.
Scaglia O, Velázquez C, Cauhepe M. 1982. Plant Composition of Coney Rat's (*Reithrodon auritus*) Diet. Acta Theriol 27(13):350-353.

Scapino R. 1974. Function of the Masseter-Pterygoid Raphe in Carnivores. Anat Anz 136(5):430.
Scapino R. 1981. Morphological Investigation into Functions of the Jaw Symphysis in Carnivorans. J Morphol 167(3):339-375.
Scapino RP. 1976. Function of the Digastric Muscle in Carnivores. J Morphol 150(4):843-859.
Schwartz GT, Enomoto S, Valiquette C, Lund JP. 1989. Mastication in the Rabbit: A Description of Movement and Muscle Activity. J Neurophysiol 62(1):273-287.
Shibata M, Shintaku Y, Matsuzaki K, Uematsu S. 2014. The Effect of Il-17 on the Production of Proinflammatory Cytokines and Matrix Metalloproteinase-1 by Human Periodontal Ligament Fibroblasts. Orthod Craniofac Res 17(1):60-68.
Sicher H. 1942. Tooth Eruption: The Axial Movement of Continuously Growing Teeth. J Dent Res 21(2):201-210.
Silva MJ, Brodt MD, Hucker WJ. 2005. Finite Element Analysis of the Mouse Tibia - Estimating Endocortical Strain During Three Point Bending in Samp6 Osteoporotic Mice. Anat Rec 283A(380-390).
Sloan P. 1978. Scanning Electron Microscopy of the Collagen Fibre Architecture of the Rabbit Incisor Periodontium. Arch Oral Biol 23(7):567-572.
Sloan P, Carter D. 1995. Structural Organisation of the Fibres of the Periodontal Ligament. In: Berkovitz B, Moxham B, Newman H, editors. The Periodontal Ligament in Health and Disease. New York: Mosby-Wolfe. p 35-54.
Smith JM, Savage R. 1959. The Mechanics of Mammalian Jaws. Sch Sci Rev 40:289-301.
Smole MS, Kleinschek K, Kreze T, Strnad S, Mandl M, Wachter B. 2004. Physical Properties of Grass Fibres. Chemical and biochemical engineering quarterly 18(1):47-54.
Sodek J. 1977. A Comparison of the Rates of Synthesis and Turnover of Collagen and Non-Collagen Proteins in Adult Rat Periodontal Tissues and Skin Using a Microassay. Arch Oral Biol 22(12):655-665.
Sodek J. 1989. Collagen Turnover in Periodontal Ligament. Biology of Tooth Movement. Boca Raton: CRC Press. p 157-181.
Spencer M. 1998a. Force Production in the Primate Masticatory System: Electromyographic Tests of Boimechanical Hypotheses. J Hum Evol 34(1):25-54.
Spencer MA. 1998b. Tooth Root Morphology and Diet in Primates. Am J Phys Anthropol(SUPPL. 26):206.
Spencer MA. 2003. Tooth-Root Form and Function in Platyrrhine Seed-Eaters. Am J Phys Anthropol 122(4):325-335.
Springer SD, Gregory PA, Barrett GW. 1981. Importance of Social Grouping on Bioenergetics of the Golden Mouse, *Ochrotomys nuttalli*. J Mammal 62(3):628-630.
Staszyk C, Hagen G. 2004. A Simple Flourescence Labeling Method to Visualize the Tree-Dimensional Arrangement of Collagen Fibers in the Equine Periodontal Ligament. Ann Anat 186(4):149-152.
Staszyk C, Wulff W, Jacob HG, Gasse H. 2006. Collagen Fiber Architecture of the Periodontal Ligament in Equine Cheek Teeth. J Vet Dent 23(3):143-147.
Steppan SJ. 1980. Revision of the Tribe Phyllotini (Rodentia: Sigmodontinae), with a Phylogenetic Hypothesis for the Sigmodontinae. Fieldiana (Zool) 1464(80):1-112.
Strait D, Wang Q, Dechow P, Ross C, Richmond B, Spencer M, Patel B. 2005. Modeling Elastic Properties in Finite Element Analysis: How Much Precision Is Needed to Produce and Accurate Model? Anat Rec 283A(2):275-287.

Stynder DD, Kupczik K. 2012. Tooth Root Morphology in the Early Pliocene African Bear *Agriotherium africanum* (Mammalia, Carnivora, Ursidae) and Its Implications for Feeding Ecology. J Mamm Evol 20(3):1-11.
Tanaka E, Inubushi T, Koolstra JH, van Eijden TM, Sano R, Takahashi K, Kawai N, Rego EB, Tanne K. 2006. Comparison of Dynamic Shear Properties of the Porcine Molar and Incisor Periodontal Ligament. Ann Biomed Eng 34(12):1917-1923.
Tanaka E, Inubushi T, Takahashi K, Shirakura M, Sano R, Dalla-Bona DA, Nakajima A, van Eijden TM, Tanne K. 2007. Dynamic Shear Properties of the Porcine Molar Periodontal Ligament. J Biomech 40(7):1477-1483.
Teaford MF, Robinson JG. 1989. Seasonal or Ecological Differences in Diet and Molar Microwear in *Cebus nigrivittatus*. Am J Phys Anthropol 80(3):391-401.
Ten Cate A. 1994. Oral Histology, Mosby, St: Louis.
Ten Cate A, Mills G, Solomon G. 1971. The Development of the Periodontium: A Transplantation and Autoradiographic Study. Anat Rec 170(3):365.
Thomason JJ. 1991. Cranial Strength in Relation to Estimated Biting Forces in Some Mammals. Canadian Journal of Zoology-Revue Canadienne De Zoologie 69(9):2326-2333.
Thomason JJ, McClinchey HL, Faramarzi B, Jofriet JC. 2005. Mechanical Behavior and Quantitative Morphology of the Equine Laminar Junction. Anat Rec A Discov Mol Cell Evol Biol 283(2):366-379.
Toms S, Dakin G, Lemons J, Eberhardt A. 2002a. Quasi-Linear Viscoelastic Behavior of the Human Periodontal Ligament. J Biomech 35(10):1411-1415.
Toms S, Lemons J, Bartolucci A, Eberhardt A. 2002b. Nonlinear Stress-Strain Behavior of Periodontal Ligament under Orthodontic Loading. Am J Orthod Dentofacial Orthop 122(2):174-179.
Turnbull WD. 1970. Mammalian Masticatory Apparatus. Fieldania: Geology(18):149-356.
Valentin S. 1996. Functional Morphology and the Masticatory Apparatus of a Small Carnivore: The American Mink (*Mustela vision*). Bulletin de la Societe Zoologique de France-Evolution Zoologie 121(1):169-170.
Verna C, Zaffe D, Siciliani G. 1999. Histomorphometric Study of Bone Reactions During Orthodontic Tooth Movement in Rats. Bone 24(4):371-379.
Viidik A. 1980. Biology of Collagen. London: Academic Press.
Vincent JFV. 1983. The Influence of Water Content on the Stiffness and Fracture Properties of Grass Leaves. Grass Forage Sci 38(2):107-114.
Wagle N, Do NN, Yu J, Borke JL. 2005. Fractal Analysis of the Pdl-Bone Interface and Implications for Orthodontic Tooth Movement. Am J Orthod Dentofacial Orthop 127(6):655-661; quiz 754.
Warhonowicz M, Staszyk C, Gasse H. 2007. Immunohistochemical Detection of Matrix Metalloproteinase-1 in the Periodontal Ligament of Equine Cheek Teeth. Tissue Cell 39(6):369-376.
Warhonowicz M, Staszyk C, Rohn K, Gasse H. 2006. The Equine Periodontium as a Continuously Remodeling System: Morphometrical Analysis of Cell Proliferation. Arch Oral Biol 51(12):1141-1149.
Watt DM, MacGregor AR, Cockburn A, Boyd JL. 1958. A Preliminary Investigation of the Support of Partial Dentures and Its Relationship to Vertical Loads. Dent Pract 9:2-15.
Weijs W. 1975. Mandibular Movements of the Albino Rat During Feeding. J Morphol 145(1):107-124.

Weijs W, Dantuma R. 1975. Electromyography and Mechanics of Mastication in the Albino Rat. J Morphol 146(1):1-33.
Weinans H, Huiskes R, Grootenboer H. 1992. The Behavior of Adaptive Bone-Remodeling Simulation Models. J Biomech 25(12):1425-1441.
Whishaw I, Sarna J, Pellis S. 1998. Evidence for Rodent-Common and Species-Typical Limb and Digit Use in Eating, Derived from a Comparative Analysis of Ten Rodent Species. Behav Brain Res 96(1):79-91.
Williams SH, Kay RF. 2001. A Comparative Test of Adaptive Explanations for Hypsodonty in Ungulates and Rodents. J Mamm Evol 8(3):207-229.
Williams W, LaPointe L, Mahan P, Cornell C, Bichajian C. 1985. Vibratory Stimulation of Jaw Muscles and Bite Force Discrimination. Am J Orthod 88(4):356-357.
Williams W, Low S, Cooper W, Cornell C. 1987. The Effect of Periodontal Bone Loss on Bite Force Discrimination. J Periodontol 58(4):236-239.
Wills D, Picton D. 1978. The Intrusion of the Tooth for Different Loading Rates. J Biomech 11(10):429-434.
Wills D, Picton D, Davies W. 1976. A Study of the Fluid Systems of the Periodontium in Macaque Monkeys. Arch Oral Biol 21(3):175-185.
Wilson A, Middleton J, Jones M, McGuinness N. 1994. The Finite Element Analysis of Stress in the Periodontal Ligament When Subject to Vertical Orthodontic Forces. J Orthod 21(2):161-167.
Woo SLY, Peterson RH, Ohland KJ, Sites TJ, Danto MI. 1990. The Effects of Strain Rate on the Properties of the Medial Collateral Ligament in Skeletally Immature and Mature Rabbits: A Biomechanical and Histological Study. J Orthop Res 8(5):712-721.
Wroe S, McHenry C, Thomason J. 2005. Bite Club: Comparative Bite Force in Big Biting Mammals and the Prediction of Predatory Behaviour in Fossil Taxa. Proc Biol Sci 272(1563):619-625.
Xia Z, Jiang F, Chen J. 2013. Estimation of Periodontal Ligament's Equivalent Mechanical Parameters for Finite Element Modeling. Am J Orthod Dentofacial Orthop 143(4):486-491.
Yeh C-K, Rodan GA. 1984. Tensile Forces Enhance Prostaglandin E Synthesis in Osteoblastic Cells Grown on Collagen Ribbons. Calcif Tissue Int 36(1):S67-S71.
Zioupos P, Casinos A. 1998. Cumulative Damage and the Response of Human Bone in Two-Step Loading Fatigue. J Biomech 31(9):825-833.